UCRL 10294

University of California

Ernest O. Lawrence Radiation Laboratory

TWO-WEEK LOAN COPY

This is a Library Circulating Copy which may be borrowed for two weeks. For a personal retention copy, call Tech. Info. Division, Ext. 5545

CONTROLLED THERMONUCLEAR RESEARCH
SEMIANNUAL REPORT
January through June 1962

LIVERMORE AND
Berkeley, California

DISCLAIMER

This document was prepared as an account of work sponsored by the United States Government. While this document is believed to contain correct information, neither the United States Government nor any agency thereof, nor the Regents of the University of California, nor any of their employees, makes any warranty, express or implied, or assumes any legal responsibility for the accuracy, completeness, or usefulness of any information, apparatus, product, or process disclosed, or represents that its use would not infringe privately owned rights. Reference herein to any specific commercial product, process, or service by its trade name, trademark, manufacturer, or otherwise, does not necessarily constitute or imply its endorsement, recommendation, or favoring by the United States Government or any agency thereof, or the Regents of the University of California. The views and opinions of authors expressed herein do not necessarily state or reflect those of the United States Government or any agency thereof or the Regents of the University of California.

Research and Development

UCRL-10294
UC-20 Controlled Thermonuclear Processes
TID-4500 (17th Ed.)

UNIVERSITY OF CALIFORNIA
Lawrence Radiation Laboratory
Berkeley and Livermore, California

Contract No. W-7405-eng-48

CONTROLLED THERMONUCLEAR RESEARCH SEMIANNUAL REPORT

January through June 1962

July 20, 1962

Printed in USA. Price $2.50. Available from the
Office of Technical Services
U. S. Department of Commerce
Washington 25, D.C.

CONTROLLED THERMONUCLEAR RESEARCH SEMIANNUAL REPORT

January through June 1962

Contents

INTRODUCTION 1

I. PYROTRON (MAGNETIC MIRROR) PROGRAM

1. Introduction and Summary (Post) 4
2. Multistage High-Compression Experiments (Coensgen, Cummins, Nexsen, Sherman, and Ellis) 5
3. Table Top III (Perkins, Post, and Carlson). 7
4. Alice (Energetic Neutral Atom Injection) (Damm, Foote, Futch, Gordon, Hunt, and Steinhaus) 15
5. P-4 (Steady-State Plasma System) (Barr, Gardner, and Oleson) 26

II. ASTRON PROGRAM

1. Introduction (Christofilos) 28
2. Astron Tank Model (Sherwood). 28
3. Plasma Diagnostics (Reagan) 29
4. Accelerator Status (Hester) 29
5. Astron Accelerator Beam-Monitoring Loops (Wright). . . . 31
6. Beam Analyzer (Sherwood) 31

III. LIVERMORE PINCH PROGRAM (Colgate and Co-Workers)

1. Summary 32

*Preceding reports: UCRL-9969, UCRL-9777.

2. Cusp-Pinch Experiment 33

3. Linear Hard-Core Pinch Experiments 35

4. Resistive Sheet Pinch Experiment 35

5. Levitron Progress 37

6. Collisionless Plasma Shock (Experimental) 38

7. Collisionless Plasma Shock (Theoretical) 38

8. Instability Theory 40

IV. BERKELEY PLASMA RESEARCH

1. Rotating-Plasma Research (Halbach, Layman, and Paxson 41

2. Hydromagnetic Waves and Cyclotron Heating (Boley, DeSilva, Forman, Hamilton, Spillman, and Cooper). 45

3. Remarks on Magnetoacoustic Waves (Kunkel) 53

4. Hydromagnetic Ionizing Fronts (Sherwood and Kunkel) . . 57

5. Crossed-Field Breakdown Studies (Bernstein, Kunkel, and Pearson) 57

6. Numerical Calculation of the Electron Energy Distribution in H_2 and D_2 in Crossed Fields for Large $\omega\tau$ (Pearson) . 59

7. Sheet Pinch Studies (Anderson) 62

8. Experiments on Lorentz Dissociation and Partially-Ionized Plasma (Pyle and Co-workers) 68

9. Wave Propagation in Hothouse II--Theoretical (Sachs) . . 70

10. The Steady-State Reflection of a Streaming Plasma by a Magnetic Field (Macmahon) 71

V. THEORETICAL AND BASIC EXPERIMENTAL PLASMA PHYSICS

1. A Self-Consistent Distribution of Electrons in the Astron E Layer (Heckrotte and Neil) 72

2. A Computation for Studying the Formation of the Astron E Layer (Killeen). 73

3. Instability of a Resistive Sheet Pinch (Furth and Killeen) . . . 73

4. Plasma Potential and Electron Energy Distributions in the Alice Experiment (Futch and Killeen) 74

5. Theory of an Electrostatic Probe in a Plasma (Hall and Geesaman) 74

6. A Statistical Theory of Transport Phenomena (Hall) 75

7. Atomic Scattering (Mittleman) 75

8. Formation of Excited Hydrogen Atoms in the Collisional Dissociation of H_2^+ Ions (Hiskes) 76

9. Magnetic Shocks (Zwick and Gonzales) 77

10. Bumpy Torus and Positron Experiment (Gibson, Jordan, and Lauer) 83

11. Atomic Scattering and Cross-Section Measurements (Baker, Brink, Chambers, McFarland, and Soltysik). 85

VI. ENGINEERING AND TECHNOLOGICAL DEVELOPMENT

1. Ultrahigh-Vacuum Development (Milleron and Levenson) . . . 88

2. Mechanical Engineering Development (Batzer). 89

3. Electrical Engineering Development (Smith, Branum, Van Ness, Cummings, Wharton, Nail, and Hopkins) 92

VII. TALKS AND PUBLICATIONS 110

CONTROLLED THERMONUCLEAR RESEARCH SEMIANNUAL REPORT*

January through June 1962

Lawrence Radiation Laboratory
University of California
Berkeley and Livermore, California

July 20, 1962

INTRODUCTION

C. M. Van Atta

The period January 1 to June 30, 1962, has been one in which the obvious construction efforts on the Alice, Astron, and the new 2X multiple-compression facility have tended to obscure the results obtained from the continuing research activities. A brief summary of the more significant developments of the past six months follows.

Table Top The experimental investigation of the stable and unstable modes of plasma confinement in the Table Top magnetic-compression mirror machine has continued. Injection at the instant of much higher field (approx 1000 gauss) during the field pulse (7.5 msec to field maximum) results in a "hot ion" plasma in which the average energy of the ions exceeds that of the electrons. The unstable mode again exhibits a rotating flute as in the "hot electron" case, but with opposite direction of rotation and lower rotational frequency.

Alice The construction of the Alice energetic neutral-atom injection mirror machine was completed, and initial operation was carried out successfully. "Total" pressure in the trapping chamber was about 10^{-8} mm Hg, which is believed to be too high by a factor of about ten for exponential plasma buildup initiated by collisions with residual gas molecules. The density of energetic ions in the plasma is estimated to have reached a value between 2×10^{7} and 1×10^{8} cm^{-3}. The ion density was observed to decay with a mean life of about 30 msec, consistent with the computed decay time due to charge exchange on the residual gas. In future operation the pressure is expected to be significantly lower as a result of installation of a water vapor curtain directed across the beam tube, which reduces substantially the gas flow into the plasma trapping region. A plasma gun is now installed for injecting a cold plasma along the axis of the field coils so that buildup initiated by charge-exchange processes in a cold plasma can also be investigated.

In surface-bombardment studies of energetic neutral atoms and ions of hydrogen (7.5 to 16 keV) on a stainless steel target, a wide range of ratios of emitted to incident particles is observed, depending upon the state and

*Work done under the auspices of the U. S. Atomic Energy Commission.

previous history of the target. For a room-temperature, unbaked target a ratio as high as ten is observed, whereas for a continuously heated (200°C) target the ratio may be less than unity. Present interpretation of the observations is that the incident particle is retained in the target material and previously absorbed gas is desorbed in the region of the thermal spike produced by conversion of the kinetic energy of the incident particle.

Toy Top The pulsed-field coil system of the Toy Top multiple-compression machine has been completely rebuilt. The new coil structure has a 9-in.-bore tube instead of the 6-in.-bore tube previously used, produces a smoother and more symmetrical field, and has a rise time of about 60 μsec instead of 270 μsec. The new arrangement is comparatively short and consists of only two stages. Full-scale operation of the modified system had just begun at the end of the report period.

Design of the larger 2X multiple-compression machine has been completed and some phases of construction work carried out.

Astron A self-consistent solution for the distribution of electrons in an infinitely thin Astron E layer has been derived analytically. This model of the E layer does not exhibit the axial bunching instability or the B_θ instability during buildup. The ampere-turn distribution at the ends of the confinement region needed to produce the desired fields in the E layer region has also been derived from this model.

Pinch Instabilities predicted by the finite-conductivity theory of plasma stability have been classified under three catagories: a long-wave "tearing" mode, a short-wave "rippling" mode, and a low-β, pressure-driven interchange mode. The Livermore pinch program is increasingly oriented toward experiments in which these instability modes can be identified and studied. A hard-core linear pinch with an outer cusp field, a cylindrical sheet or "triaxial" pinch, a large new linear hard-core pinch, and the Levitron (toroidal hard-core pinch) are the experimental devices in which the importance of the "rippling" and "tearing" modes can be evaluated.

Bumpy Torus Considerations of plasma confinement in a bumpy torus type of field have included (a) a study of stabilization against interchange instability, (b) computation of the loss rate of ions back out through the horseshoe shaped injection channel, and (c) analysis of the conservation rules applicable to particles during transition from oscillation between adjacent magnetic mirrors to complete rotational traversal of the torus. Iron pole pieces to be placed between the coils of the Bumpy Torus to introduce shear in the field and improve plasma stability are being designed.

Homopolar V A new design of the rotating-plasma device, Homopolar V, has been in operation throughout the report period. The major improvements over the Homopolar IV consist of the better base pressure ($< 10^{-7}$ mm Hg), more symmetrical injection of the gas pulse to initiate the discharge, and a new coil assembly providing greater flexibility in field configuration and higher magnetic field strength. Electrical measurement of angular momentum yields plasma peripheral velocities up to 6×10^7 cm/sec, corresponding to an ion drift energy of about 4 keV. The conditions during initiation of the discharge are such

that the average Larmor energy should equal the drift energy. Since the ion density is about 10^{15} cm^{-3}, neutrons should be produced, and they are observed. The neutron output is expected to increase as the magnetic and electric fields applied to the device are increased. After the higher field conditions are realized an objective will be to determine the origin and time dependence of the neutron output.

Hothouse II The turbulence previously reported in observations of Alfvén waves in Hothouse II (ion cyclotron heating) has been greatly reduced by placing a conducting screen over the quartz window on the end of the machine for the purpose of anchoring the magnetic field lines. Probe measurements of the wave amplitude are much smoother as a result of decreased turbulence. These measurements indicate that about half the rf power output of the 8.3-Mc oscillator used in exciting the wave appears in the plasma wave and that at least 90% of the wave energy is absorbed from the wave at the magnetic beach (region of ion cyclotron resonance).

Positive Column Instabilities Investigation of the instability of the positive column discharge in a longitudinal magnetic field has been extended to the case of an alternating applied electric field. The onset of instability is observed to occur at higher magnetic field values as the frequency of the electric field is increased in the range 0 to 70 kc. At high frequency (>30 kc) the form at the onset of instability appears to be more complex than in the dc case, and more nearly resembles the complex states obtained in the dc case with magnetic fields much greater than the critical value. The experimental results are in qualitative agreement with theoretical results obtained by extending the theory of Kadomtsev and Nedospasov to higher modes ($m > 1$).

I. PYROTRON (MAGNETIC MIRROR) PROGRAM

1. INTRODUCTION AND SUMMARY

Richard F. Post

First operation of the ALICE experiment, reconstruction of the coil system of the multistage experiment, and additional experimental investigation of the "rotating flute" instability in Table Top were the main activities of the mirror group during this report period. In addition, some significant measurements on the release of adsorbed gas from surfaces under energetic particle bombardment, and on the electrical breakup of excited atoms, were made in connection with the ALICE experiment. First measurements at low temperatures were also performed on the full-scale coil which has been constructed to test the feasibility of cryogenic coils with ultrapure sodium conductors.

In addition to the above experimental activities, significant progress was made toward the design and construction of the new "2X" multistage mirror facility.

A continuing effort has been made to reconcile both the observed stability and the unstable plasma behavior observed in the Table Top and in the multistage experiment with theory. Of considerable interest in this connection is the fact that it has been confirmed that the same type of rotating flute seen with a "hot electron" plasma in Table Top has been seen with a "hot ion" plasma, except that in the latter case the flute is observed to rotate in the opposite direction, i.e., in the sense expected if the plasma potential is positive. It also seems that the rotating instability observed is the <u>only</u> instability that occurs in the Table Top plasmas; that is to say, when the rotating flute is not present, no other instability seems to be operative, either. A complete proof of this conjecture would, however, require accurate quantitative measurement of the collisional end losses, for comparison with diffusion theory.

The Table Top and multistage experiments, taken together, at present seem to indicate the following about confinement in simple mirror machines:

(a) Confinement that is stable against the flute instability is possible under the proper circumstances.

(b) High-mode-number flutes are not observed; m = 1 (or nonlinear forms of it) are most prevalent (this from Table Top and early multistage evidence).

(c) Nonlinear effects are important; growth rates of the instability, for example, do not seem to be as rapid as simple theory would indicate. Also, in Table Top, definite evidence is observed of instability "triggering thresholds," or of shock-like phenomena which lead to sharpening of the shape of the rotating flute.

(d) Diffusion of particles and electrical conduction (through particle flow) along the magnetic lines through the mirrors seem to play a significant, though not always understood, role in the observed stabilizing effects.

(e) The instability may be self-destroying; in many cases it has been observed that instability, accompanied by rapid radial diffusion, may begin, only to disappear before the plasma reaches the chamber wall (this from Table Top).

The above observation suggest that several different effects are operative in determining the boundaries between stable and unstable behavior. Among those which seem plausible are:

(a) The "finite orbit" stabilizing mechanisms calculated by Rosenbluth et al.

(b) "Drift smearing" effects arising from both magnetic and electrostatic gradients in the plasma.

(c) Slowing of instability growth rates by flow of charges out the mirrors; this may possibly lead to overall stability when coupled with (a) and (b).

(d) "Line tying" arising from the anchoring of magnetic lines in the conducting surfaces external to the plasma, owing to the presence of cold plasma outside the mirrors.

We hope that, by understanding the above effects in detail, and by exploiting the predictions of the theory of stabilization of hydromagnetic instabilities, we will be able to expand the regime of stably confined plasmas into larger volumes and higher temperatures, ones which more nearly approach thermonuclear goals.

2. MULTISTAGE HIGH-COMPRESSION EXPERIMENTS

Frederic H. Coensgen, William F. Cummins, William E. Nexsen, Jr., Arthur E. Sherman, and Robert E. Ellis

Toy Top III S

On January 5, 1962 one of the pulsed magnets of the 6-inch system failed owing to breakdown of insulation between windings. Consequently, no further data than reported previously (UCRL-9969) were obtained from the system. Rather than rebuild the 6-inch system, we constructed an improved 9-inch system. For the past 5 months almost the entire group effort has been devoted to the design of symmetric magnets, their construction, and the precise detailed magnetic measurements of the individual magnets as well as the assembled system. The new 9-inch system was designated as Toy Top III S and has become known as the III S system; i.e., the short, symmetric, stabilized system. It is short, as it consists of only two stages. The symmetry is such that the magnetic field contour lines at the 9-in. diameter are circular within ± 1/8 in. Deviations from symmetry of the magnetic surface which should bound the plasma are less. Improved hydromagnetic stability should result from the elimination of the sharp bends in the magnetic field lines such as were present in the 6-inch system. Stabilizing windings similar to those used by Ioffe are located between the vacuum chamber and the pulsed-magnet system.

Operation of the completed III S system has just started and neutrons have been observed. Currently, we are trying to increase the reaction rate to the point where it can be followed as a function of time. Other diagnostics are being installed.

As the compression time in the III S system is about one-quarter that of the 6-inch system, comparison of the time dependence of the reaction rates in the two systems should enable one to determine whether or not the early decay of the reaction rates observed in the 6-inch system were due to cooperative effects (including instabilities) or due to atomic processes such as charge exchange or excessive Coulomb scattering from the slower components of the injected plasma.

The increased size of the compression chamber should, also, slow down loss due to the cascade process, suggested as a possible explanation of the mode II decays discussed in the preceding report. Initial wall bombardment should be reduced in the larger compression chamber.

Plasma Injections

The equivalent of at least 100 Toy Top injectors will be required for the 2X experiment. Consequently, considerable effort is being devoted to the simplification of injector construction, improvement of reliability, and increase of plasma output. The output from a larger model has been found to increase approximately linearly with the diameter of the injector orifice. Provided the angular distribution of the ions is not changed radically a smaller number of larger injectors may be used in the 2X experiments.

A gas-fed plasma gun of the LASL type (Osher) is in operation and measurements of the ion energy distribution are in progress. Although the gun is now operated in zero field, its performance in the presence of a magnetic field will also be investigated. Because of the reported high average ion energy and the large plasma output, we have considerable interest in this type of injector. Therefore upon completion of the III S construction considerable effort has been transferred to this work.

2X Facility

Most of the 2X design was completed by the end of January. Subsequently the detailed electrical, mechanical, and construction engineering was initiated and completed. Much of the construction is now in progress and will be reported by the various engineering groups.

The development of the low-inductance magnets for the symmetric fields of III S can be regarded as development of the 2X pulsed magnets. Although the preliminary pulsed magnet design has been completed, construction of the 2X pulsed magnets will not be started until the performance of the III S system is evaluated.

Magnetic Field Codes

To analyze the results of high-compression experiments (in which considerable inductive coupling exists between the various pulsed coils as well as between pulsed coils and dc coil shielding) it might be necessary to know the magnitude and direction of the magnetic field, as a function of time, at all points in the space occupied by a plasma. For any particular coil configuration and system geometry, actual measurements could be made for given values of capacitor bank voltage, firing delays, etc. On the other hand, considerable experimental time might be saved if reliable calculations of the time-varying fields, field gradients, lines of magnetic induction, forces on conductors, etc., were available. An IBM 7090 code is being developed for this purpose, involving the solution of k sets of coupled ordinary linear differential equations, where k is the total number of energizing or crowbar switches that have been closed during the operational sequence. There are 2n equations in each set, where n is essentially the total number of loops, or coil circuits (including the passive shielding loops) that have been closed, up to and including the time at which the kth switch is closed. The input parameters involved are the mutual and self-inductances, resistance and capacitance of each loop, and capacitor bank voltage. The output is the loop current as a function of time. This output will in turn be used as a scale factor in the input for an IBM 7090 code which has been developed at Oak Ridge for the calculation of magnetic fields for cylindrically symmetric rectangular coils by the method of zonal harmonics. The solution for the loop currents was originally obtained in terms of the natural modes of the system by the usual method of Laplace transforms. Difficulties inherent in this method, due to the necessity of solution of the algebraic characteristic equation, essentially of degree 2n, will, we hope, be by-passed by a method of matrix iteration suggested by R. Von Holdt in which it is unnecessary to determine the natural modes and which utilizes the capabilities of the computer to greater advantage. Parametric studies of the effects of mutual inductance on the magnetic field in complicated coil systems will be undertaken with relation to possible effects on plasma confinement during the compression cycle.

3. TABLE TOP III

Continued Experimental Studies of an Instability

Walton A. Perkins, Richard F. Post, and Norris W. Carlson

In the preceding report we reported our discovery that the unstable plasma was rotating around the chamber and that the mechanism for escape to the walls was the $\vec{E}\times\vec{B}$ drift caused by a flutelike form.[1]

An explanation for the rotation is as follows: when the plasma is injected into the initially low magnetic field (10 to 50 gauss), the high-energy ions from the source spiral into the walls while the electrons with smaller

[1] Walton A. Perkins, Richard F. Post, and Norris W. Carlson, in Controlled Thermonuclear Research Semiannual Report, UCRL-9969, Jan. 1962, p. 10.

gyroradii are trapped. The electrons are "hotter" than the ions before and after the compression, and a plasma with a negative potential is created. The radially inward $\vec{E}$ field causes an azimuthal $\vec{E}\times\vec{B}$ drift for both electrons and ions in the direction that electrons precess in the midplane of a mirror machine. When the instability occurs, the unstable plasma moves outward and continues to rotate to conserve angular momentum. Of course, the rotating form loses momentum by collisions with probes, chamber walls, background gas, and other plasma. It is observed that the rotation velocity decreases, but at a rate much slower than 1/B during compression, and it continues to decrease while the magnetic field is decaying.

A good test of the explanation that the plasma-produced $\vec{E}$ fields causes the rotation would be to create a positive potential plasma and see if the rotation occurs in the opposite direction. Table Top III was designed to trap and contain a "hot ion" plasma, and such a plasma should have a positive potential. The main difference is that the initial fields are greater (500 to 2000 gauss) and the hot-ion component ($E \approx 1$ keV) from the source is trapped. Here scattering losses cause a depletion of electrons and thereby a positive potential plasma is created.

The instability was detected at relatively low injection densities. Figure I-1 shows an accumulation of the main results. The top left trace is an electrostatic probe signal indicating an instability from 1 msec to 5 msec (injection time is 200 μsec). The top right traces are from two electrostatic probes at opposite sides of the chamber. There are four main differences in the electrostatic probe signals in the hot ion case:

(a) By using a fixed and a movable probe we determined that the rotation is in the opposite direction.

(b) Here the positive part passes by first and the negative second. The polarization must be in this direction for the instability $\vec{E}\times\vec{B}$ drift to be outward.

(c) The relative pulse heights of the positive and negative parts of the electrostatic probe signals indicate that the negative region is closer to the probe--i.e., farther from the axis--than the positive region. Also, the observed direction of rotation would require an outward radial $\vec{E}$ field.

(d) The rotation period in the hot ion case is typically 20 μsec, compared with the typical 2-μsec periods in the hot electron case.

The middle left trace shows a fairly common occurrence in which the electrostatic probe signals change character (here at 5 msec) and the signal changes from predominantly negative to positive. By using two electrostatic probes in the midplane a quarter of the circumference apart, it was determined that direction of the later rotation is opposite that of the hot ion plasma (or the same as that for a negative potential plasma).

This is explained along the lines of the above exposition for the rotation. The plasma potential is positive when the hot ion plasma becomes unstable. The unstable, rotating plasma form acquires an angular momentum for this direction of $\vec{E}\times\vec{B}$, which it conserves except for collisions.

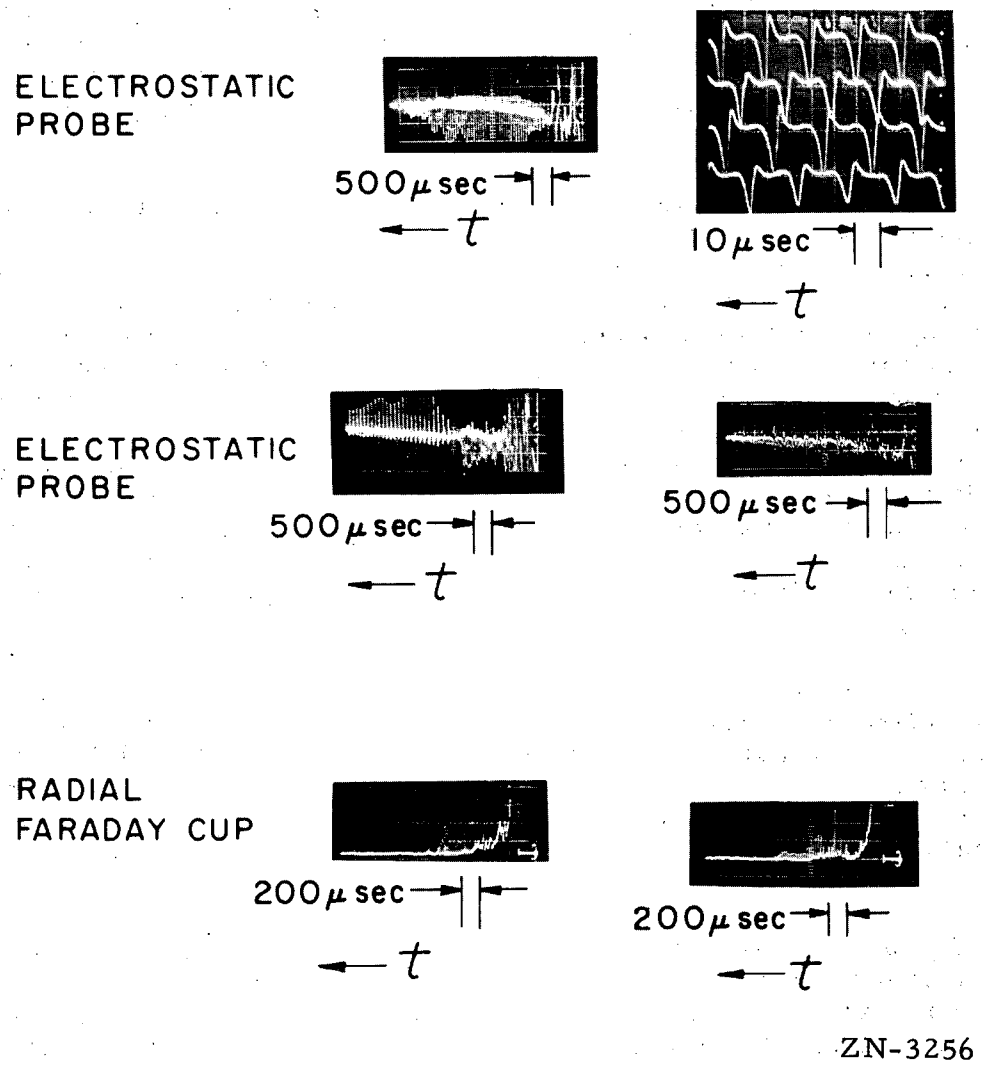

Fig. I-1. Electrostatic probe and screened collector cup signals for the "hot ion" plasma.

As time goes on, free plasma (not contained in the unstable rotating plasma form) is compressed by the magnetic field (7.5 msec rise time) and hot ions are lost by the instability and charge exchange. Therefore, the potential of the plasma changes from positive to negative and the second unstable plasma form rotates in the opposite direction from the first. Note that the second rotation is much slower than in the usual hot electron case, indicating that a much weaker electric field is formed here.

In the middle right trace the negative-potential rotating form starts before the positive-potential rotating form dies out, and we have plasma forms rotating in opposite directions at the same time. The question immediately arises: How can they collide with so little interaction? Here, the two rotating forms may be at different radii, as the electrostatic probes detect at a distance. In cases discussed previously[2] the two forms rotating at different velocities which were detected by a scintillation probe appeared to be at the same place at the same time. The plasma densities here are 10^7 to $10^9/cm^3$ and particle collisions are not important. If the rotating forms are of different sizes, it is possible to envision a collision in which a small, dense plasma passes through a large lower-density plasma. Another explanation may be that they are different points in space. For example, if they are at two different radii, the inner form might push up plasma as it goes around.

The two bottom traces are typical signals from a screen-covered Faraday collector cup that "protrudes" radially in the midplane. The line structure of the signals indicates the rotation. Time-correlation studies showed that the collection cup line signal occurred at the time the rotating form, detected by the electrostatic probe, passed by. The polarity of collector signals was reversed by reversing the bias voltage between the screen and cup.

In hot electron experiments, the radial distribution of the escaping end flux was measured with a 0.25-in.-diameter scintillator for the low-density unstable case and the high-density seemingly stable case. The results are shown in Fig. I-2. The solid curve is a least-squares fit to the experimental points. In the high-density case it was necessary to use two Gaussians--one for the points near the axis and another with a slower drop-off for the rest of the points. The small end detector showed sharp readjustments in density. Instabilities occurred between 0.5 msec and 8.0 msec in the central region. Apparently the stabilizing mechanism was strong enough to stop the instability, because it was not detected by the radial scintillator at 10 cm from the axis. In taking our experimental points for the figure we used only those points in which no instability was detected before 7.5 msec (peak magnetic field), or extrapolated the signals before an instability occurred to 7.5 msec. The voltage on the photomultiplier was 2500 V for the low-density case (2.0 kV on source) and 1500 V for the high-density case (6.5 kV on source). Actually, the peak end signals differ by a factor of 10^4. A calibration of the scintillation detector indicated a peak density (6.5 kV on source) of about $10^{11}/cm^3$.

Some evidence of the inner shape of the rotating plasma form was obtained with this 0.25-in.-diameter end scintillator. End and radial scintillator probe traces are shown in Fig. I-3 for a triggered instability (triggered by pulsing a nearby axial magnetic coil). The top traces show the end scintillator

[2] Ibid., see Fig. I-3, bottom trace.

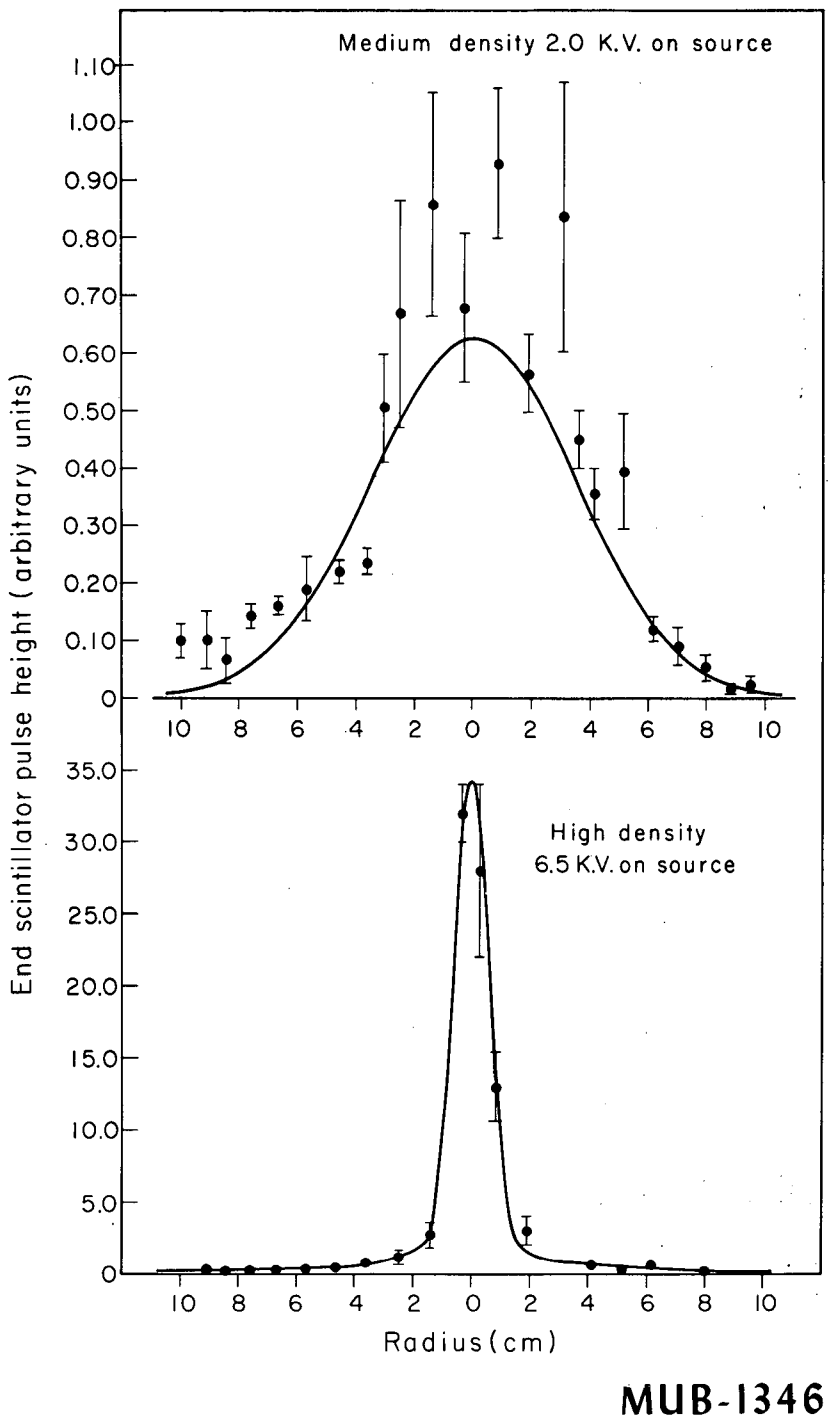

Fig. I-2. End-escaping flux as a function of radius for the low-density unstable case (top) and the high-density stable case (bottom). The bottom curve should be multiplied by 280 to give comparison signal intensities.

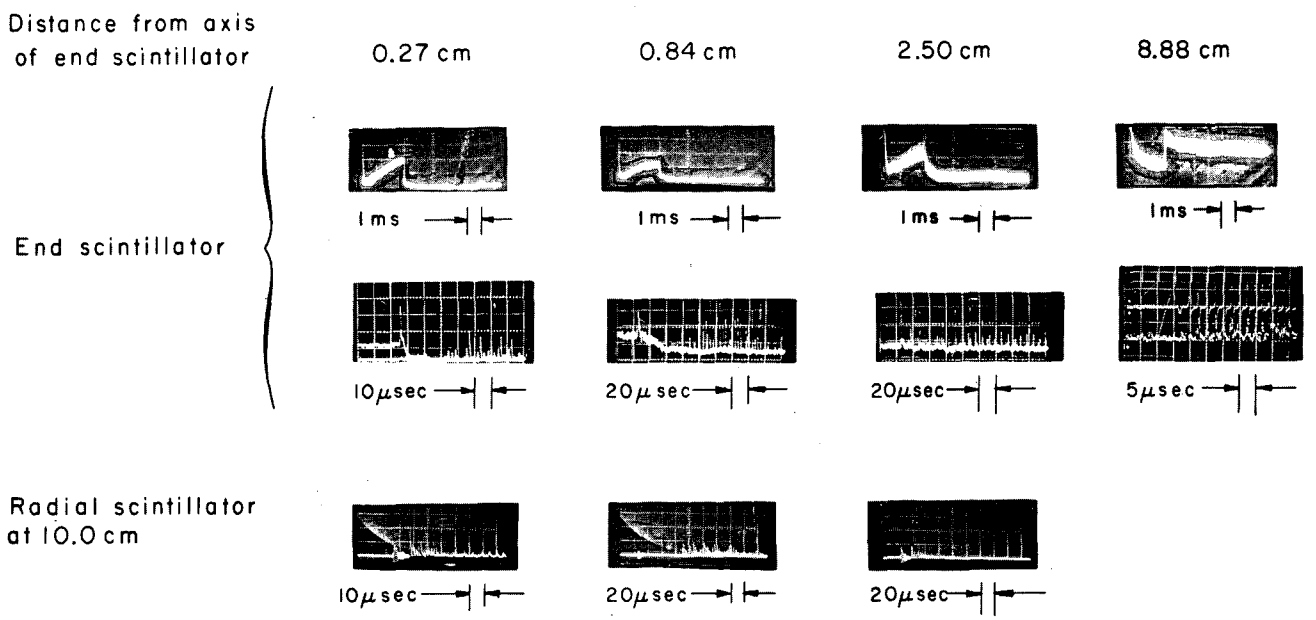

ZN-3253

Fig. I-3. End and radial scintillation probe signals for a triggered instability. The 0.25-in.-diameter end probe is set at various distances from the axis as noted on the figure. At the 10-cm position the electrostatic probe signal is shown just above the end-probe signal.

signal for the first 10 msec, giving an overall picture. The middle set shows on a fast sweep of the interesting region, and the bottom set has the corresponding radial scintillator probe signals. Some interesting points:

(a) There is a sharp momentary increase in end flux when the instability is triggered (earlier oscillation on radial probe trace is caused by triggering mechanism).

(b) The instability causes the plasma to leave the central region. Next the rotating instability is detected by the radial probe, and finally a line-structure signal is detected on the central end scintillator.

(c) With the end probe detecting plasma at 2.50-cm radius and radial probe at 10-cm radius there is a 1:1 correspondence in the line structure for the first 40 μsec of the signal. At the 8.88 cm position there is also 1:1 correspondence between the end and electrostatic probe signals (same picture).

(d) Since the rotation is detected at 2.5 cm and 10 cm at the same time, we must rule out the model of a "rotating wave on a disk."[3] Since the unstable plasma moves off-axis, a "spinning arm" seems unlikely.

(e) These results are consistent with a "rotating column," which would be an M = 1 mode flute instability. It should be noted that this evidence of the rotating forms shape was obtained only in triggered instabilities.

Another detector that we have recently found useful is a light monitor, i.e., a photomultiplier monitoring the light from the background gas that is ionized by the plasma. Over short periods the gas density is quite constant, so one has a measure of how the density varies. Figure I-4 shows two cases of triggered instabilities. In Fig. 4a the triggering mechanism was the crowbarring of the pulsed mirror field, and in Fig. 4b pulsing an axial magnetic field nearby. Note in Fig. 4a that the light monitor signal shows a sharp drop along with end scintillator signal when the instability occurs at 8 msec.

[3] Ibid., see Fig. I-4.

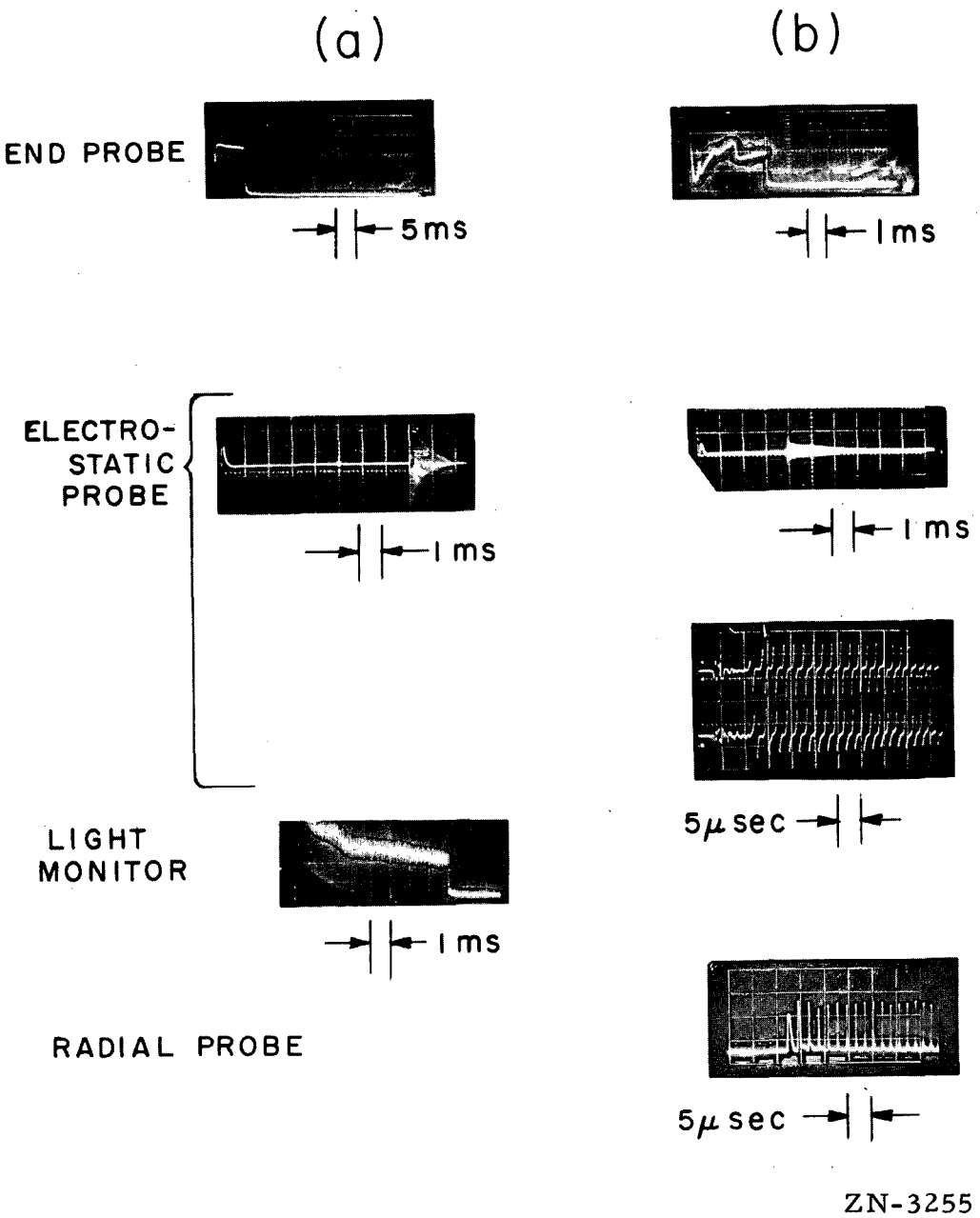

Fig. I-4. Triggered instabilities. The triggering mechanism is in (a) crowbarring the pulsed mirror field, and (b) pulsing an axial magnetic field coil nearby to 2 kilogauss.

STUDY OF THE ROTATING-FLUTE INSTABILITY IN A RAPIDLY RISING MIRROR FIELD

Walton A. Perkins and Norris W. Carlson

A small magnetic mirror machine was assembled in the Table Top area. One of the main purposes of this machine was to study the flute-type instability (described in the Table Top Section) in a fast-compression mirror machine. The rise time of the Table Top mirror machine is 7.5 msec, and we are interested in shortening the rise time of the magnetic field toward that of the θ pinch devices. So far we have studied this instability with coils of 60 μsec and 35 μsec rise time. In both cases the rotating instability was easily observed with scintillation detectors. Electrostatic probe signals also showed the rotation. Because of the fast pulsed magnetic fields, a glass vacuum chamber was used, whereas Table Top has a stainless steel chamber in the diagnostic section of the machine. The use of electrostatic probes is greatly hindered in the glass chamber because of its sensitivity to extraneous pickup. This is probably why electrostatic probes are not used more extensively in plasma physics.

4. ALICE (ENERGETIC NEUTRAL ATOM INJECTION)

Alice Trapping Experiments

Charles C. Damm, James H. Foote, Archer H. Futch, Frank J. Gordon, Angus L. Hunt, and James F. Steinhaus

Assembly of the Alice mirror machine and beam tube has been completed and initial trapping experiments have begun.

As arranged for these experiments, the beam tube was 34 ft long from ion source to burial-chamber target. The ion source was 16 ft from the axis of the mirror machine. The beam was collimated by a system of apertures to 0.8×2.5 in. The vertical half-angle at full width of the beam was 8.6 milliradians, and the horizontal half-angle at full width was 30 mr. Beam-intensity profile measurements have not been made under these conditions. During the trapping experiments, the transmitted beam of 20-keV H^0 atoms was 40 mA (equivalent), or approximately 1.8×10^{16} atoms/cm^2 sec.

The interior of the mirror-machine chamber was coated with evaporated molybdenum, so that a very large fraction of the surface area was covered. For the lowest base pressures and maximum pumping speed, the walls in the trapping region were cooled to liquid nitrogen temperature. Base pressures were about 3.5×10^{-10} mm Hg. With the beam traversing the chamber, the pressure increase was 4.8×10^{-9} mm Hg. This number includes a gauge calibration for hydrogen gas, and a thermomolecular correction because the gauge operated at room temperature.

The estimate of local gas density in the trapping region must include the molecular streaming from the beam-neutralizing gas cell. This was measured by means of the movable ionization gauge shown in Fig. I-5, when this gauge was located within the beam volume. With a typical operating pressure of 1 micron of water vapor in the gas cell (and without the fast atom beam) the streaming density was equivalent to 2.3×10^{-9} mm Hg. Although the calibration factor of this gauge for water is not known, work at this Laboratory on other gauges indicates a value of about unity.[1] In addition it is known that the charge-transfer cross section for protons in water vapor is about the same as in hydrogen,[2] so that the gauge reading can be used directly as an equivalent hydrogen pressure.

Unfortunately, two gasket leaks were encountered when the magnetic coils were cooled to liquid nitrogen temperature, raising the base pressure to 2.7×10^{-9} mm Hg. During operation, therefore, the total equivalent pressure in the trapping region was about 1×10^{-8} mm Hg, or six to ten times what is estimated as necessary for exponential growth of the plasma density. Because of this high pressure, we could expect to achieve a plasma density corresponding to trapping on residual gas, or about $2\times10^{7}/cm^{3}$. This was confirmed by the signal on the fast atom detector (Fig. I-5) when the coils were energized. At a field of 20 kilogauss, the magnet was on for about 10 sec at a time, and the beam was gated on for controlled periods. The secondary electron current of the fast atom detector was 1×10^{-8} A, and if the appropriate geometrical factors, secondary electron coefficient, and neutral gas density are used, the estimate of fast-ion density falls between 2×10^{7} and $1\times10^{8}/cm^{3}$. A more refined analysis of this signal is under way. When the atom beam was gated off, the characteristic decay time of the ion density was measured to be 29 msec. From the pressure estimate, the charge-exchange time is predicted to be 28 msec, which is in reasonable agreement with the direct measurement.

During the next few months we will attempt to achieve a higher plasma density, using a cold plasma as the ionizing medium. In addition, we will attempt to reduce the operating pressure so as to approach an exponentiating condition. Some progress in this endeavor has already been made (see section on Neutralization).

It is interesting to note that no significant contribution to the trapped-ion density is evident as a result of Lorentz ionization of atoms in excited states. Some increase in ion density was expected from this effect, especially in view of the results of Sweetman.[3] One possible explanation (suggested by John Hiskes) of our negative result is a de-excitation of the atoms during the traversal of the fringe field of the mirror magnet, i.e., a Stark shortening of the excited-state lifetimes. Analysis of this aspect of the trapping continues.

---

[1] A. H. Futch, Rev. Sci. Instr. 32, 1263 (1961).

[2] A. H. Futch and C. C. Damm, Charge-Transfer and Ionizing Collisions of Hydrogen Beams with Water Vapor, UCRL-6956-T Abstract, June 1962.

[3] D. R. Sweetman, Nucl. Fusion Suppl. Part I, 279 (1962).

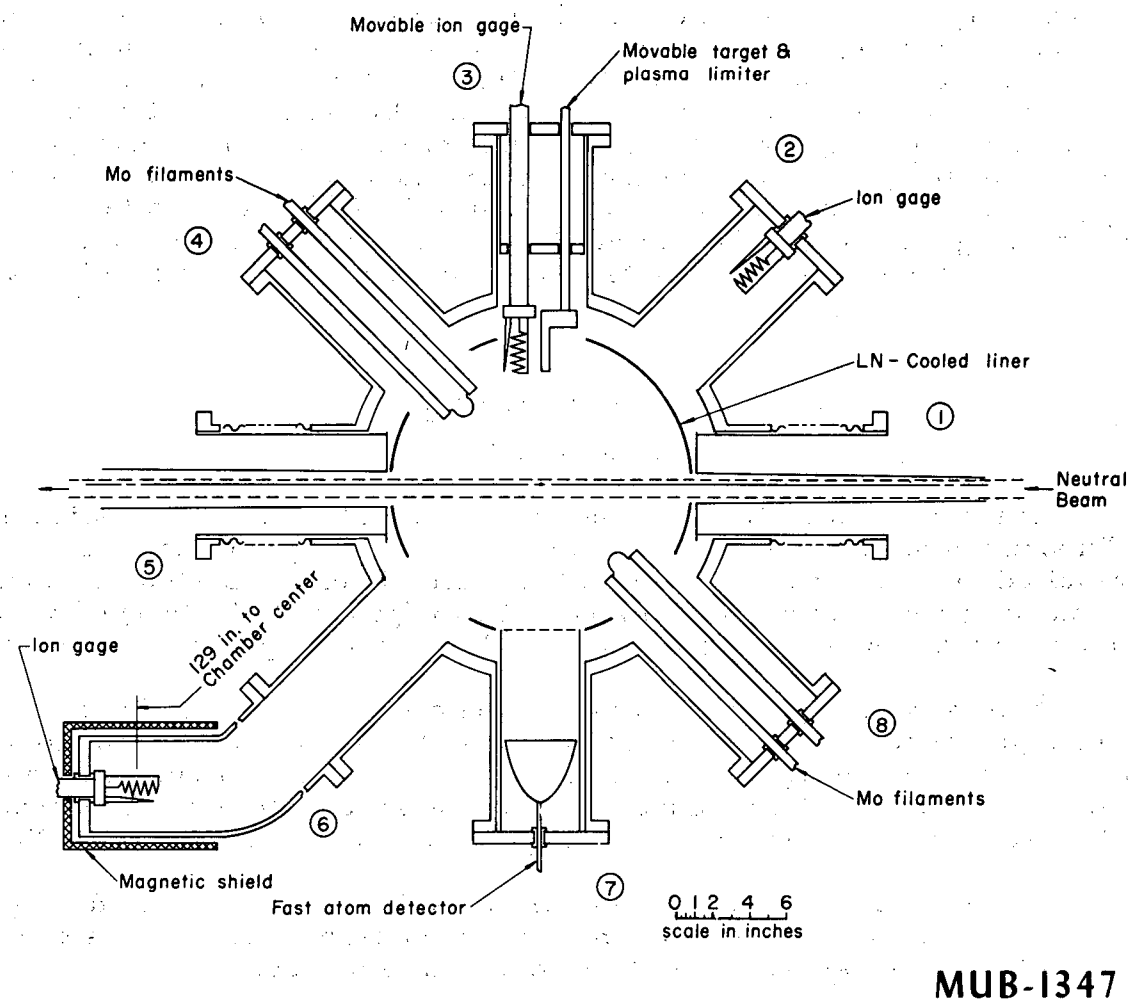

Fig. I-5. Schematic of Alice trapping chamber.

Neutralization

Charles C. Damm

The streaming of molecules from the neutralizer through the trapping chamber results in a local density on axis of the mirror machine which is itself too high to allow exponential plasma density growth. In an effort to reduce this streaming, a molecular beam of water vapor has been introduced, crossing the beam tube approximately 18 in. downstream from the neutralizer. This crossed beam is formed by a grid of tubes 0.025 in. diameter by 0.30 in. long, covering an area of about 1×6 in. Preliminary measurements indicate a reduction in streaming, so that the reading on the movable ionization gauge while it is within the stream is reduced from 2.3×10^{-9} mm Hg to less than 5×10^{-10} mm Hg. It will not be known whether this is a minimum until provision is made for increasing the water vapor pressure behind the collimating grid.

Ion Source Development

Frank J. Gordon

The more restrictive baffling described in the section on Alice Trapping Experiments, together with an increase in the length of the beam tube, has resulted in a decrease in the total transmitted beam reported previously.[1] These changes result in a beam of about 40 mA (power equivalent) of 20-keV H^0 atoms, and this was the beam intensity during the trapping experiments.

A subsequent reduction in initial beam radius from 3.5 in. to about 3.35 in. together with a source rotation of about 1.5 deg brought the atomic beam up to about 50 mA (power equivalent). Deuterium was run with no other changes in a source which produced 45 mA of atomic hydrogen. It produced 36 mA of atomic deuterium, which is slightly better than would be predicted.

Changing the accelerating slit from carbon to water-cooled copper has recently produced 57 mA of atomic hydrogen beam. This points toward future work on dimensional stability of the source slit system.

---

[1] Charles C. Damm and Frank Gordon, in Controlled Thermonuclear Research Semiannual Report UCRL-9969, Jan. 1962, p. 21.

Trapping with Cold Plasma

James F. Steinhaus

The preceding report covered pressure measurements associated with the occluded gas, cold plasma source, and a partial spectroscopic analysis.[1] In the succeeding period we have completed the spectrographic work, made calorimetric plasma profile and energy measurements, and studied the plasma electron densities with microwave techniques.

The previous spectroscopic observations were made perpendicular to the directed plasma; in recent work observations were made longitudinally down the axis of the mirror magnetic field, looking directly at the source. This provided us with not only species identification, but also Doppler-shift measurements of their velocities. Spectral lines from the plasma column were compared to those born in the bore of the source. A summary of the spectroscopic work appears on page 27 of this report.

The calorimetric measurements were made by using a small thermistor mounted behind a 0.5-in.-long tubular grid containing 190 tubes, each 0.025 in. in diameter. An electromagnet was mounted perpendicularly across the axis of the grid, and its field could be raised to and beyond the point where all charged particles were cut off in the grid. The entire grid-thermistor mechanism could be moved on a radius around the source to permit profile measurements of the particles emerging from the source. The total energy density coming from the source, operated in a 3-kG field at 10 keV and a 200-μsec pulse length, was found to be 1.8 joules. Total energy density was the same, within experimental error, with no magnetic field. Energies measured with this technique allow us to calculate average ion velocities present in the plasma. These calculations appear to be in good agreement with the Doppler-shift measurements. Probe data from time-of-flight measurements will also be analyzed. Velocity data are still being compiled, and it is clear at this point that values will be considerably less than those obtained with the ringing discharge type of operation used by Coensgen et al.[2]

Microwave data were taken by using 10-, 8-, and 3-mm-wavelength equipment. Observed electron densities varied with the pulse-line charging voltage of the source, pulse length, and magnetic field. Densities in excess of 1×10^{14} electrons/cm^3 were observed with the magnetic field on, and curves showing the rate of buildup and decay of plasma as a function of time were obtained for different conditions. These data also indicate the length of time that densities remain above certain levels. Densities in the midplane region were found to be related, but not critically, to the number of firings given a titanium hydride washer, to the pulse-line voltages, and to pulse length, as well as to the on-axis positions of the source relative to the mirror.

Using 8-mm and 3-mm microwave gear simultaneously, and measuring their transmission and interferometer patterns, we derived an estimate of the plasma diameter and spatial distributions.

Some small holes were observed in some of the plasma shots which have prompted us to consider making some fast framing and streak photographs of its behavior. Preparations for these measurements are under way.

---

[1] James F. Steinhaus and Charles C. Damm, in Controlled Thermonuclear Research Semiannual Report UCRL-9969, Jan. 1962, p. 25.

[2] F. Coensgen, W. Cummins, and A. Sherman, Toy Top Plasma Injector, UCRL-5603-T, May 28, 1959.

The cold-plasma trapping scheme for the Alice machine has been assembled in place, but not yet fired with Alice in operation.

The following people have assisted in this experiment: Norman L. Oleson, overall data analysis, William L. Barr, spectrographic measurements, and Ronald Hawke and Charles Wharton with the microwave measurements.

Alice Diagnostics

James H. Foote and Archer H. Futch

Fast-Atom Detector Calibration

Before our fast-atom detector[1] was placed in the Alice trapping chamber, we checked its operation and performed an initial calibration. The ion source and west arm of the "Diagnostic Development and Testing" area equipment were used for this purpose. The calibration permits us to quote probably upper limits for the effective secondary-electron emission coefficient (δ) for hydrogen and deuterium atoms incident upon the detector. We need to know the effective δ because we obtain the flux of fast atoms from Alice at the detector by observing the current flow necessary to replace the emitted secondary electrons. Measurements of δ were made in the energy range 10 to 30 keV. At 20 keV, the energy presently being used in Alice, we found, for the given experimental setup, $\delta \approx 4.5$ for H^0 and $\delta \approx 3.9$ for D^0. Because the pressure in Alice is lower than in the calibration setup, and the surfaces are cleaner, the coefficient δ is expected to be lower under actual operating conditions.[2] The cleaner conditions of Alice may well reduce the values of δ by a factor of two below those quoted here. However, we feel that knowledge of δ to within this uncertainty is satisfactory at this time. If deemed desirable later, we can make further calibration measurements with a cleaner system.

Low-Current Source

The low-current source described in an earlier report[3] has been modified. This current source consists of an evacuated glass tube with an electron gun sealed into one end and a metal collector plate sealed into the other. The electrons striking the plate are drained off to the external circuitry, thus providing a current flow from an isolated target--a situation similar to the fast-atom detector. We have extended the usefulness of this current source by placing a band of conducting material inside the glass tube, near the collector plate. An electrical lead to the band allows one to bias it positive when desired, thus collecting secondary electrons when the plate is bombarded by the electron beam. By using a plate surface with a high secondary-electron emission coefficient, we can obtain a net flow of electrons to the plate along its electrical lead. Removal of the positive bias from the band reverses this electron flow. Thus we can now obtain both directions of current flow along the plate lead, making this low-current source more versatile than before.

---

[1] This detector was briefly discussed by J. H. Foote and C. C. Damm, in Controlled Thermonuclear Research Quarterly Report, UCRL-9598, March 1961, p. 19.

[2] L. N. Large and W. S. Whitlock, Proc. Phys. Soc. (London) 79, 148 (1962).

[3] J. H. Foote and C. C. Damm, in Controlled Thermonuclear Research Quarterly Report, UCRL-9777, Aug. 1961, p. 20.

Fast-Atom Detector Electronics

The low-current source just discussed has been used to test electronics associated with the fast-atom detector. As mentioned in an earlier report,[3] a square-wave signal can be obtained from this current source by modulating the grid of the electron gun with a similar signal. With this square-wave output, we were able to examine, at low current levels, response times of several amplifiers. Other amplifier characteristics investigated were noise and saturation levels. Also, we checked recovery times of certain amplifiers and oscilloscope preamplifiers after they had been saturated with excessively strong input signals, in preparation for possible future electronic applications. The amplifier selected for initial use was a Keithley 414 Micro-Microammeter. Its characteristics appeared suitable for beginning Alice operation.

Scintillation Counter for Low-Energy Particles

Considerable improvement in the detection of low-energy particles with a CsI(Tl) scintillation counter has been made by the substitution of a low-noise EMI 6255S photomultiplier tube for the RCA-6810 tube used previously. Figure I-6 shows the pulse-height distribution obtained with a counter consisting of a 1.5-in.-diameter CsI(Tl) crystal mounted directly on the face of a 6255S photomultiplier tube with Dow-Corning high-viscosity silicone oil. The pulse-height distribution is for a 26-keV hydrogen atom beam.

The temperature dependence of the counter was determined over the range from 19° C to -39°C. The counter noise was lower by approximately a factor of ten at the lowest temperature. A corresponding increase of about 20% in the pulse height of the detected particle was also observed.

Lorentz Ionization Experiment

Archer H. Futch and Charles C. Damm

With the completion of measurements of charge-exchange and ionization cross section of water vapor, work has been resumed on the Lorentz ionization of neutral hydrogen atoms produced by charge-exchange collisions with various gases. The Faraday cup detector has been replaced by a CsI(Tl) scintillation counter described under "Alice Diagnostics". A flag that may be rotated in front of the neutral atom beam allows measurements to be made of both the ionized component and the total neutral beam with the same scintillation counter. The recently installed von Ardenne source has been operating at an energy as high as 44 keV for this experiment.

Measurements have recently been made of the fraction of neutral atoms in the excited states that may be neutralized by electric fields from 0 to 200 keV/cm. Two gases have been used for neutralizing, water vapor and lithium. A typical curve for water vapor at 37 keV energy is shown in Fig. I-7.

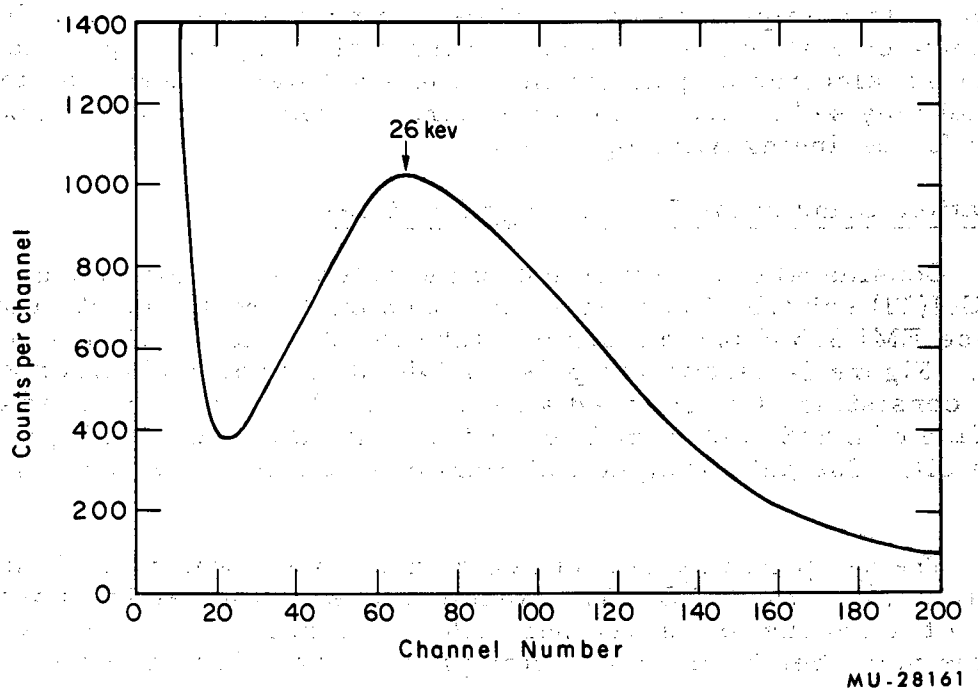

Fig. I-6. Pulse-height spectrum of a 26-keV hydrogen beam from a CsI(Tl) scintillation counter.

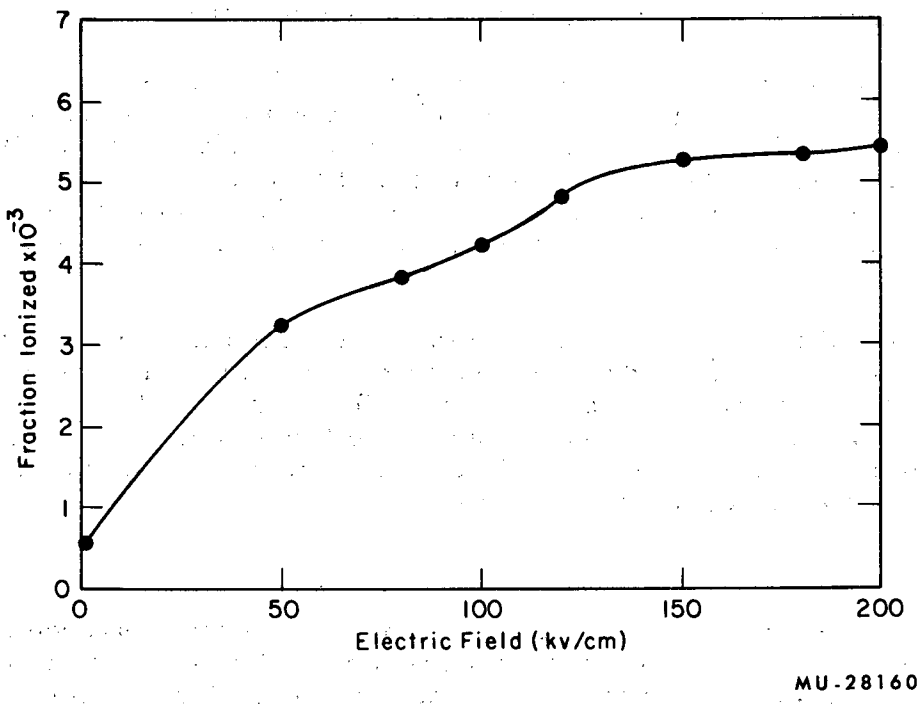

Fig. I-7. Fraction of a 37-keV neutral beam ionized versus electric field.

Vacuum and Surface Studies

Angus L. Hunt and Charles C. Damm

Surface Bombardment Studies

An apparatus has been developed for bombarding a target of representative wall material with beams of hydrogen or deuterium atoms and observing the gas evolved from the surface as a function of the target temperature, the energy and flux density of the bombarding particles, and the composition of the residual gases surrounding the target.

The beam of hydrogen or deuterium atoms enters a target chamber of known volume through an orifice and strikes a target of known temperature. The target-chamber volume includes a mass spectrometer and two ionization gauges. During bombardment, the target chamber is evacuated at a known rate, so that the pressure rise is a measure of the total gas evolved from the target surface, while the mass spectrometer determines the gas composition.

To differentiate the partial-pressure rise due to the bombarding particles from that due to hydrogen contamination, it is convenient to use a deuteron beam rather than a proton beam. The mass spectrometer then monitors the partial pressure of the deuterium in the target chamber as a function of time to distinguish the beam particles from the hydrogen evolved from the surface due to impingement of the beam.

Apparatus

The apparatus consists of a small von Ardenne source followed by a 30 deg bending magnet for mass separation, and an electrostatic lens system. The beam then enters a water-vapor neutralizer. After leaving the neutralizer the beam passes through three stages of differential pumping with collimating orifices between each stage before entering the target chamber. A beam of charged particles can be used, if the water vapor is removed from the neutralizer. The source and electrostatic lens systems are pumped by titanium evaporation. The water vapor neutralizer is pumped by a liquid-nitrogen-trapped system, and the three stages of differential pumping are provided by water-cooled evaporated molybdenum films. The target is pumped by the third stage of differential pumping through the beam orifice. It has been found possible to obtain pressures in the target chamber as low as 10^{-9} mm Hg by baking only the target chamber.

Results

In the first experiments, proton beams of energies 7.5 to 16 keV and current densities of from 1 to 5 $\mu A/cm^2$ were directed normally on a 304 stainless target or a silver target which had been previously baked under vacuum to $400^{\circ}C$ as in the usual bakeout procedure. The ratio of the number of desorbed particles to the number of incident particles was highly variable, and depended on the duration of the bombardment period, but it was not unusual to observe ratios of five. If only the target was heated to about 200° C the ratio could be

reduced to less than unity, but after this target had cooled the ratio of emitted particles to incident particles slowly increased with time. For an unbaked surface the ratio of emitted particles to incident particles exceeded 10. It was evident from these preliminary results that the interaction of energetic particles with the vacuum chamber surface could be an important factor in maintaining plasma purity.

Because of the implications of this result, additional experiments were performed to ascertain the nature of the interaction of the 304 stainless steel surface with a D^+ beam. The use of a charged beam eliminated uncertainties in measuring the total beam current by calorimetry or the secondary-electron-emission method.

The data are consistent with the following qualitative model for protons or deuterons normally incident on a stainless steel surface. The incident particle is not reflected from the surface but is buried within the surface. The thermal spike associated with the loss of kinetic energy within a few thousand angstroms of the surface[1] desorbs loosely bound surface contamination. Under continued bombardment, the increase in the concentration of buried particles results in diffusion of the particles to the surface of the stainless steel, where they desorb as molecular hydrogen or deuterium.

The observations that support this interpretation are as follows:

Initially, the target retains all the incident D^+ beam, with the D_2 in the gas phase increasing only slowly with continued bombardment. The concentration of D_2 in the gas phase increases with target temperature and with beam current. D_2 is desorbed from the stainless steel target between 65°C and 150°C, as the target is rapidly heated after a period of bombardment. The pressure rise that occurs in times less than 10 sec, as measured from the time the D^+ beam initially strikes the target, is due to desorbed contamination and not due to D_2.

The D_2 is accumulated in the bulk of the target, for the cold target surfaces were saturated with a high residual partial pressure of H_2 which would interfere with D_2 adsorption on the surface. Further, more than monolayer amounts of D_2 could be accumulated on a room-temperature target, if it is assumed that 10^{15} molecules/cm^2 constitutes a monolayer surface density. Supporting evidence for the accumulation of D or D_2 in the bulk structure and not on the surface was obtained by measuring the secondary-electron-emission coefficient as a function of the duration of bombardment. The secondary-electron-emission coefficient was independent of the duration of bombardment but not independent of surface contamination, as a higher coefficient was obtained for an aged, cold target.

[1] J. R. Young, J. Appl. Phys. 27, 1 (1956).

5. P-4 (STEADY-STATE PLASMA) SYSTEM

Electron Beam Interaction with the Plasma

William L. Barr, Andrew L. Gardner, and Norman L. Oleson*

One of the aims of the present study is to determine the rate of loss of energy, $-\left|\frac{dE}{dx}\right|$, of an energetic electron beam as it passes lengthwise through the plasma column.

A simple technique for evaluation of the remaining energy of electrons that have traversed some of the plasma consists of measuring the x rays produced when the electrons are allowed to impinge upon a target. Our attempts to employ this method have been only partially successful, however, because the x-ray target (either a "rotating probe" wire or the cathode of the discharge chamber) has been in electrical contact with the plasma, and an accurate determination of the collected current of the electron beam has not been feasible in the presence of the plasma current fluctuations.

The discharge chamber has now been modified to permit a portion of the electron beam to emerge through a small hole (1/16-in. diam) in the cathode after traversing the entire length of the plasma. The pencil of plasma that also emerges (or is created by the "canal rays") is terminated at a biased iron disc located at a magnetic cusp. The energetic electron beam, however, passes through a small (1/4-in. -diam) hole in the disc into a low-pressure region where it may be analyzed. Measurements are now getting underway with this arrangement. Initially the x-ray technique will again be used, although more conventional methods may now be employed and may be needed to resolve questions of energy distribution.

An 8-mm waveguide has been installed at the back of the cathode plate of the discharge chamber to couple to the energetic electron beam as it emerges, but measurements of modulation on the beam have not yet been attempted.

Difficulties have been experienced with the bombarder of the electron gun, which was designed for operation in a sealed-off klystron. Presumably some contamination on the filament shield causes thermionic emission from the shield itself, which results in further heating, and a runaway condition can develop. Modifications are being made in an attempt to relieve this situation.

Plasma Compression

Plans have been made to perform a modest compression on the helium plasma of P-4 (or a hydrogen plasma with some helium present) and to optically follow the heating and plasma motion with the light emitted from He^+.

---

*U. S. Naval Postgraduate School, Monterey, California.

A quartz tube approx 8.5 in. long and 2.5 in. i.d. will enclose the plasma in the compression region for the initial tests. The plasma characteristics before compression, particularly the magnetic-guide field and the neutral pressure, will depend somewhat upon proximity effects of the quartz wall; however, one may expect on the order of 10^{13} ions/cc with approx 8 eV ion temperature in a B_z field of about 1 kG and with a background neutral pressure of 1 or 2×10^{-5} mm Hg. The ion-ion collision time for such a plasma is about 5 μsec.

A small bank (approx 5 kJ) is available which will permit rise times of a few microseconds in a small coil with 3.5 in. between mirrors and a maximum central field of 20 to 40 kG.

Spectroscopy

William L. Barr

A spectroscopic study was made of the plasma ejected from a hydrogen-loaded titanium washer source. This was done to help determine the feasibility of using such a source to supply the cold plasma background in the Alice experiment. The results can be summarized as follows:

(a) The spectra of H, Ti, Ti^{+}, Ti^{++}, Ti^{+++}, O^{+}, O^{++}, Al, Al^{+}, Al^{++}, and Ta were observed.

(b) From a consideration of the ionization and excitation energies involved it is concluded that the mean electron energy both inside the gun and out in the plasma is around 30 eV. Ti^{++++} must also be abundant, but its spectrum is not detected because the maximum electron energy appears to be less than 70 eV.

(c) Doppler shifts in the spectral lines indicate axial velocities that range from 5×10^{5} cm/sec for neutral H to 3×10^{6} cm/sec for Ti^{+++}. Small shifts in the lines of neutral Ti and neutral Al were detected.

(d) From the time dependence of the intensities it is clear that the radiation is a result of excitation by electron collisions rather than recombination.

Other spectroscopic work involved preparation for the beam-plasma interaction and the compression experiments to be done on P-4.

II. ASTRON PROGRAM

1. INTRODUCTION

Nicholas C. Christofilos

The main component of the Astron experimental facility, the electron accelerator, is now approaching completion. It is expected that debugging of the electron gun will start in August. The completion of the six accelerator units will follow soon thereafter. The progress of the accelerator construction is described in the Engineering and Technological Development Section.

The E layer electrons are injected intermittently, forming rings of rotating electrons of intensity of several thousand amperes. The injection of each electron bunch or ring in the E layer tank may excite electromagnetic modes in it. The frequency of these modes depends on the geometry of the tank. In order to avoid the excitation of a mode of frequency equal to the Larmor radius of the electrons it is contemplated to form a low-density plasma column along the axis of the tank. For the purpose of studying the rf properties of the E layer tank, a quarter-scale model is now under construction. This model is described in more detail in Section II-2.

The behavior of the E layer is now being studied by Warren Heckrotte and Kelvin Neil. A simplified model of a thin E layer was assumed. Time-dependent solutions of the buildup of the E layer were developed and the electron momentum distribution was calculated. Preliminary results of this study indicate that the E layer, up to a loading factor $\zeta = 1.2$ (i.e., 20% of field reversal), is not subjected to the so-called spontaneous azimuthal magnetic field instabilities. Thus, according to present theoretical work on simplified E layer models, it appears that there is no apparent instability of the E layer within the limits of field reversal as presently contemplated.

2. ASTRON TANK MODEL

William A. Sherwood

Past experience with the 700-keV Astron machine showed that electromagnetic modes excited in the trapping tank by injected electrons overwhelmed monitoring targets, pickup loops, etc., that were being used in the experiments. Suppression of these modes by introducing lossy elements allowed experiments to continue.

It is possible that the same type of trouble will occur in the 5-MeV Astron machine, and it will provide a great saving if this trouble can be anticipated and the most predominant of these modes suppressed in the initial assembly.

Analytic treatment of the entire Astron tank assembly is difficult. The cantilevered stubs are of unequal length and have two diameters. Tank ends--formed by pumping stations--are far from ideal shorts. The cantilever supports constitute unknown impedances, and resistor mounts provide many places for local reflections to be set up. In short, attempts at closed-form solutions of

the field equations fail because of the discontinuous boundary conditions. Section-by-section analysis may yet prove fruitful, but can only be approximate. Hence, the Astron tank modes should be measured.

For the purposes of determining (some of) the natural resonant modes of electromagnetic energy propagation in the Astron tank, and finding means to suppress or change the more dominant of these modes, a 1/4-scale model of this tank is being constructed.

The cavity is approximately a combination of two dissimilar quarter-wave stubs with a section of cylindrical guide in between. The size and mechanical design of the model will allow frequent disassembly for experiment with internal structure and mode-suppressor design.

3. PLASMA DIAGNOSTICS

Daryl D. Reagan

The radio-frequency skin-effect apparatus is now operating. To test this equipment, we have a hydrogen discharge in a 1×12-in. pyrex pipe, operating at a pressure near 100 μ, at energy of about 20 joules per pulse. At 150 Mc, for example, one observes conductivities ranging from about 1000 mho/meter down to about 10 mho/meter during a period of about 100 μsec after the pulse.

Another possibility for small sample plasma measurement is being explored. This technique would measure kinetic pressure, nkT, by compressing magnetic fields, which can be generated by a current of a few hundred amperes in a small loop around the plasma to be measured. For $n = 10^{13}$ ions/cm^3, $T = 10^4$ °K, for example, one needs about 20 gauss. One requires, however, a very fast rise time. For a plasma 1 cm in radius, with conductivity 100 mho/meter, one needs a rise time better than 10^{-8} sec so that the field will not penetrate the plasma instead of compressing it. For a first attempt, we have built a triggered air gap, discharging a 50-ohm cable, to produce the pulse. Previous experience has shown that pulse rise times approaching 10^{-8} sec are possible with this kind of gear.

We have purchased a fast image-converter camera, with exposure times down to 10^{-8} sec, which will be useful in observing the compression.

An image splitter, using five photomultipliers, is being built. It will give us another tool for observing plasma motions.

4. ACCELERATOR STATUS

Ross E. Hester

In the last six months most of the emphasis has been on the construction of the Astron accelerator.

Upon receipt of a vacuumtight metal and ceramic accelerating column, 14 in. in diameter, the mechanical assembly of the 720-keV electron gun was completed. The unit has been installed in the pressurized freon tank and the internal electrical connections were individually checked with pulse equipment.

Five of the 48-core 575-keV accelerator units have been assembled, and the sixth unit is under construction.

The Astron requires a very-high-quality high-current beam. At low energies the electrostatic defocusing forces are very large. To compensate for the large defocusing forces the initial beam diameter is 22 cm, and the accelerating column is designed in such a manner that the space charge is compensated by the gradient of the accelerating field.[1] As the beam is accelerated the defocusing force diminishes. The relevant equation of motion for the beam due to space charge forces is

$$m\frac{d^2r}{dt^2} = Ee - B_\theta ev,$$

where E = electrostatic field due to beam charge,

B_θ = self-magnetic field of the beam,

v = electron velocity

m = relativistic electron mass.

In terms of beam parameters this equation becomes

$$m\frac{d^2r}{dt^2} = \frac{Ie}{2\pi rv\epsilon_o} - \frac{I\mu_o}{2\pi r}\, ev,$$

where I = beam current,

r = beam radius (mks units).

This equation may now be written

$$m_o\gamma\frac{d^2r}{dt^2} = \frac{Ie}{2\pi rv\epsilon_o\gamma^2},$$

where $\gamma = \left(1 - \frac{v^2}{c^2}\right)^{-1/2}$

and m_o = electron rest mass.

Therefore, as the beam is accelerated, the diminished space-charge forces allow the beam radius to be reduced by conventional electron optics without loss of beam quality. A system of periodic solenoidal lenses has been designed to accomplish this. Mechanical fabrication of this system is about 90% complete.

[1] N. Christofilos, High-Current Pulsed Electron Accelerator, UCRL-5951-T, June 1960.

5. ASTRON ACCELERATOR BEAM-MONITORING LOOPS

Robert E. Wright

A short section of air dielectric coaxial line was constructed to simulate the Astron beam traveling through a tube. A square pulse of current (200 A) was directed through the line and absorbed in a characteristic terminal resistance. The E and H fields in the air space between the center and outer conductors should approximate those in a tube through which a 200-A pulse of electrons travels.

The behavior of several shapes and sizes of magnetic signal pickup loops was investigated when located in the dielectric region of the coaxial line. Two loops, located on opposite sides of the center conductor, but at the same radius with respect to the axis of the system, yield a signal which is sensitive to a 7 to 10% displacement of the inner conductor from the center line when the loop signals are differentially coupled.

An integrated signal from either loop shows the current passing the loop as a function of time.

6. BEAM ANALYZER

William A. Sherwood

The Astron beam-analyzer magnet has been calibrated for median plane trajectories of 350-, 400-, 500-, 600-, 700-, and 800-keV electrons. The floating-wire method of trajectory simulation was used (see UCID-4476). Six small Faraday cups have been made for measuring relative beam currents on these trajectories. To facilitate analyzer conversion for beam analysis at higher energies, these cups will be positioned on a movable jig plate inside the analyzer target tank.

For maintaining constant performance of gaussmeters used on the beam analyzer and other Astron magnets, a Helmholtz coil set has been built. Relative field strengths on the coil-set axis are accurate to less than ± 0.25% which is more than four times as accurate as our best gaussmeter.

A jig has been made which simultaneously locates a reference flip-coil probe, the analyzer turning and target tanks, and the magnet relative to the accelerator axis.

Beam-analyzer magnet calibrations for higher-energy increments can now be completed less than 20 man-days with trajectory accuracies less than ± 1 cm and estimated energy accuracies of better than 10%.

III. LIVERMORE PINCH PROGRAM

Charles K. Birdsall, Dale H. Birdsall, Stirling A. Colgate, Harold P. Furth, Charles W. Hartman, Charles E. Kuivinen, Ross L. Spoerlein, and Alvin W. Trivelpiece

1. SUMMARY

A complete elementary theory of the finite-conductivity stability problem has now been formulated.[1] This theory predicts three basic types of "resistive" instabilities: a long-wave "tearing" mode, corresponding to break-up of a current layer along current-flow lines; a short-wave "rippling" mode, due to the flow of current across the resistivity gradients of the layer; and a low-β, pressure-driven interchange mode, that grows in spite of finite magnetic shear. The time scale for these modes is set by the resistive-diffusion time τ_r and the hydromagnetic-transit time τ_h of the current layer. For large $S = \tau_r/\tau_h$, the growth of the "tearing" and "rippling" modes is of order $\tau_r^{-3/5}\ \tau_h^{-2/5}$, and that of the pressure-driven mode is of order $\tau_r^{-1/3}\ \tau_h^{-2/3}$.

The predictions of the present theory appear to fit known experimental results far better than do the predictions of the classical infinite-conductivity theory. Now that the basic finite-conductivity theory is known, our efforts to establish close correspondence between experimental and theoretical stability results are being accelerated. Growth times, wall stabilization effects, magnetic-curvature effects, etc., can be predicted and are being checked experimentally. On the other hand, the theory is still somewhat idealized in its present form and needs to be extended in order to achieve satisfactory reliability.

The basic effects of viscosity, thermal conductivity, plasma compressibility, and Joule heating are understood, but the corresponding analysis has not been carried out in full detail. Perhaps the most important inaccuracy of the present theory is in its use of the hydromagnetic approximation. In most of the experiments, the ion gyro-radii are not small compared with typical skin-depth dimensions during instablity growth times. The possible stabilizing effect that results has not been evaluated.

The specific experiments that bear on the "resistive" instability question are:

(a) A hard-core pinch experiment with an outer cusp field, to study the importance of field curvature.

(b) A "triax" or resistive-sheet-pinch experiment to study the "tearing" instability.

(c) A large new hard-core pinch experiment (in construction), with special diagnostic equipment to study the "rippling" and "tearing" modes.

[1] H. P. Furth, J. Killeen, and M. N. Rosenbluth, Hydromagnetic Instabilities of a Plane Resistive Current Layer, submitted to Phys. Fluids (July 1962).

(d) The levitron experiment itself, which is aimed primarily at the question of plasma-containment under such conditions that the infinite-conductivity stability theory is satisfied, and which therefore will provide decisive information on the importance of the "rippling" mode and the pressure-driven "resistive" mode in causing plasma diffusion.

2. CUSP-PINCH EXPERIMENT

Initial experiments with a hard-core pinch and outer cusp field have been reported previously.[2] The object is to study a current layer in a "magnetic trough," where the absolute magnetic field strength is increasing in all directions away from the plasma.

The initial experiments were dominated by gross current filaments emanating from port holes in the cathode. Current filaments appeared simultaneously along the length of the pinch, with nearly zero pitch and no apparent rotation in time. Azimuthal modulation of the total current as high as about 30% was observed. Only partial compensation for cathode ports could be made by the omission of several units from the ring of cathode spark triggers. The particularly strong influence of the cathode on the apparent stability and symmetry of this pinch led to exploration of several cathode types, with a final choice of a radial-fin stainless steel cathode. With the fin cathode, the turbulence could be reduced in amplitude by an order of magnitude, and more useful probe data could be obtained. (The study of cathode-initiated streamers, which in itself has some relevance to the "resistive" instability question, is being pursued further in other experiments.)

Inverse-pinch configurations (B_θ at the rod, 5000 gauss) have been studied with no initial B_θ, as well as with initial forward and reverse $B_{\theta 0}$ (2500 gauss at the rod) in average cusp fields of 3 and 6 kilogauss, and with 100 μ D_2 or He. In regions between cusps, a degree of coupling to the axial field that is comparable to the usual coupling to a pure B_z field is observed for all initial B_θ's. In the cusp regions, with no initial or with forward $B_{\theta 0}$, a current layer is formed near the outer wall, where presumably viscosity and wall mass emission impede the rotational motion. A characteristic B_θ distribution for $B_{\theta 0} = 0$ is shown in Fig. III-1, upper. Typical rotational velocities in the cusp regions, as inferred from Doppler shifts, are 2×10^6 cm/sec. Contact of the current layer with the wall precludes a meaningful assessment of stability for these configurations.

Pinches formed with reversed initial B_θ tend to exhibit high reproducibility. The use of reversed B_θ gives rise to current layers that are well separated from the insulating wall at low cusp fields ($B_z \approx 3$ kG). As the cusp field is increased, wall currents again form, and stability disappears. No Doppler shift is observed for the stable distributions, establishing an upper limit on rotational velocity of about 0.5×10^6 cm/sec.

The remarkable stability of the reverse-B_θ-plus-weak-cusp-field configurations (see Fig. III-1, lower) contrasts with the familiar instability of all

[2] C. K. Birdsall et al., in Controlled Thermonuclear Research Semiannual Report, UCRL-9969, December 1961.

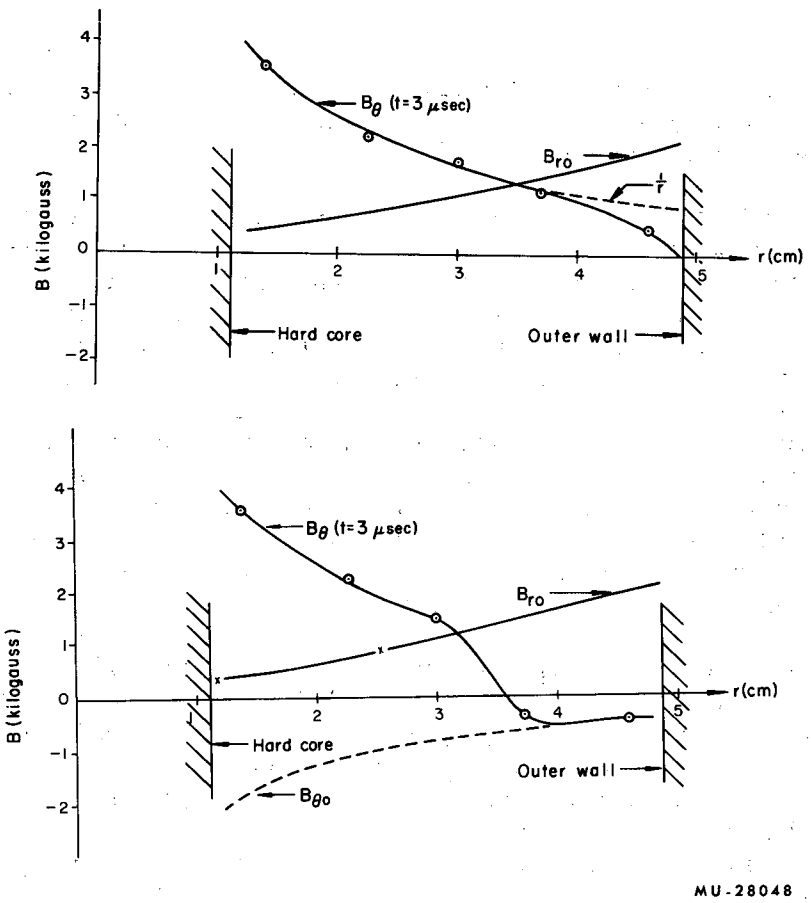

Fig. III-1. Upper: B_θ and initial B_r in cusp region for no initial B_θ, 100 μ D_2, 3 μsec rise time.

Lower: B_θ and initial B_r in cusp region for reverse initial B_θ, 100 μ D_2, 3 μsec rise time.

the reverse-B_θ-plus-B_z configurations.[3] In the present experiment the "cuspiness" of the initial field can be varied continuously from pure B_z to a perfect cusp field, and at the same time the reverse-B_θ discharge is observed to go from substantial instability to apparent quiescence. This phenomenon, which was discovered experimentally, can be explained in terms of the finite-conductivity stability theory. The "rippling" and "tearing' modes, which presumably are responsible for instability in the pure-B_z case, involve displacement of hot plasma outward from the zero-order position. If there is a strong increase of absolute magnetic field strength away from the plasma, as well as a high β, then such plasma displacements give rise to a restoring force which can overcome the driving forces of the rippling and tearing modes. A detailed analysis of this effect is given in Ref. 1.

The cusp field, unlike the pure B_z field, presumably gives rise to some plasma rotation, and this could also be argued to have an influence on the observed stabilization phenomenon.

3. LINEAR HARD-CORE PINCH EXPERIMENTS

A 12-inch hard-core pinch with multiple probe ports and light ports is under construction. The purpose is to get detailed measurements on "resistive" instabilities, particularly those of the rippling and tearing types. The study will be centered on the transition from initial quiescence to turbulence.

A preliminary investigation of the initial growth of pinch instabilities has been made with a 4-inch linear inverse stabilized pinch (using the same facility as the cusp pinch experiment). Thus far, the influence of the electrodes on gross symmetry has been examined with B_θ magnetic loops external to the pinch. The anode is found to have negligible effect on symmetry, while the cathode exerts a dominant influence. Current filaments having the same sense of pitch as the magnetic field are observed to grow simultaneously along the length of the discharge. It is also observed that even during the reproducible initial phase of pinch formation that is indicated by magnetic probes within the plasma the probe signals from the outside loops are already irreproducible. This result is indicative of finite-conductivity effects. Since the pinch is driven from the inside ("unpinch" operation), the outer signals depend on resistive diffusion of field through the plasma.

4. RESISTIVE SHEET PINCH EXPERIMENT

Initial experiments have demonstrated the "tearing" instability of the current layer at D_2 densities above 100 μ. The illustrative Kerr-cell pictures of Fig. III-2 were taken through the screen electrode of the pinch tube. For 10 kV and 300 μ D_2, the current rises in 5 μsec to 200 kA and is then crowbarred, with a 1/e time of 25 μsec. The pictures of Fig. III-2 were taken at 1 and 10.5 μsec after pinch initiation. Initially the discharge is seen to be quite uniform, while after about 10 μsec an asymmetric light distribution takes place.

[3] S. A. Colgate and H. P. Furth, Phys. Fluids 3, 982 (1960).

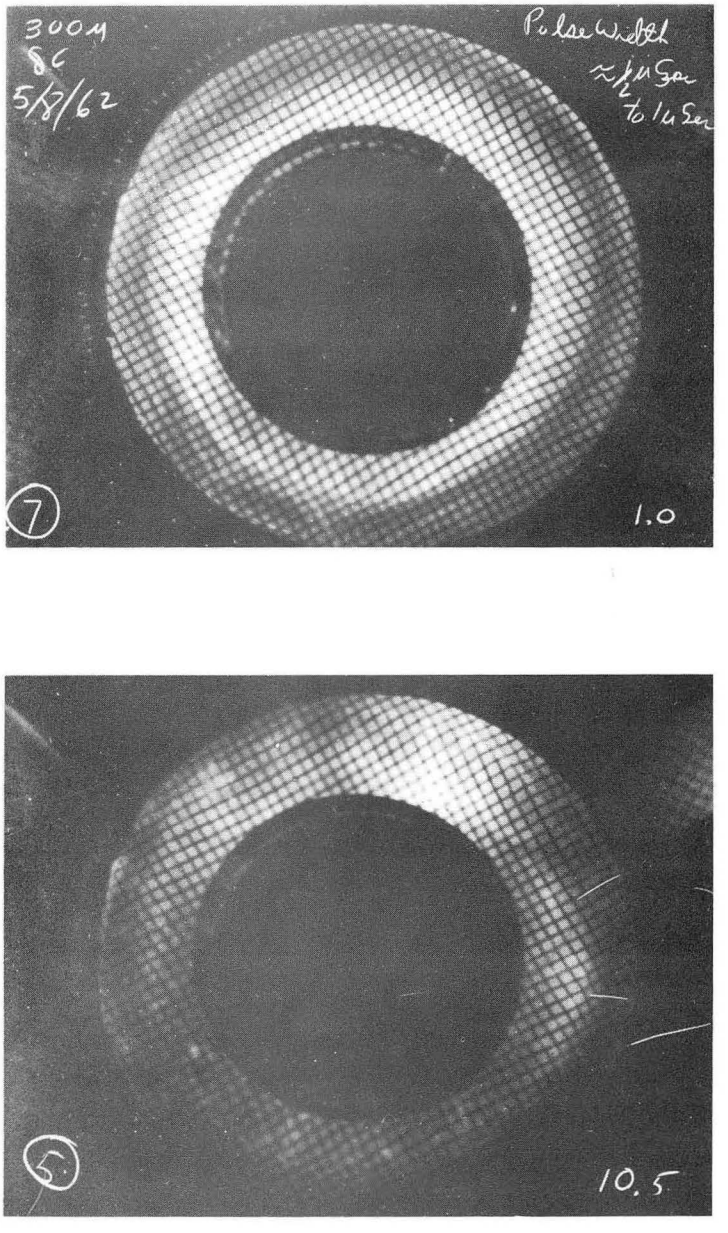

ZN-3257

Fig. III-2. End views of tubular pinch, 300 μ D_2, 10 kv, taken at 1 μsec and 10.5 μsec after initiation.

Measurements with eight magnetic pickup loops placed around the periphery of the tube confirm that the light asymmetry is correlated with current channeling.

At still higher densities, the current channeling becomes more sharply localized, while at densities below 100 μ the discharge remains essentially uniform throughout the pinch time. These results suggest that the observed instability may depend on very-low-temperature effects, such as ionization and Joule heating. In order to demonstrate the type of tearing instability that our theory envisages for a fully ionized plasma of fairly good conductivity, it is desirable to operate below 100 μ. The observed nonoccurrence of the instability in the range below 100 μ may be due to wall stabilization. The discharge may be passing sufficiently close to the inner glass wall and return conductor (see Fig. III-2) so as to fall within the theoretically predicted stable zone. The apparatus has now been modified to center the discharge more accurately and to increase the separation between the return conductors. Further experiments will either permit documentation of the present theoretical predictions or else indicate new stabilizing effects that are not yet taken into account. A second avenue of study will be to extend the present theory to include low-temperature effects, and then to make detailed comparisons with the instability that is already being observed in Fig. III-2.

5. LEVITRON PROGRESS

The levitron has been assembled and preliminary vacuum tests completed. In the initial pumpdown, the liner pressure was 2×10^{-6} mm Hg after 24 hours of pumping. The annular space reached 5×10^{-4} mm Hg in this same period. It is planned to conduct liner bakeout tests and make additional vacuum checks before installing the magnetic-field-generating windings.

Preliminary cryogenic pump tests for the levitron looked encouraging and a final design has been worked out. A liquid-helium-cooled finger trap is inserted into the discharge region for high-speed pumping and then removed transiently during a discharge. This will be assembled and tested in the Mechanical Engineering Laboratory prior to installation on the levitron.

The major delay in reassembling the levitron has been the development of an insulating coating for the main toroidal vacuum and flux-concentrating copper shells. Since this coating must be continuous from inside the annular space (between shell and stainless steel liner) to the outside of the shell, hold 5 kV everywhere (including the vacuum seals at the major and minor coating line), and in addition withstand 1/2 watt/cm^2 radiant heat load in vacuum, the solution has taken considerable time.

Phenolic proved to be unsatisfactory for a shell coating even though in all preliminary testing it looked ideal. One shell was successfully coated but considerable trouble was experienced in coating the second half. It was found that the combination of high temperatures and heat cycling caused hairline cracks to develop in the surface even though adhesion to the copper was relatively good.

Many combinations of coatings were tried, and in almost every case either adhesion was poor owing to oxidation of the copper or else the coating became brittle. The following combination proved satisfactory and was used in the present assembly of the levitron. The copper shell was first sand-blasted and then brush-plated with nickel to prevent oxidation. A phenolic primer was applied, and the remainder of the coating was a new material by DuPont called Pyre ML. This is a polyamide varnish which has superior high-temperature properties and a film strength approaching that of Mylar. The material was brush coated, since this appeared to give more satisfactory results than spraying.

A hollow-cathode-discharge plasma source for the levitron has been constructed and is now under test. The source is to operate in a radial port, injecting plasma radially onto flux surfaces as they are swept inward. A thermionic cathode is used. Pulsed D_2 is injected into the hollow cathode region and a 50 to 100-ampere discharge is formed to a tubular anode. The plasma is allowed to expand to a 1-inch column in the present straight test section. Densities up to $10^{13}/cm^3$ and electron temperatures of roughly 10 to 30 eV have been measured.

6. COLLISIONLESS PLASMA SHOCK (EXPERIMENTAL)

The importance of theoretically predicted plasma-constrastreaming instabilities depends critically on the temperature of the electron-neutralizing background. For the experimental conditions investigated (10^{15} to 10^{16} D^+/cm^3, 1 keV kinetic energy), collisional heating of electrons by the ion streams may provide sufficiently high electron temperature for instabilities to appear, if impurity radiation is unimportant. Magnetic probes have indicated an increase in electron temperature from about 10 eV, for no contrastreaming, to 20 to 30 eV during contrastreaming. Interpretation of magnetic pressure measurements is made difficult by changes in the shape of the moving plasma charge as well as by the excitation of large-amplitude radial magnetosonic modes. Spectroscopic studies of highly ionized states of C, O, and N are being made, which should provide better temperature estimates.

7. COLLISIONLESS PLASMA SHOCK (THEORETICAL)

Instantaneous pictures of electron and ion phase space (each dot represents a particle) and potential, taken after five ion plasma periods, for the sheet-code electrostatic-shock calculations are shown in Fig. III-3. The shock wave is propagating in the positive direction away from a stationary reflecting wall at $x = 0$. Shocked plasma is at rest, unshocked plasma is streaming with velocity $v_o = -1$ in the negative direction, and the shock velocity is +1. The mass ratio is 10, distance is measured in units of v_o/ω_{pe}, and the ion energy at velocity v_o corresponds to a potential of 5 units, where potential troughs attract electrons. Figure III-3 is taken before thermalization of the contra-streaming shocked plasma has occurred, but illustrates the mechanism that persist at later times.

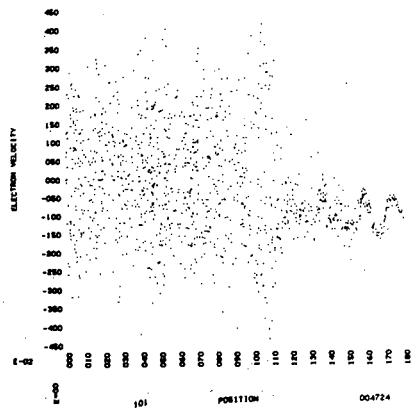

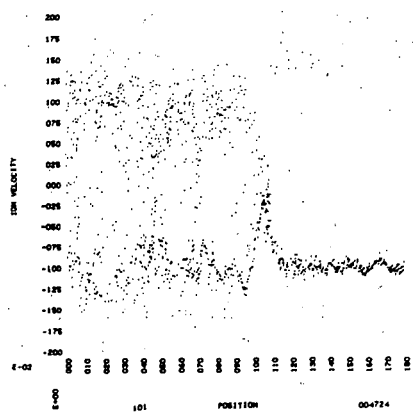

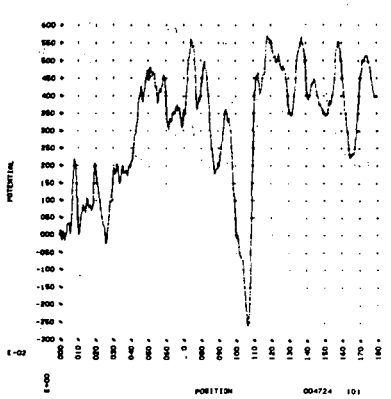

MUBI344

Fig. III-3a. Electron phase space for mass ratio 10 shock calculation, $t = 5\ T_{pi}$.

3b. Ion phase space for mass ratio 10 shock calculation, $t = 5\ T_{pi}$.

3c. Potential for mass ratio 10 shock calculation, $t = 5\ T_{pi}$.

The potential wave for $x > 120$ fluctuates at about the ion plasma frequency and is produced by the excitation of electron plasma oscillations in the incoming plasma by energetic ions of low density. The dominant shock interaction occurs at the primary density gradient of the front. A sheathlike potential well is formed at $x = 107$ by energetic electrons in the shocked region. The incoming ion stream is decelerated to about $1/3\ v_o$ while electrons are accelerated to nearly the ion kinetic energy. Equivalently, the adiabatic compression which heats electrons increases the amplitude of the electron plasma oscillations as well. For $x < 107$ the potential distribution is established by large-amplitude electron oscillations and ion plasma waves, which are maintained by contrastreaming behind the front. Eventual thermalization of the ion distribution occurs after 12 ion plasma wavelengths interpenetration.

Initial mass-ratio-100 calculations could not be carried to complete thermalization of the ion distribution because of limitations of running time and machine storage. Another calculation with 1/3 the sheets per Debye length has been started, and appears not to differ substantially from the initial results.

8. INSTABILITY THEORY

The stability studies for collisionless anisotropic plasmas and sheet pinches that have been previously reported in this section have now been consolidated into an over-all theory.[4]

An approximate analysis has been developed for sheet pinches in which both finite conductivity and finite electron mass are important. (The latter limit corresponds to the collisionless sheet pinch model). For this purpose the dj/dt term in Ohm's law, as well as the ηj term, is used in the analysis of Ref. 1, and the results are modified by replacing $\tilde{\eta}$ by $\tilde{\eta} + p/4\pi n r_e a^2$, where $r_e = e^2/mc^2$. The finite mass becomes important for instability growth rates above $2 \times 10^{-5}\,(nT)^{-3/2}\,\mathrm{sec}^{-1}$, where T is the electron temperature in eV; and the growth rate of the tearing mode then scales like $n^{-3/2}$.

[4] H. P. Furth, A Prevalent Instability of Nonthermal Plasma (UCRL-6907, May 28, 1962), submitted to Phys. Fluids.

IV. BERKELEY PLASMA RESEARCH

1. ROTATING-PLASMA RESEARCH

Klaus Halbach, Robert W. Layman, and G. Donald Paxson

In January 1962 Homopolar V was operational for the first time. The electrode structure of this device, which is shown schematically in Fig. IV-1, is identical with the one used in Homopolar IV device. The improvements over Homopolar IV concern mainly the following points:

(a) Through replacement of all rubber gaskets by specially treated Teflon gaskets and the use of two Vacion pumps, (instead of one) the base pressure could be reduced by a factor of 10, to less than 10^{-7} mm Hg.

(b) The magnetic field coils are more flexible and, owing to stronger construction, they will allow us to go to higher magnetic fields as soon as the 1-megajoule capacitor bank is operational.

(c) A newly designed fast-acting valve proved more reliable than the one used in Homopolar IV.

(d) The cavity that contains the deuterium now has a cylindrical shape and is located in the very center of the apparatus. This insures the azimuthal symmetry of the gas release, which was very sensitive to machining tolerances in the annular cavity used in Homopolar IV. We believe that it is because of this change of the shape of the cavity that practically 100% of the shots with Homopolar V show a backvoltage, whereas only 20 to 30% gave a backvoltage in Homopolar IV.

Figure IV-2 shows typical current and voltage traces obtained with Homopolar V. From the thermonuclear point of view, the most important feature of the voltage trace is that owing to the low-impedance supply circuit, the voltage does not decrease appreciably during the main ionizing discharge. This means that the randomized Larmor energy[1] of the ions in the drift frame at the time the plasma is created must be nearly the same as the organized rotational energy of the ions at that time, provided that the measured voltage does not appear mainly across a thin plasma sheath. It seems, however, that this latter possibility can be ruled out, because (a) both "crowbar" (shorting) experiments and experiments with an inductance in series with the driving capacitor show that the machine reacts like a well-behaved hydromagnetic capacitor and that the angular momentum imparted to the plasma by the radial current can be recovered; (b) the charge going through the machine during the ionization and acceleration phase agrees with the charge calculated from the applied voltage and the equivalent capacity of the hydromagnetic system if it is assumed that the whole plasma participates in the rotation. The highest drift velocity calculated from experimental data on this basis has been 6×10^{7} cm/sec, corresponding to 4 keV ion energy.

The sudden drop of the voltage across the machine to less than 100 volts after 19μsec (Fig. IV-2) is most likely due to an internal short. We

[1] The Larmor energy is randomized in the sense that for every radius the Larmor velocity distribution of the nearly monoenergetic ions in a plane perpendicular to the axis of the system is isotropic, since the ions are formed in a time long compared with the Larmor period.

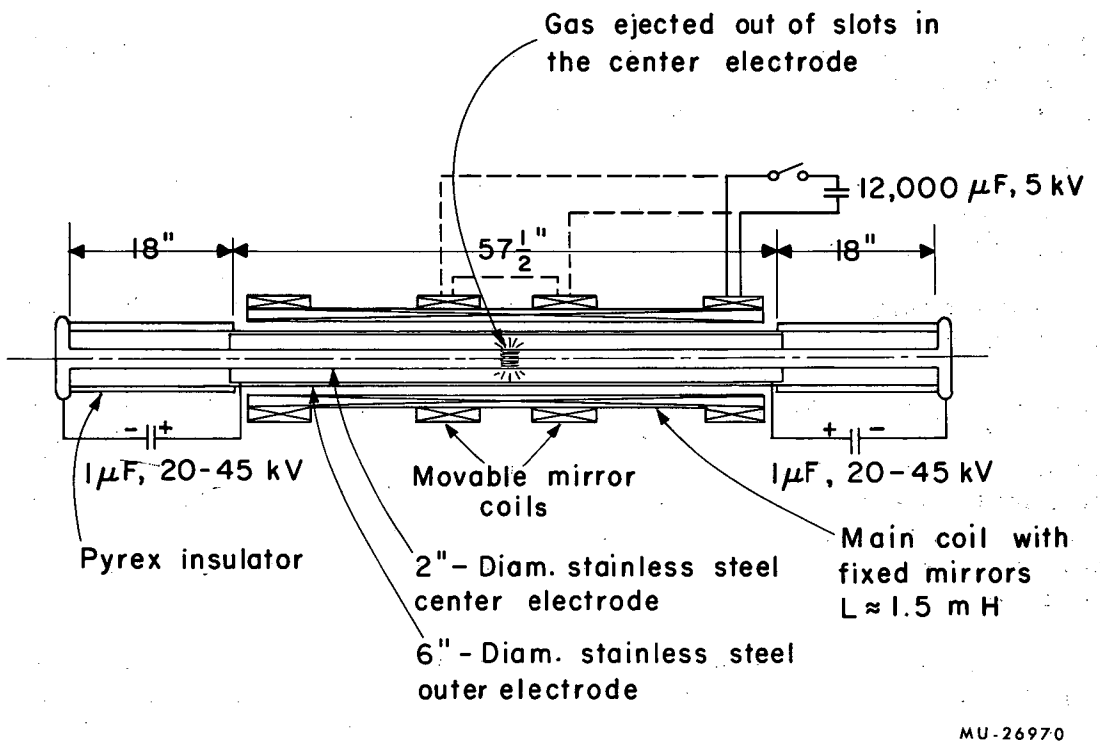

Fig. IV-1. Schematic diagram of Homopolar V device.

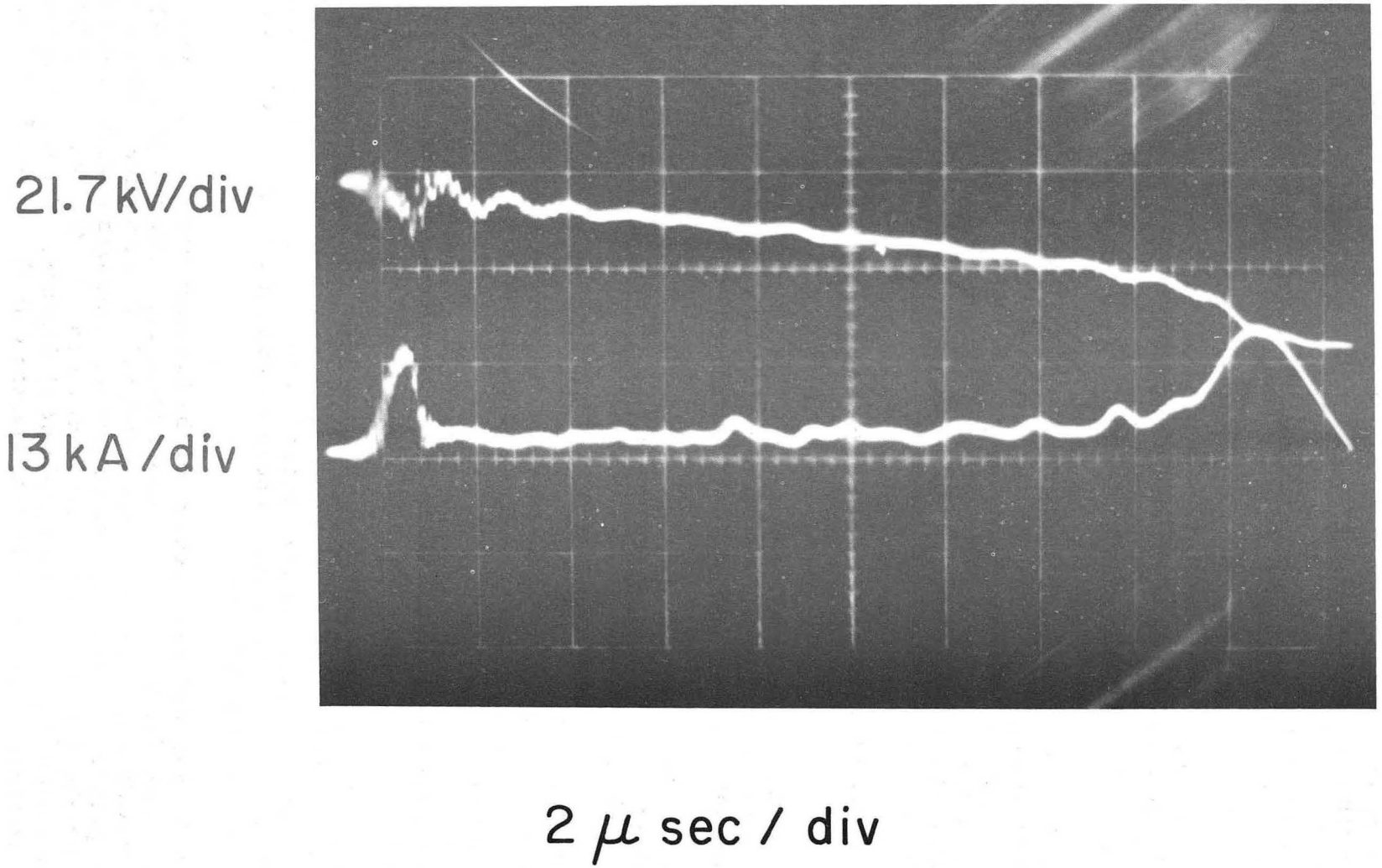

ZN-3262

Fig. IV-2. Oscilloscope trace of Homopolar V current and voltage.

believe that, owing to the heating of the electrons by the ions and the extremely fast thermalization among electrons, electrons escape through the mirrors and establish conductivity between the electrodes along magnetic field lines. The large current that accompanies this drop of the voltage is the discharge current of the external capacitor into this short circuit. The loss of rotation due to this crowbar does not, however, mean that we lose the plasma at this time. Microwave transmission experiments show that the electron density is higher than $10^{13} cm^{-3}$ until the magnetic field drops to 2 to 5 kG, which occurs (depending on the magnetic field configuration) 5 to 9 msec after the discharge took place. It should be noted that the randomized ion energy in the drift frame should not be altered directly by this internal or an external crowbar.

Since the valve releases typically 30 to 50 μl D_2 into the apparatus, the findings described above indicate that we are dealing with a D plasma of 1 to 4 keV randomized ion energy at a density of 10^{14} to 10^{15} ions/cm^3. We therefore investigated the neutron production of this plasma with LiI, Hornyak, and plastic scintillators in conjunction with photomultipliers. The results of these experiments are the following:

(a) There is no detectable neutron production before the onset of the main discharge.

(b) The total neutron production, which has a maximum value of the order of 10^5 neutrons per shot, is not affected when the machine is crowbarred externally after the main discharge current ceases to flow.

(c) Preliminary time-resolved neutron studies show that neutrons are produced for at least 20 μsec after the main discharge current drops to low values, whether or not an external crowbar is applied after that time.

In addition to these methods to detect the occurrence of D-D reactions, we tried to detect the protons that are produced in this reaction by placing a thin plastic scintillator in the vacuum system and observing the scintillations with a photomultiplier. Because of the x-ray and γ background produced by the device, this has been unsuccessful so far, but we hope that we can improve this method enough to obtain useful information. Furthermore, we intend to use a stilbene crystal in conjunction with a photomultiplier and a pulse-shape discriminator circuit, which should allow us to differentiate clearly between scintillations produced by γ's and those by fast neutrons. As soon as the 1-megajoule capacitor bank is completed, we will be able to increase the electric and magnetic field, and if everything goes according to expectations, this will increase the neutron output to the point where we can monitor the neutron production with an activation counter.

To make a direct measurement of the ion velocities, we used two detectors that could detect the fast neutrals resulting from charge exchange between slow neutrals and fast ions. They consisted of a secondary electron emitter and a properly biased electron collector. One was mounted close to the outer electrode, the other at a distance of 60 cm with the connecting line intersecting the outer electrode at an angle of 45 degrees. The detector close to the outer electrode yielded a pulse that started with the onset of the discharge

current and disappeared shortly after the current reached its maximum value. The fact that no neutrals were detected after that time indicates that the plasma is highly ionized as long as there are high-energy ions in the plasma. The second detector showed a signal that was spread in time somewhat and had a time-of-flight delay that indicated a maximum velocity that was in agreement with twice the drift velocity at the outer electrode as calculated from the electrical data.

We are presently testing a neutral detector with a fast-acting valve mounted very close to the point where the neutral detector is attached to the outer electrode. By releasing gas at any desired time and observing the output of the neutral detector, we hope to find out how long the energetic ions are present after the ionization current ceases to flow.

All the experiments mentioned above were performed with a negative center electrode. Preliminary experiments with the opposite polarity resulted in the production of a rotating plasma with the neutron yield reduced by a factor of 15. We intend to study the operation of Homopolar V with this polarity in more detail.

2. HYDROMAGNETIC WAVES AND CYCLOTRON HEATING

Ion Cyclotron Resonance Experiment

Forrest I. Boley, Alan W. DeSilva, Peter R. Forman, and Gordon W. Hamilton

During the period covered by this report the ion cyclotron resonance apparatus has been operated in a form modified somewhat from that described previously. The evidence[1] for the control of turbulence by insertion of a conducting screen perpendicular to the magnetic field at one end of cylindrical plasma devices has prompted the introduction of such a screen into the ion cyclotron resonance apparatus. To allow this modification the slow bank ionizing voltage is applied to the same electrode that supplies the wave-inducing rf field. The opposite end of the tube is thus free to accept the conducting screen, as shown in Fig. IV-3. Some of the wave-field measurements described in earlier reports have been repeated with the screen in place. The radial and axial dependence of the azimuthal wave-field component b_θ has been measured. The results and the corresponding wave energy are presented here.

Introduction of the conducting screen substantially reduced the time dependence of the b_θ wave-field amplitude. This reduction in "hashiness" suggests reduced turbulence associated with the wave propagation, and has allowed measurement of wave amplitude over relatively sharply defined periods of the wave-propagation time. Thus the extensive time averaging used in earlier data reduction was eliminated.

[1] John M. Wilcox, William S. Cooper III, Alan W. DeSilva, George R. Spillman, and Forrest I. Boley, Swirls Produced in a "Crowbarred" Rotating Plasma, UCRL-10010, Jan. 12, 1962.

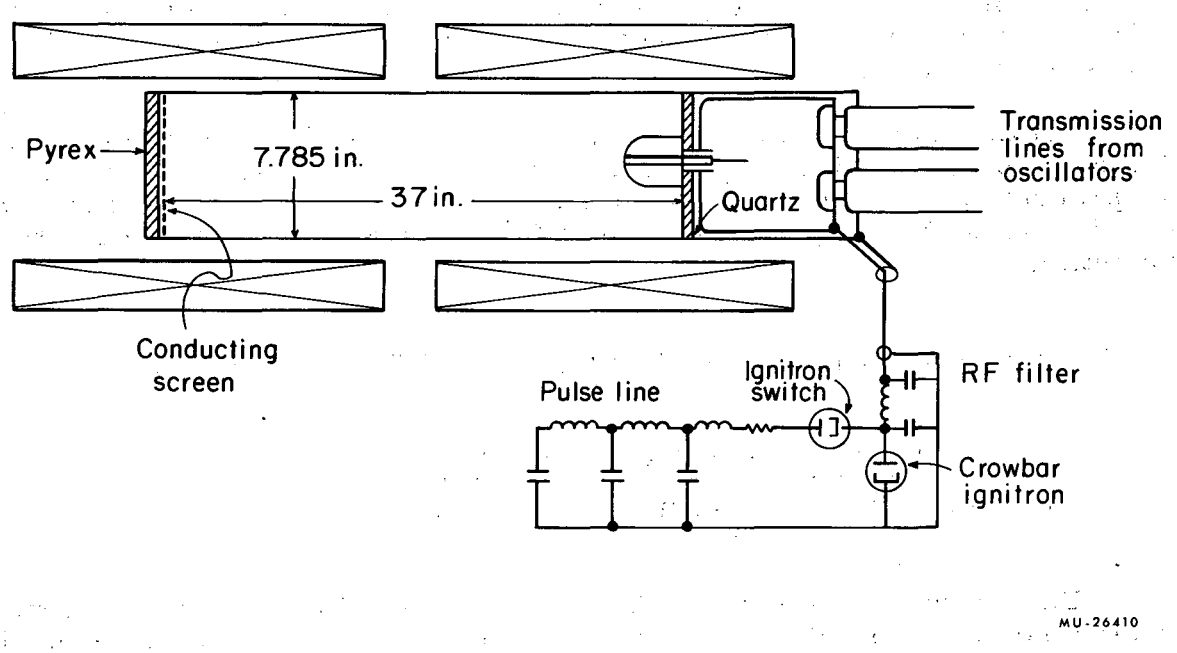

Fig. IV-3. Modified ion cyclotron resonance apparatus with conducting end screen in place.

Application of the 8.3-Mc radial electric field to the coaxial electrodes produces a predominantly torsional hydromagnetic wave in which the azimuthal component b_θ is approximately proportional to $1/r$ at the electrodes. As the wave propagates down the tube, the total wave energy per unit length and hence the wave amplitude is expected to rise owing to the spatially decreasing magnetic mirror field and the consequent drop in wave velocity. The energy per unit volume is only slightly reduced by the increasing cross section of the wave front. As the resonance region is approached, most of the energy of the wave is expected to be converted into thermal energy. Figure IV-4 shows $b_\theta(r)$ at four axial positions 800 μsec after the wave-inducing field is applied. The general behavior of b_θ is as expected.

Figure IV-5 shows in a more detailed manner than Fig. IV-4 the amplitude of b_θ as a function of axial position. These measurements were made at a constant radius midway between the electrodes. A sharp decrease in amplitude near resonance is apparent, as is the slow increase in amplitude with distance from the driving end immediately prior to resonance due to the decrease in wave velocity.

Figure IV-6 gives the b_θ phase shift with z at 800 μsec after application of the wave field. The wave velocity can be obtained from the slope of the data in Fig. IV-6, and this velocity is indicative of the plasma density. At the driving end the density so indicated at 800 μsec is 14% of the initial neutral atom density. This density has not been confirmed by other techniques.

Calculated from the wave-field data presented above, the theoretical ratio of b_r/b_θ, and the wave velocity determined from the phase-shift data, the total wave power is 270 kW. The corresponding total input power from the oscillator at 800 μsec is 550 kW. Thus the efficiency of power transfer from the oscillator into hydromagnetic wave motion is approximately 50%.

It is concluded that a substantial portion of the power from the oscillator can be coupled into torsional hydromagnetic waves in a highly ionized plasma by direct application of an oscillatory radial electric field. These waves propagate in a relatively steep magnetic mirror field to an ion cyclotron resonance region at the mirror center, where at least 90% of the wave energy is lost from the wave.

Spectroscopic measurements designed to measure ion and electron temperature are under way. These observations are to be made at both visible and ultraviolet wavelengths.

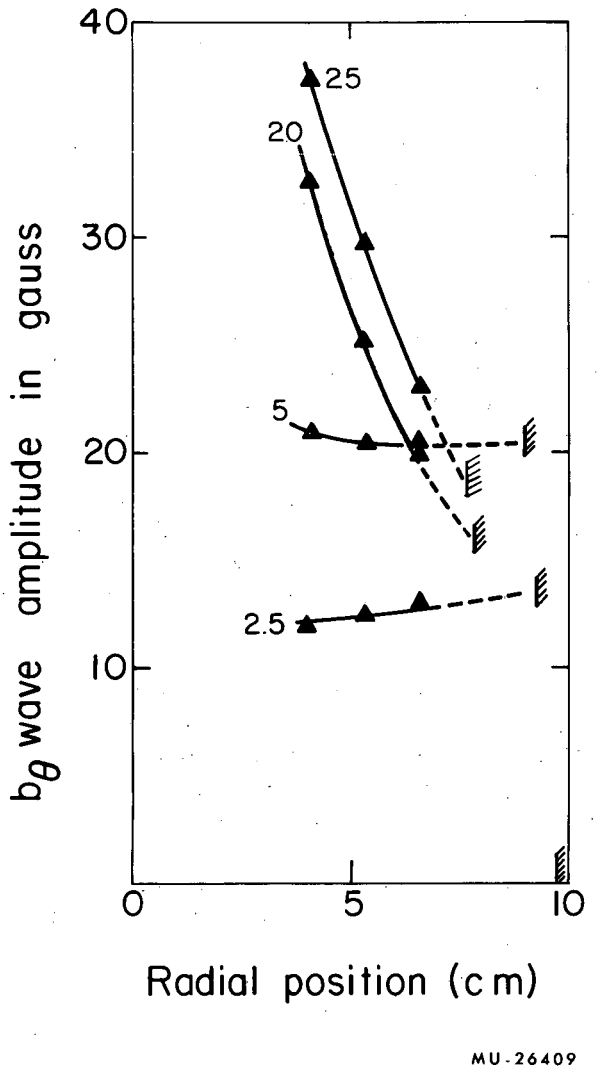

Fig. IV. -4. Azimuthal component of the wave amplitude as a function of radius at four axial positions. Number affixed to each curve is axial distance from midplane in cm.

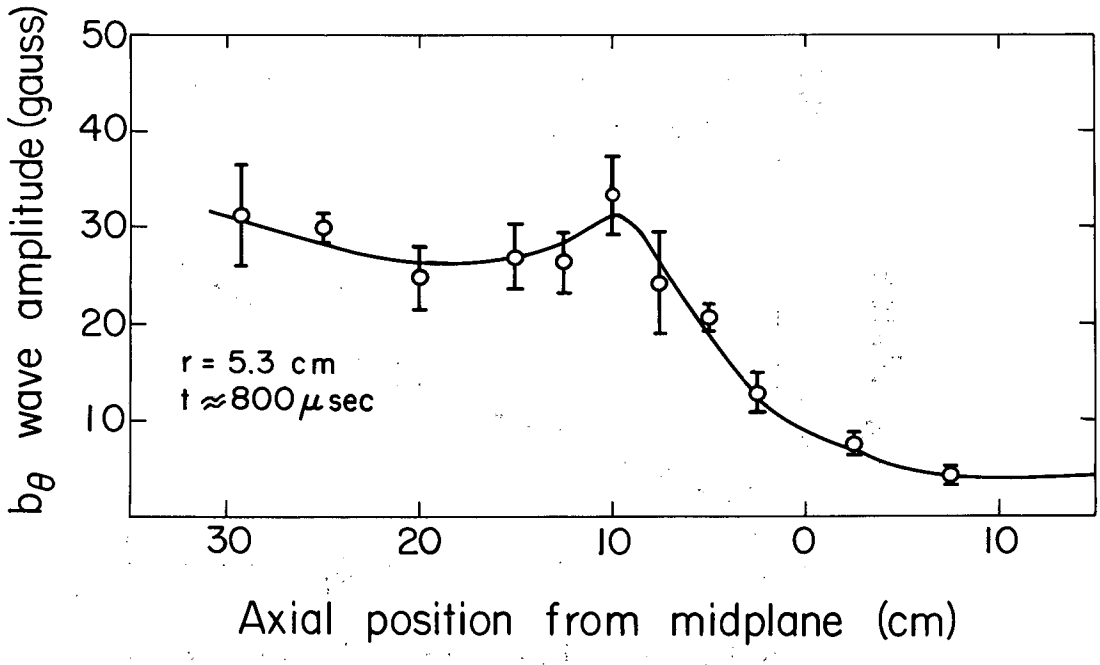

MU-26408

Fig. IV-5. Azimuthal component of the wave amplitude as a function of axial position at a fixed radius.

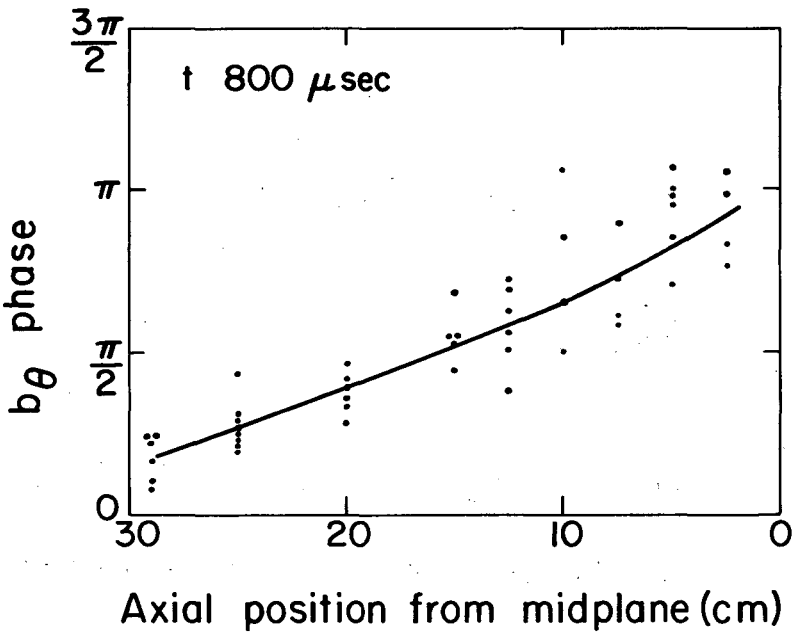

MU-26412

Fig. IV-6. Phase shift of b_θ as a function of axial position at 800 μsec after application of the wave fields.

Plasma Core Device

George R. Spillman* and Forrest I. Boley

The behavior of plasma produced by ionizing fronts of the type discussed by Kunkel and Gross[2] has been described for cylindrical geometries in which conductive containing walls are in close contact with the plasma.[1] A preionizer has been described[3] in which the conducting walls were replaced by Pyrex ones. The related behavior has now been observed when the cylindrical Pyrex confining walls are removed from the immediate vicinity of the plasma. To provide an appropriate geometry for the observations, the inside diameter of the Pyrex portion of the preionizer device was enlarged from 3.0 to 6.0 in. The diameter of the front launching section was thus less than half that of the enlarged Pyrex section.

In the absence of a conducting screen at the end of the Pyrex section the plasma spreads beyond the area of the launching section in a manner shown by the Kerr-cell photograph in Fig. IV-7. A grounded conducting screen placed in the end of the Pyrex tube opposite the driver section was observed to virtually stop the spreading motion and confine the plasma to the cross section of the launcher.

Ion-density measurements were made by observing Stark-broadened H_β line profiles. These measurements were made with a viewing path at an angle to the tube axis so as to exclude light from the launching section. At 40 μsec after initial breakdown and 16 μsec after the electrodes were short-circuited the ion density was observed to be 150% of the initial neutral atom density, thus implying a net influx of neutrals into the plasma region.

Kerr-cell photographs were also taken viewing at an angle to the axis. Such photographs taken with uniform and nonuniform magnetic fields indicated that the plasma was formed within a boundary defined by a flux surface intercepting the outer wall of the launching section.

Polychromator Modification and Data Reduction

George R. Spillman,* Gordon W. Hamilton, William S. Cooper III, and Forrest I. Boley

The polychromator previously described[4] has been modified to provide additional sensitivity and an increase from 9 to 18 channels. Both these modifications increase the utility of the device in examining spectral line profiles. To help provide the increased sensitivity, a long-focal-length

*1st Lt. U. S. Air Force. The opinions expressed by the Air Force author are his own and do not necessarily reflect those of the United States Air Force or of the Department of Defense.

[2] Wulf B. Kunkel and Robert A. Gross, Hydromagnetic Ionizing Fronts, UCRL-9971, Dec. 14, 1961.

[3] In Controlled Thermonuclear Research Semiannual Report, UCRL-9969, Jan. 19, 1962, p. 57.

[4] George R. Spillman, William S. Cooper III, and John M. Wilcox, Nine-Channel Polychromator for Observation of Time-Dependent Spectral Line Profiles, UCRL-9843 Rev., Jan. 22, 1962.

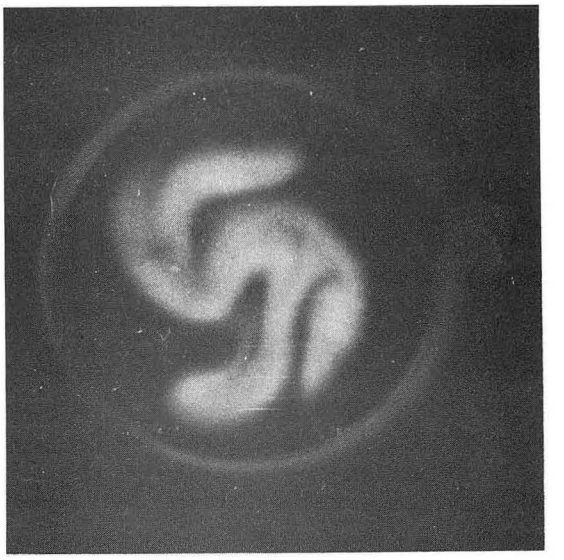

80

ZN-3252

Fig. IV-7. Kerr-cell photograph of plasma core device viewed along the axis 82 μsec after initial breakdown.

cylindrical lens has been used to focus the light in the direction of the slit length, thereby concentrating the light in the center of the light pipes. By use of the focusing lens and modified light pipes the sensitivity of the polychromator has been doubled.

In order to process efficiently the data from the 18-channel polychromator a compueter program has been written by Harold Hanerfeld and Edna Williams of the computing group. This program fits the theoretical Stark-broadened line profiles to the experimental data, using the ion density as a fitting parameter. This program has been run successfully and has been joined to a program written for reduction of polychromator data to line profiles by use of the OSCAR (a scanning machine which punches data into IBM cards). The program takes input data from the OSCAR and produces as output (a) the ion density as a function of time and (b) plots of the experimental line profiles together with their best-fit theoretical profiles.

3. REMARKS ON MAGNETOACOUSTIC WAVES

Wulf B. Kunkel

In connection with the research on hydromagnetic waves of various types that is being carried out at Berkeley it became obvious that we did not have a clear picture of the physical difference between the so-called fast and slow waves of compressible magnetohydrodynamics.[1] The following simple analysis was performed to shed light on the matter.[2]

Our starting point is the familiar set of linearized equations of magnetohydrodynamics of a dissipationless fluid. With the help of either Fourier analysis[3] or the method of characteristics,[1] and by using the continuity equation to eliminate the density as a variable, these are readily transformed into

$$c^2 \mu\rho \mathbf{v} = a^2 \mu\rho (\mathbf{n}\cdot\mathbf{v})\, \mathbf{n} + c\mathbf{B} \times (\mathbf{n} \times \mathbf{b}), \tag{1}$$

$$c\mathbf{b} = \mathbf{n} \times (\mathbf{B} \times \mathbf{v}). \tag{2}$$

Here $\mathbf{v}$ and $\mathbf{b}$ signify the small disturbances of the fluid velocity and of the magnetic induction, respectively. The undisturbed medium is characterized by a density ρ and a speed of ordinary sound a, and is assumed to be permeated by a magnetic field $\mathbf{B}/\mu$. The signals are propagating at speed c in the direction of the wave normal $\mathbf{n}$.

[1] K. O. Friedrichs and H. Kranzer, in Nonlinear Wave Motion, Notes on Magnetohydrodynamics, VIII, U. S. Atomic Energy Commission, New York Operations Office Report NYO-6486, July 1958 (unpublished).

[2] W. B. Kunkel, Phys. Fluids 5 851 (1962).

[3] L. D. Landau and E. M. Lifschitz, Electrodynamics of Continuous Media (Pergamon Press, New York, 1960), p. 219.

For $\mathbf{n}\cdot\mathbf{v} \neq 0$, i.e., in cases of "magnetoacoustic" waves, the coplanarity of $\mathbf{b}$, $\mathbf{v}$, $\mathbf{n}$, and $\mathbf{B}$ can immediately be deduced from (1) and (2). Inspection of these equations also reveals that the mutual orientation of the vectors in question must be of the type sketched in Fig. IV-8 for the domain $\mathbf{n}\cdot\mathbf{B} > 0$ and $\mathbf{b}\cdot\mathbf{B} > 0$. It will be recognized as an interesting physical feature that in fast waves $\mathbf{n}\cdot\mathbf{v}$ and $\mathbf{b}\cdot\mathbf{B}$ have the same sign, but in slow waves they have opposite signs.

A convenient quantitative relation between the direction of $\mathbf{v}$, defined by $\mathbf{v}\cdot\mathbf{B} = vB\cos\phi$, and the direction of propagation $\mathbf{n}$, defined by $\mathbf{n}\cdot\mathbf{B} = B\cdot\cos\theta$ (see Fig. IV-8), is readily obtained if we use elementary vector algebra to eliminate c, $\mathbf{b}$, and $|\mathbf{v}|$ from (1) and (2). One can show, for instance, that $(\mathbf{B}\cdot\mathbf{v})(\mathbf{B}\times\mathbf{v}) = \mu\rho a^2(\mathbf{n}\cdot\mathbf{v})(\mathbf{n}\times\mathbf{v})$. If we introduce the abbreviation $r = \mu\rho a^2/B^2$, this can be written very simply as $\sin 2\phi = r \sin 2(\phi - \theta)$. In terms of the discriminant of magnetoacoustics, defined by $q^2 = r^2 - 2r\cos 2\theta + 1$, the relation between ϕ and θ takes the explicit form

$$\sin 2\phi = (r/q)\sin 2\theta. \tag{3}$$

Since the propagation speed in this notation is given by $c^2 = (1+r+q)B^2/2\mu\rho$, the positive root $q > 0$ obviously refers to the fast wave, while $q < 0$ belongs to the slow wave. At a given angle θ, then, Eq. (3) yields two admissible basic solutions for ϕ which differ by $\pi/2$. Evidently these are the two orthogonal directions labeled $\mathbf{v}_f$ and $\mathbf{v}_s$ in Fig. IV-8.

A plot of ϕ vs θ for various values of r is presented in Fig. IV-9. For $r \gg 1$, the fast wave very clearly approaches pure compression ($\phi = \theta$), whereas for $r \ll 1$, $\mathbf{v}_f$ is transverse to the magnetic field at all values of θ. It is remarkable that for values of r of only 4 and 1/4, respectively, the maximum deviations from these limiting directions amount to only about 7 deg.

The angle ϕ for slow waves is indicated by broken lines in Fig. IV-9. At the point $\theta = \pi/2$, the direction of $\mathbf{v}_s$ changes by π. This occurrence is connected with the fact that both c_s and $\mathbf{n}\cdot\mathbf{v}$ go to zero at this point.[1, 4]

The magnitudes of $\mathbf{v}$ and $\mathbf{b}$ are, of course, uniquely related to each other. After some algebraic manipulation, this relation in terms of q and r is found to be

$$2b^2 = \mu\rho v^2 [1 + (1 - r)/q]. \tag{4}$$

The case $r = 1$ deserves special attention. Equation (4) states that as far as relative amplitudes are concerned, there is no distinction between fast and slow waves under this condition. And in Fig. IV-9 we see that in the directions $\theta = 0$ and $\theta = \pi$ the fast and slow waves are not only indistinguishable but also in a certain sense exchange roles. This is also apparent when $c(\theta)$, for the case of $r = 1$, is shown in a polar plot.[4]

---

[4] J. Bazer and O. Fleischman, Phys. Fluids 2, 366 (1959).

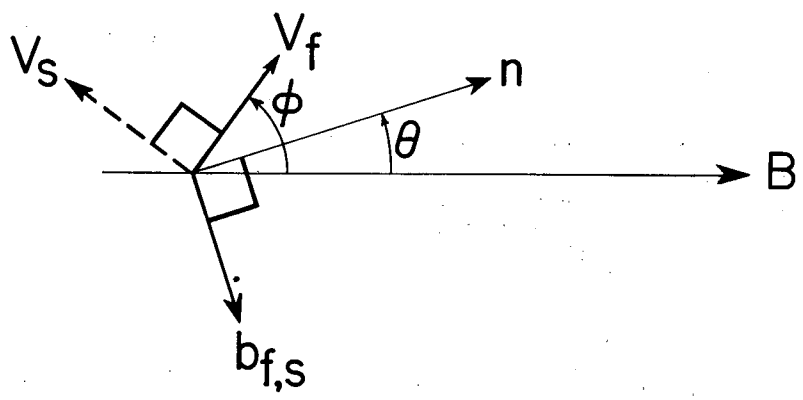

MU-26200

Fig. IV-8. Orientations of the vectors in magnetoacoustic waves.

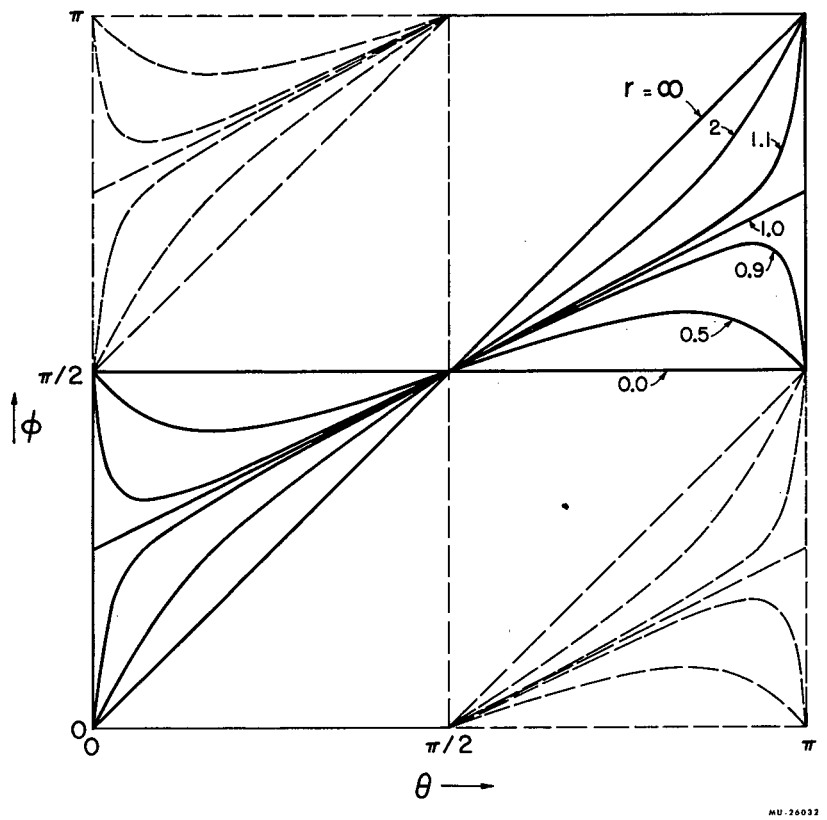

Fig. IV-9. The angle ϕ as function of θ for various values or $r = \mu\rho a^2/B^2$. The solid curves refer to the fast wave, the broken curves to the slow wave.

4. HYDROMAGNETIC IONIZING FRONTS

Arthur R. Sherwood and Wulf B. Kunkel

Construction of the major components of the apparatus for the experimental investigation of hydromagnetic ionizing fronts has been completed.[1] The device has been assembled and vacuum-tested. Dummy load tests of the driving current source have revealed unequal current distribution among the feed cables connecting the current source to the electrodes of the apparatus. As a result the current source has been rebuilt, and further dummy load tests now in progress indicate that the problem has been eliminated.

A probe allowing axial positioning and angular orientation of a search coil has been constructed for investigation of the quasi-static vacuum magnetic field. The probe will be used for calibration of the magnitude of this field, to check that the axis of the field is parallel with the axis of the annular experimental region, and to check the uniformity of the field in the experimental region.

[1]Arthur R. Sherwood and Wulf B. Kunkel, in Controlled Thermonuclear Research Semiannual Report UCRL-9969, January 1962, p. 65.

5. CROSSED-FIELD BREAKDOWN STUDIES

Melvin J. Bernstein, Wulf B. Kunkel, and Gary A. Pearson

Measurements of the formative time lag for crossed-field breakdown in H_2 were reported previously.[1] We have since discovered that the gap widths and voltages used were not sufficiently large to cause "single avalanche breakdown, i.e., the electron crossing times were smaller than the formative time lags. Thus, the attempts to compare with earlier experiments and with theory must include the effects of the electrodes; with this in mind, further experiments should be done.

There is still reason to expect the total current to increase exponentially during the formative time. This has been observed directly by using the electrode arrangement described previously[1] and the circuit shown in Fig. IV-10. The cathode was illuminated with ultraviolet light. The procedure consisted of momentarily closing switch S_1 to bias the gap and draw electrons from the cathode. Then the vacuum relay switch S_2 was closed, which disconnected the power supply from the 1.0-μF capacitor and fired the delay chassis. The two outputs were timed in such a way that the pulse generator was fired about 2 μsec before the hydrogen thyratron. The length of the pulse closing the 2N316A transistor was adjusted to be just long enough to short out the current charging the gap so that the oscilloscope amplifier would not be overloaded. The 1N355R Zener diode kept the voltage rating of the 2N316A triode from being exceeded. The voltage rise time was about 0.5 μsec.

[1]Melvin J. Bernstein and Wulf B. Kunkel, in Controlled Thermonuclear Research Semiannual Report UCRL-9969, Jan. 1962, p. 67.

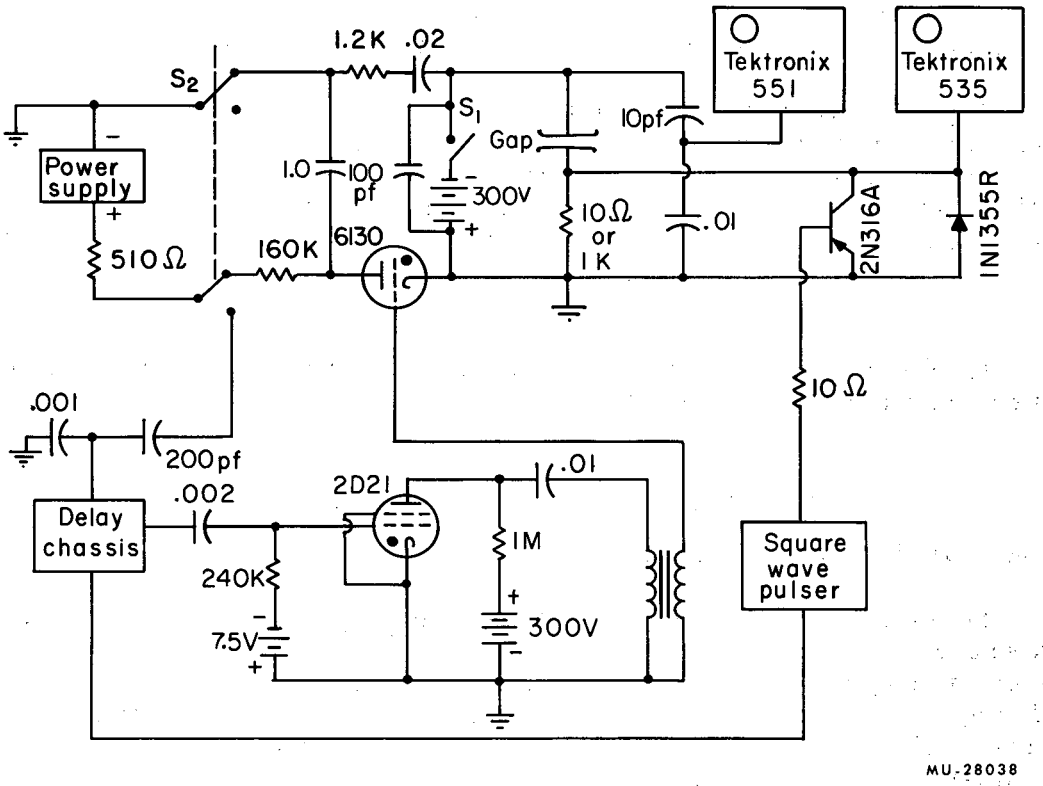

Fig. IV-10. The circuit used to observe the prebreakdown current. Capacitance is in μF unless noted otherwise.

At each setting of physical parameters, three or four shots were photographed at each of nine current sensitivities, which range from 5×10^{-6} to 5×10^{-3} A/cm. The currents obtained from the photographs were plotted as in the example given in Fig. IV-11, using those photographs which corresponded most closely to the average formative time lag. The electrode gap was 0.8 cm, and E, B, and p ranged respectively from 2.0 to 2.9 kV/cm, 8 to 10 kG, and 0.027 to 0.11 mm Hg of H_2. In all cases the current rose exponentially at the smaller currents, but often the rate of current increase fell at anywhere from 20 to 5 mA.

Again, because the breakdown is not "single avalanche," comparison of the measured rate of current increase with theory is difficult. However, by dividing the time for a tenfold increase of current into the formative time lags, it was found that breakdwon corresponded to an increase of the current by a factor of 10^9 to 10^{12}. We had speculated that this factor would be 10^8 to 10^{11}.[1]

6. NUMERICAL CALCULATION OF THE ELECTRON ENERGY DISTRIBUTION IN H_2 AND D_2 IN CROSSED FIELDS FOR LARGE $\omega\tau$

Gary A. Pearson

The numerical computations on the problem outlined previously[1] have been completed on an IBM 7090 computer. The cross sections used, the details of the analysis, and a complete compilation of the results is given elsewhere.[2]

This calculation was made primarily to find the rate of ionization of the gas by electron impact. This problem has recently been studied experimentally by Bernstein,[3, 4] who measured the first Townsend coefficient α, the drift velocity v_E (Bernstein's $V_\perp$) of the electrons parallel to $\vec{E}$, and $D_{||}$, the coefficient for diffusion along $\vec{B}$. For large $\omega\tau$ and low electron density the electron energy distribution $f_0(\epsilon)$ depends only upon the $\vec{E} \times \vec{B}$ drift speed v_d (Bernstein's $V_\perp$ or E/B), and is independent of the gas density n_g and the electron density. The number of electrons and the current thus increase exponentially in time as $\exp(\beta t)$, where β/n_g depends only on v_d. From the definition of α, we see that $\alpha = \beta/v_E$; for large $\omega\tau$, α/B depends only on v_d. Figure IV-12 shows a comparison of the calculated result (Curve 1) with Bernstein's experimental result. The agreement is reasonably good, in view of the large uncertainty in the cross section for electronic excitation. It was found that by increasing this cross section by a factor of 4.7, good agreement is obtained, as shown by Curve 2 in Fig. IV-12.

---

[1] Gary A. Pearson, in Controlled Thermonuclear Research Semiannual Report, UCRL-9969, Jan. 1962, p. 76.

[2] Gary A. Pearson, Electron Energy Distributions and Ionization Rates in Hydrogen with Crossed Electric and Strong Magnetic Fields, UCRL-10366 (in preparation).

[3] Melvin J. Bernstein, Townsend Ionization Coefficient for Hydrogen in a Transverse Strong Magnetic Field (UCRL-10017, Jan. 1962), Phys. Rev. 127, 342 (1962).

[4] Melvin J. Bernstein, Electron Drift and Diffusion Measurements in H_2 and D_2 with Crossed Electric and Strong Magnetic Fields (UCRL-10016, Jan. 1962), Phys. Rev. 127, 335 (1962).

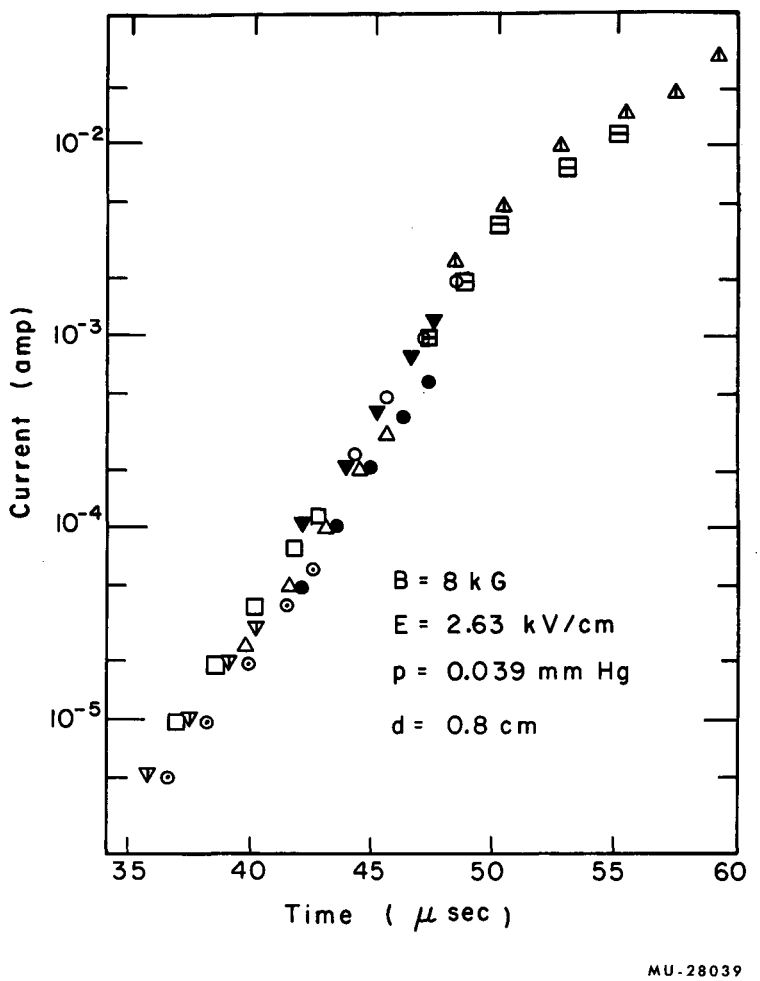

Fig. IV-11. An example of the prebreakdown current in H_2 as a function of time. For these physical parameters the formative time lag was about 64 μsec. Each symbol is a shot at a different sensitivity.

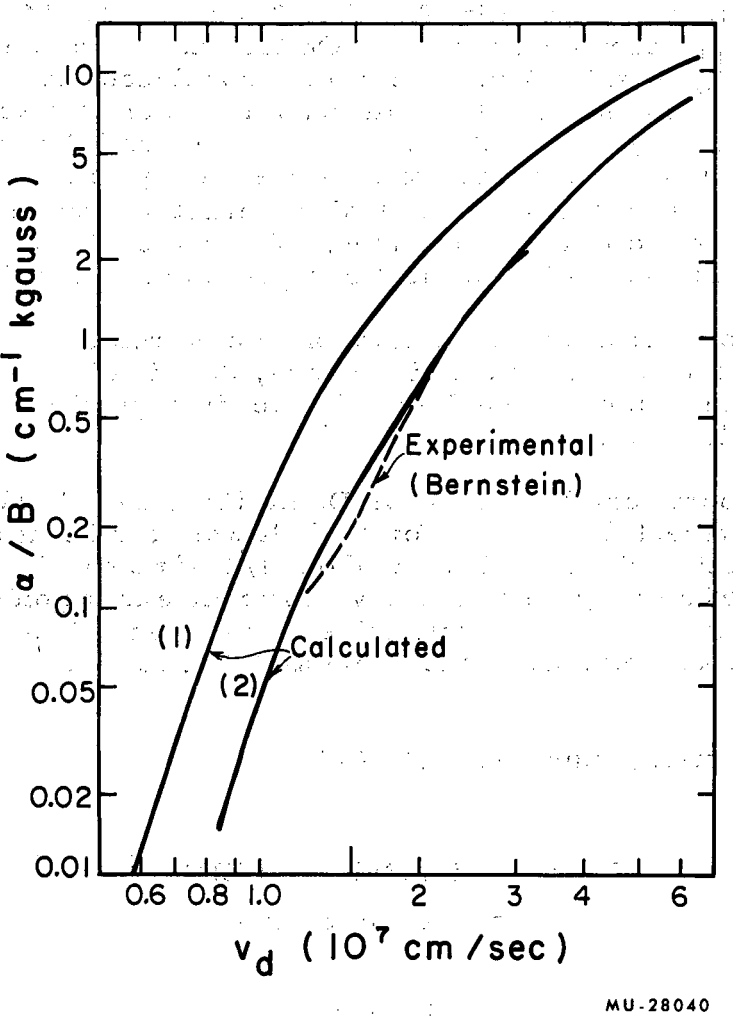

Fig. IV-12. Ratio of the first Townsend coefficient α to the magnetic field B in H_2 as a function of the $\vec{E}\times\vec{B}$ drift speed v_d. Curve 2 was calculated by using a cross section for electronic excitation which was 4.7 times that used in calculating Curve 1.

These results on the ionization rate provide the basis for qualitative predictions of the formative time lag in single-avalanche breakdown. They also provide part of the information necessary to discuss the prebreakdown current and formative time lags observed experimentally by Bernstein.[5]

Comparison of the calculated values of V_E and $D_{||}$ with Bernstein's experimental values are given in Fig. IV-13 and Fig. IV-14. On our model, Bv_E/n_g and $n_g D_{||}$ depend only on v_d. On the basis of an analysis that assumed Maxwellian energy distributions, Bernstein concluded that these experimental results are made consistent only by increasing the elastic scattering cross section by about 10 to 20% for electrons with energies of 0.3 to 4 eV. Such an assumption would also be necessary to improve the agreement shown in Fig. IV-13 and Fig. IV-14. From the same analysis, Bernstein derived the mean energy of the assumed Maxwellian distributions. The comparison of these with the mean energies obtained in the present analysis is shown in Fig. IV-15.

The gross features of the calculated electron energy distributions are quite similar to those of a Maxwellian energy distribution, although the high energy "tails" are somewhat depleted; this tends to justify Bernstein's analysis. A typical example is shown in Fig. IV-16.

The experimental results for D_2 in Figs. IV-13, IV-14, and IV-15 are considerably different from those for H_2. It was found that assuming the energy loss to vibrational excitation of D_2 is about 1/4 of that in H_2 could account for these results. The cross section for vibrational excitation of D_2 has not been investigated. For $\vec{E} \times \vec{B}$ drift velocities above about 10^7 cm/sec, the results for D_2 should be approximately the same as those for H_2.

[5] Melvin J. Bernstein, this report, IV-5.

7. SHEET PINCH STUDIES

Oscar A. Anderson

6×10 Triax

The results of the Triax pinch research will soon be written up for publication. Hence the work done during the past six months is only briefly summarized here.

Flare effects in the Triax, as previously reported, are mostly caused by small particles that crumble from the insulating wall. This annoying phenomenon has been extensively studied in order to find ways to minimize it. Data have been taken on the relative frequency of flares of various locations, both for deuterium and for helium as the working gas. It has been concluded that the insulator deteriorates less rapidly with helium but that the very small particles that cause most of the flares are still almost as numerous.

Two changes were made on the condenser banks, with the object of increasing the peak current while reducing the insulator damage. The bank capacity was increased from 200 μF to 340 μF. Also, small series resistors

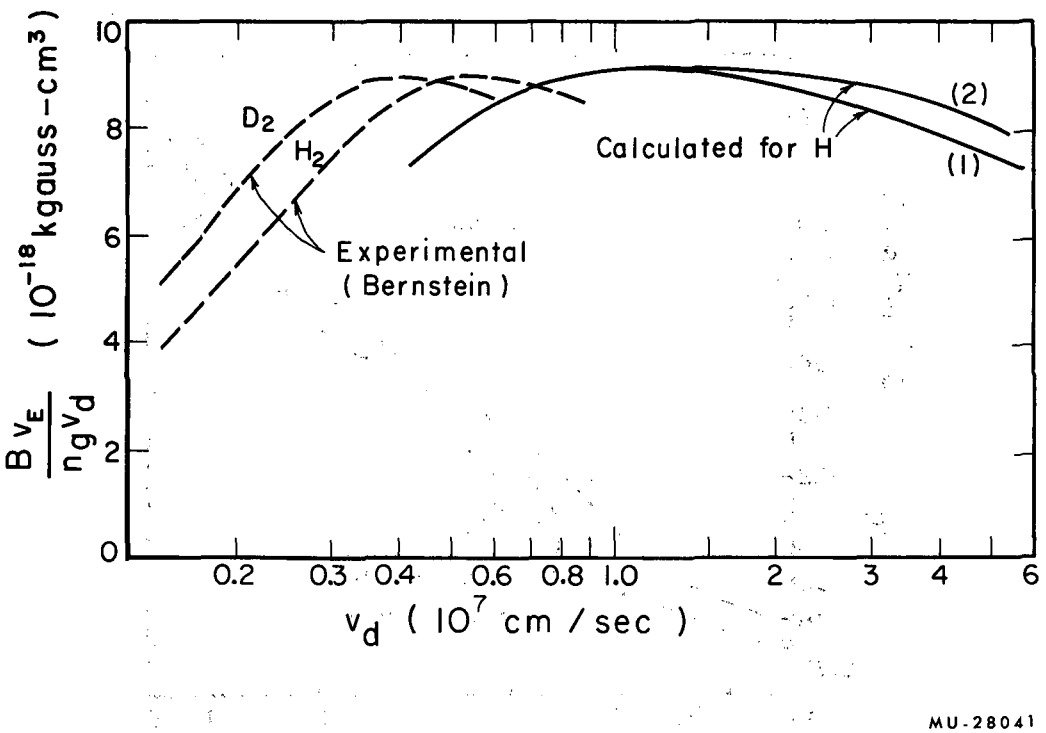

Fig. IV-13. $Bv_E/n_g v_d$ as a function of the $\vec{E}\times\vec{B}$ drift speed v_d, where v_E is the electron drift speed parallel to E, B is the magnetic field strength, and n_g is the gas density. Curve 2 was calculated by using a cross section for electronic excitation which was 4.7 times that used in calculating Curve 1.

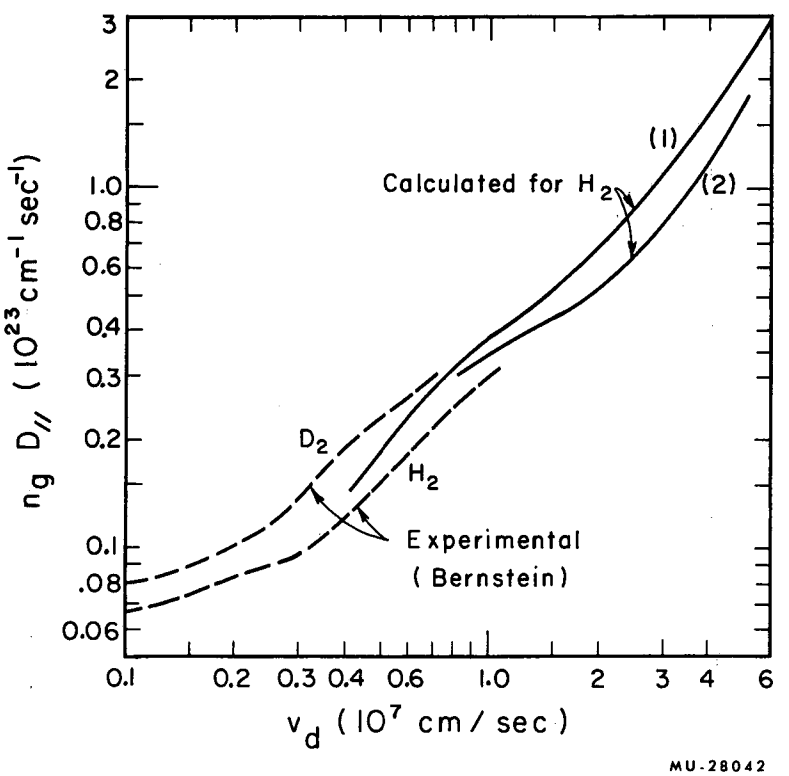

Fig. IV-14. The product of the gas density n_g and $D_{||}$, the coefficient for diffusion for electrons along $\vec{B}$, as a function of the $\vec{E}\times\vec{B}$ drift speed v_d. Curve 2 was calculated using a cross section for electronic excitation which was 4.7 times that used in calculating curve 1.

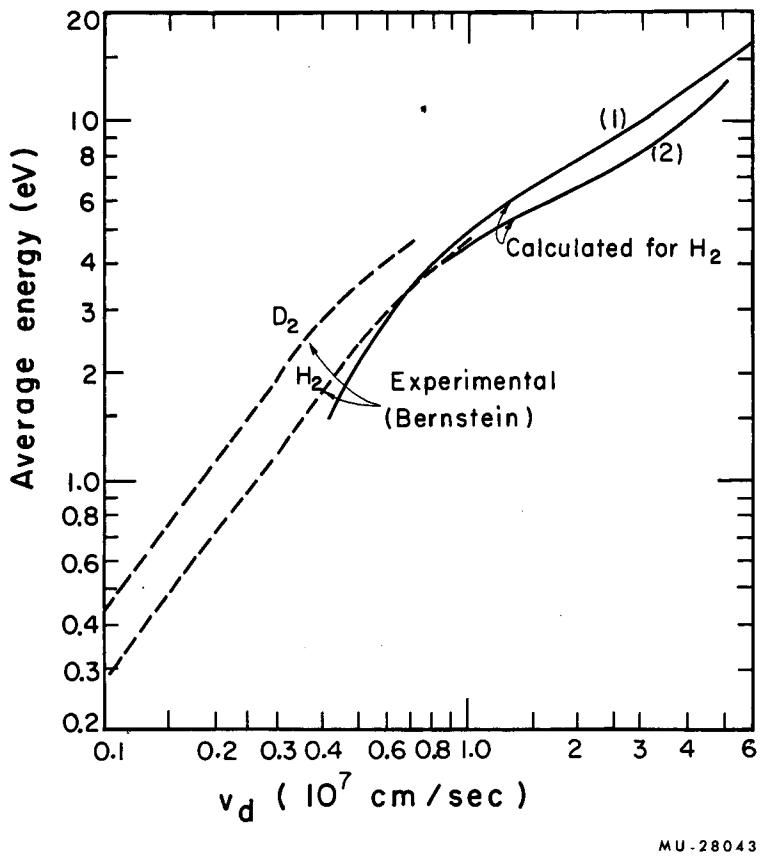

Fig. IV-15. The average energy of the electrons as a function of the $\vec{E}\times\vec{B}$ drift speed v_d. Curve 2 was calculated using a cross section for electronic excitation which was 4.7 times that used in calculating curve 1.

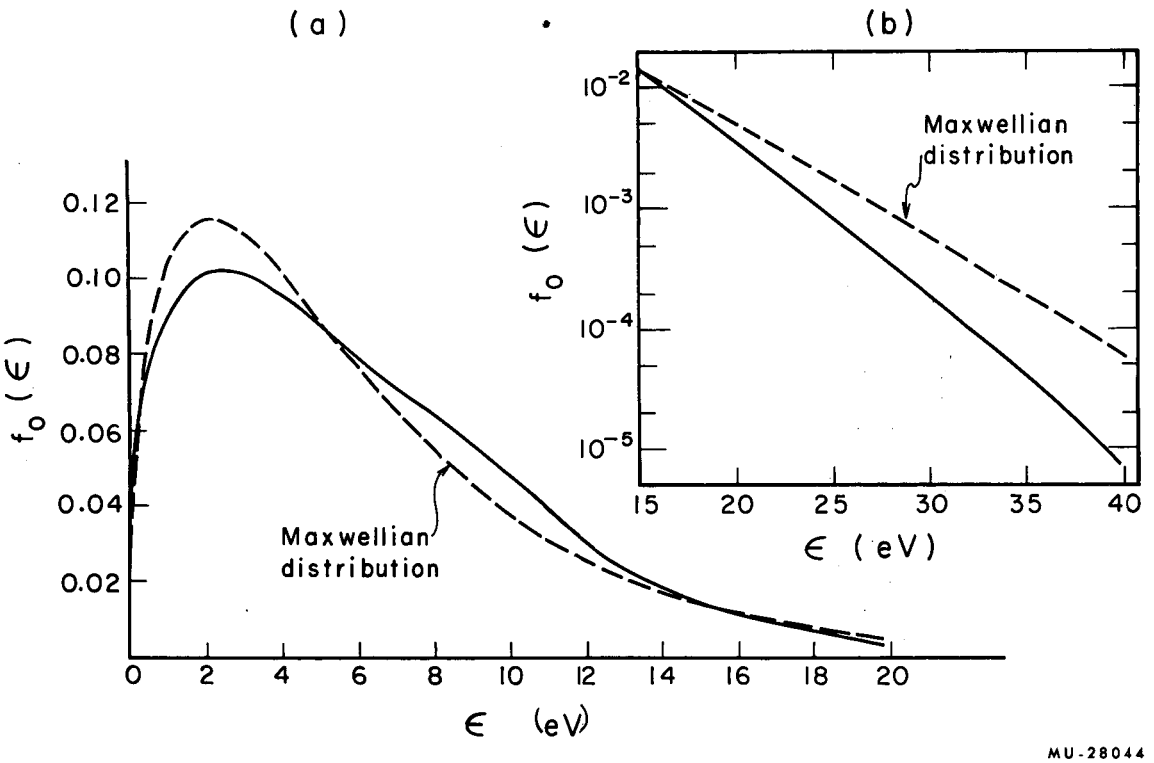

Fig. IV-16. The distribution of electron energy $f_0(\epsilon)$ in H_2 when the $\vec{E}\times\vec{B}$ drift speed is 1.88×10^7 cm/sec. The Maxwellian distribution has the same average energy. Fig. IV-16a shows the distribution of the bulk of the electrons, and Fig. IV-16b is a logarithmic plot showing the details in the "tail" of the distribution.

were installed having about 15% of the value required to critically damp the circuit. Because of the nonlinear nature of the switches and load, these resistors stop the ringing of the condensers much more quickly than would be expected. In spite of the changes in the bank, it was found unnecessary to make any major modifications to the switches, since added capacity and damping resistors have opposite effects on switch performance.[1] The operation is now actually more reliable than before.

High power operation of the Triax is now in progress. Optical, spectroscopic, and neutron-flux measurements are being made, which will be discussed in the forthcoming paper.

Ribbon Pinch

An STL image-converter camera has been used to study the dynamics of the ribbon pinch under fairly high-level conditions. This had been difficult with the Kerr cell because of its poor open-to-closed transmission ratio. The STL camera has the additional advantage of providing three independently adjustable exposures per shot, which can be as short as 5×10^{-9} sec.

These latter features were useful for studying the plasma behavior around the time of most rapid motion, i.e., when the edge collision takes place.[2] It was found that there is no bounce after this collision, unlike the case of compression in the thin direction. Furthermore, the plasma appeared to be confined in the central region for about 1.5 μsec after the edges pinched together. This is consistent with the surprisingly long duration of the neutron burst, previously reported.[2]

A rotating valve has been designed that will open a 1-in. hole in approximately 25 μsec. With this acting as a gate between an aperture in the anode and a separate evacuated chamber, plasma can be axially ejected from the pinch for diagnostic purposes. Use of the ribbon pinch as a source of energetic plasma can also be investigated.[2]

[1] Oscar A. Anderson, in Controlled Thermonuclear Research Quarterly Report, UCRL-9598, March 1961, p. 44.

[2] Oscar A. Anderson, in Controlled Thermonuclear Research Semiannual Report, UCRL-9969, Jan. 1962, p. 81.

8. EXPERIMENTS ON LORENTZ DISSOCIATION AND PARTIALLY IONIZED PLASMA

Klaus H. Berkner, Vincent J. Honey, Robert V. Pyle, Henry F. Rugge, and J. Warren Stearns have contributed in various ways to the following experiments. In addition, Selig N. Kaplan and George A. Paulikas are associated with the detachment and dissociation experiments.

Magnetic Field Detachment and Dissociation of D^-, H^0, and H_2^+

The experiment to observe the detachment of electrons from fast D^- ions in a magnetic field[1] has been completed and the data are partially reduced. For 20-MeV D^- ions the process $D^- \rightarrow D^0 + e^-$ commences at a magnetic field somewhat larger than 80 kG and is complete at about 100 kG. The equivalent electric fields are 3.6×10^6 V/cm and 4.4×10^6 V/cm, respectively. These limits are in agreement with recent calculations by Hiskes;[2] they will be known more precisely after the emulsion scanning is complete. The percentage detachment vs magnetic field for $D^- \rightarrow D^0 + e^-$, and an estimate for the subsequent process $D^0 \rightarrow D^+ + e^-$, will be obtained from the data.

A preliminary experiment to measure the detachment probability, $H^0 \rightarrow H^+ + e^-$, has been carried out at the Hilac, using neutrals obtained by breaking up 20-MeV H_2^+ ions in argon and helium. The detachment produced by the Lorentz force of a magnetic field appears to be quite large--1 to 2% for magnetic fields in the range 6 to 18 kG--but further measurements must be made to establish the reliability of the data. Results of this magnitude might be expected for recent estimates by Hiskes.[2] This technique may be useful for producing neutral beams in the energy range 50 to 100 keV for injection experiments.

Further data on the Lorentz dissociation of H_2^+ from the gas stripping of H_3^+ have been obtained and are being reduced. Brief attempts to produce beams of HeH^+ ions were made by Basil F. Gavin and Kenneth W. Ehlers, using a high-voltage PIG source and a high-current arc source, respectively. No appreciable currents of this ion were observed in either case, although other workers have apparently obtained respectable amounts. We hope to discover the secret and perform magnetic dissociation experiments.

---

[1] In Controlled Thermonuclear Research Semiannual Report, UCRL-9969, Jan. 1962, p. 85.

[2] John R. Hiskes (Lawrence Radiation Laboratory), private communication.

ac Positive Column

The investigation of the macroscopic instability of the positive column of an ac discharge in a longitudinal magnetic field[3] has been continued using sinusoidal and square-wave applied voltages. The growth time of the instability is typically about 100 μsec in the dc case, and should decrease with increasing magnetic field. We have examined discharges in H_2, D_2, He, Ne, and Ar at applied frequencies from 0 to 70 kc and found that the onset of instability is pushed to higher fields with increasing frequency. Although the (m = 1) theory of Kadomtsev and Nedospasov is not specifically applicable to time-dependent discharges, the experimental observation that the critical magnetic fields are closely the same in dc and half-wave-rectified (i. e. unidirectional) high-frequency discharges encourages a comparison between the ac experiments and the dc theory. The effects of higher m-value modes have been calculated and results showing qualitative agreement with theory have been obtained.

At low frequencies, e. g. 1 kc, streak-camera photographs show the development of the spiral instabilities previously observed in the dc case. At very high frequencies, e. g, 30 kc or more, the nature of the instability is not easily discerned from the photographs, which resemble the complex states obtained in the dc case with magnetic fields much greater than the critical field.

Expressions for the radial energy transport in a dc positive column in a very large magnetic field have been developed by Kadomtsev[4] and shown to be completely analogous to turbulent transport in an incompressible fluid. We have examined energy losses and streak photographs of dc discharges at magnetic fields several times greater than critical. The photographs show complex patterns, but in general seem to retain some spiral structure. These studies are only preliminary.

An interesting instability has been observed in a low-pressure Ar dc discharge in a magnetic field. At pressures of about 50 μ, the electron mean free path is long enough that a constricted discharge runs the length of the 2-meter tube. When the magnetic field is raised sufficiently the discharge blows up radially at a point near the anode, the blowup occurring in an axial distance of a few centimeters. As the magnetic field is increased the instability point moves toward the cathode. The nature of this phenomenon has not yet been studied.

---

[3] In Controlled Thermonuclear Research Semiannual Report, UCRL-9969, Jan. 1962, p. 91.

[4] B. B. Kadomtsev, Zh. Tekhn. Fiz. 31, 1273 (1961).

Hollow-Cathode Discharges

The measurements of the absorption of resonance radiation by Sr^+ ions from a hollow-cathode discharge[1] were discontinued while better Fabry-Perot coatings and spacers were being constructed. Good optical resolution is now being obtained and the Sr^+ density and temperature measurement will be continued.

A study of 2- to 50-kc oscillations occurring in the hollow-cathode discharges is in progress. The oscillation frequencies and amplitude show strong dependences on discharge parameters and involve rotation and (or) some other phenomenon, originally thought to be standing ion sound waves because their dependence on electrode spacing was in reasonable agreement with calculations of ion-sound velocities. Recent measurements with multiple probes show, however, that the phases of these oscillations vary in an unexpected way from point to point; they are not understood at present.

9. WAVE PROPAGATION IN HOTHOUSE II--THEORETICAL

David L. Sachs

A study of electromagnetic waves in nonuniform plasma is in progress, including a particular study of the plasma in the cylindrical geometry of Hothouse II.[1] In Hothouse II the axial magnetic field decreases with axial distance to a magnetic beach. Effects of Hall current, finite electron mass, and conductivity are retained in a two-fluid model at zero pressure. Retention of these effects in cylindrical geometry leads to a fourth-order differential equation for the wave fields. The behavior of the wave fields away from the beach and the energy transmission, reflection, and absorption by the beach will be calculated by asymptotic expansion of solutions of the fourth-order scalar differential equation. Previous workers in this field have omitted various effects in order to reduce the wave field equation to two second-order differential equations which are uncoupled or weakly coupled.[2]

---

[1] In Controlled Thermonuclear Research Semiannual Report, UCRL-9969, Jan. 1962, p. 57; and this report, IV. 2.

[2] T. H. Stix, Phys. Fluids 3, 19 (1960).

10. THE STEADY-STATE REFLECTION OF A STREAMING PLASMA BY A MAGNETIC FIELD

Alan Macmahon

Rosenbluth[1] and Beard[2] have discussed the steady-state reflection of a streaming plasma by a magnetic field. Rosenbluth considers only the case in which the streaming plasma is incident normally on a plane boundary. Beard treats arbitrary angles of incidence. Both make the approximation of quasi charge neutrality and neglect the ion current. This calculation has been carried out in the quasi-neutral approximation for arbitrary directions of incidence with the ion current included. One interesting result, which is a consequence of the charge-neutrality approximation, is that the magnetic-field profile is independent of the component of plasma velocity parallel to the boundary. In general, there is an electric field outside the plasma and normal to the plasma surface. This field may cause long-wavelength instabilities similar to those found by Northrop in the MHD approximation.[3]

---

[1] M. N. Rosenbluth, Infinite Conductivitity Theory of the Pinch, Los Alamos Scientific Laboratory Report LA-1850, Oct. 1954.

[2] David B. Beard, J. Geophys. Research 65, 3559 (1960).

[3] T. G. Northrop, Phys. Rev. 103, 1150 (1956).

V. THEORETICAL AND BASIC EXPERIMENTAL PLASMA PHYSICS

1. A SELF-CONSISTENT DISTRIBUTION OF ELECTRONS IN THE ASTRON E LAYER

Warren Heckrotte and V. Kelvin Neil

It has been possible, within certain rather good approximations, to calculate a steady-state, self-consistent distribution of electrons that possesses the properties desired in the Astron E layer. This work is reported in detail elsewhere.[1] The cylindrical layer is assumed to have zero radial extent and to be neutralized by stationary positive ions. All electrons have the same canonical angular momentum and are sufficiently relativistic that the rest energy may be neglected in comparison with the kinetic energy. Boundary conditions on the magnetic self-field are such that the self-flux of the layer is confined to the E layer region of the axis. The problem of providing the external field necessary to insure the desired layer properties is defined but not solved. The model used is stable against the axial bunching instability.[2] It is also stable against B_θ instability if the self-magnetic field is less than 1.2 times the externally applied field.[3]

At the time UCRL-6942 was written it was thought that by varying the total number of electrons in the model one approximated the distribution of particles at different stages of the layer's formation. However, it is now apparent that increasing the number of particles in the model in fact increases the density of particles in axial phase space. Since this is impossible, we conclude that, although our model may be valid during some stage of the build-up process, the time-dependent problem is yet to be solved.

---

[1] Warren Heckrotte and V. Kelvin Neil, A Self Consistent Distribution of Electrons in the Astron E Layer, UCRL-6942, June 8, 1962.

[2] V. Kelvin Neil, Stability of Thin Electron Layers, Phys. Fluids 5, 14 (1962).

[3] Harold P. Furth, A Prevalent Instability of Nonthermal Plasmas, UCRL-6907, May 1962.

2. A COMPUTATION FOR STUDYING THE FORMATION OF THE ASTRON E LAYER

John Killeen

During the past six months substantial progress has been made with the Larc code called LAYER, which has been described previously.[1] A first version was completed in the fall of 1961, but many changes have been made since then to improve the accuracy of the computation. Electrons of 5 MeV energy from a 100-A source are injected at the end of the device. They are injected into a given mirror field. A property of the particular mirror field chosen is that there is a zero of the radial force on the electrons near the injection, i.e., a potential trough is formed about that radius. The electrons can move into 43,890 positions in phase space--21 in the z coordinate, 10 in the radial coordinate, 19 in v_z, and 11 in v_r. This phase-space motion is governed by the numerical solution to the collisionless Boltzman equation, including time dependence. At each time step an integration over velocity space is carried out to compute the current density, and the field due to this current is added to the vacuum field and the force terms in the Boltzman equation are appropriately modified. At the present stage the phase space fills up correctly, and the current and field are computed properly, but various difficulties have prevented us from carrying the calculation to a point where the external field is appreciably modified by the layer.

A separate write-up of this code is being prepared and will be issued as a UCID report.

[1] John Killeen, in Controlled Thermonuclear Research Quarterly Report, UCRL-9598, March 1961, p. 62.

3. INSTABILITY OF A RESISTIVE SHEET PINCH

Harold P. Furth and John Killeen

The study of the effect of finite conductivity on the hydromagnetic stability of a plane current, layer which has been reported previously,[1,2] has been continued. Considerable analytic work has been done in collaboration with M. Rosenbluth with the model in the high-conductivity limit. A dispersion relation has been obtained which describes growing modes of the "tearing" and "rippling" types. An interchange instability due to gravitational field has also been derived. The effects of plasma compressibility, viscosity, and thermal conductivity have been evaluated. These results are being submitted for publication in Physics of Fluids.

[1] Harold P. Furth and John Killeen, in Controlled Thermonuclear Research Quarterly Report, UCRL-9777, Aug. 1961, p. 91.

[2] Harold P. Furth and John Killeen, in Controlled Thermonuclear Research Quarterly Report, UCRL-9969, Jan. 1962, p. 135.

Further numerical work has been done with the time-dependent model, using the code RIPPLE. A range of conductivities has been studied for several perturbation wavelengths.

4. PLASMA POTENTIAL AND ELECTRON ENERGY DISTRIBUTIONS IN THE ALICE EXPERIMENT

Archer H. Futch, Jr., and John Killeen

The code for solving the Fokker-Planck equations which has been used for energy-transfer problems[1] has been modified to include source and loss terms and the calculation of the plasma potential. The code solves for the electron velocity distribution as a function of time. There is a source of hot ions and cold electrons. The ion-distribution function is assumed to remain constant in time. The ion density as a function of time is assumed from the build-up calculations.[2] The plasma potential is computed at each time step of the calculation by requiring charge neutrality. A critical velocity $v_c(t)$ is determined by the condition that electrons with $v < v_c$ are not lost and those with $v > v_c$ can be lost by scattering off other electrons or ions. At each time step the electron density from the code is compared with the given ion density and the velocity v_c modified accordingly. An iterative procedure is employed at each time step. The plasma potential is obtained from

$$e\phi = 1/2\ Mv_c^2.$$

This work will be presented in a separate report.

[1] J. Killeen, W. Heckrotte, and G. Boer, Energy Transfer from Hot Ions to Cold Electrons in a Plasma, UCRL-6383, June 1961.

[2] A. H. Futch, W. Heckrotte, C. C. Damm, and L. Mish, Plasma Production by Neutral Atom Injection: Equations and Numerical Solutions, UCRL-6728, Jan. 1962.

5. THEORY OF AN ELECTROSTATIC PROBE IN A PLASMA

Laurence S. Hall and Donald P. Geesaman

The problem and the methods of solution are described in previous Controlled Thermonuclear Research Quarterly and Semiannual Reports. A working code is now available for the computation of potential distributions about spherical and cylindrical probes. Unfortunately the code is very time-consuming and, for this reason, is somewhat impractical for parametric studies. Work is presently directed towards speeding the computations, and several new codes, not yet completely operational, have been written in the hope of materially shortening the computation times.

6. A STATISTICAL THEORY OF TRANSPORT PHENOMENA

Laurence S. Hall

Preliminary work was completed on a statistical theory of transport phenomena and a report has been issued, covering all results to date.[1] In this paper a systematic procedure for the derivation of transport equations from the Liouville equation through the use of the BBGKY hierarchy is put forward. The unique feature of the analysis is the use of statistical considerations to determine the method of truncating the hierarchy. A variational technique for the performance of Gibb's ensemble average, which amounts essentially to an a priori assumption of an H theorem, is used to determine the missing information when a lower member of the BBGKY hierarchy is substituted for the Liouville equation. The procedure is illustrated for the case of truncation at the lowest level in the hierarchy, and in a certain approximation the Fokker-Planck equation is recovered. However, in order to effect a complete evaluation of the coefficients of the Fokker-Planck term at this level, it is found that a new physical principle, implicit in conventional derivations of the Fokker-Planck coefficients, must be postulated. A discussion of this feature and a proposed experimental check on the analysis are given.

[1] Laurence S. Hall, A Statistical Theory of Transport Phenomena, UCRL-6751, Jan. 1962.

7. ATOMIC SCATTERING

Marvin H. Mittleman

Numerical calculations of 2s excitation of atomic hydrogen have been extended to include excitation to higher states and subsequent decay to the metastable 2s state.[1] The calculation is shown to have direct applicability to a proposed experiment.

A long-overdue calculation of the scattering of light by atomic hydrogen has been carried out numerically (with Fred A. Wolfe). The results are shown to be unambiguous below threshold but to depend on the state of target gas above threshold.[2]

The contribution of "free molecular" effects to opacity have been evaluated for a partially ionized hydrogen gas. The contributions are significant in a restricted high density range.[3]

[1] Marvin H. Mittleman, "Excitation of Atomic Hydrogen by Fast Protons," UCRL-6808-T (Rev.) June 1962.

[2] Marvin H. Mittleman and Fred A. Wolfe, "Coherent Scattering of Protons by Atomic Hydrogen," UCRL-6897-T, April 1962.

[3] UCRL report in preparation.

A calculation of charge exchange of protons in heavy gases is under way.

The general problem of rearrangement collisions is being investigated further (with James Quong). A simple physical problem in which rearrangement is possible has been programmed for numerical solution. Transition probabilities for rearrangement are obtained numerically. This will be compared with the results of all the existing approximation schemes to ascertain the region of validity of each.

8. FORMATION OF EXCITED HYDROGEN ATOMS IN THE COLLISIONAL DISSOCIATION OF H_2^+ IONS

John R. Hiskes

The formation of energetic excited hydrogen atoms and their subsequent Lorentz ionization inside a magnetic field is of interest as a means for injecting and trapping energetic ions inside fusion machines. The formation of excited hydrogen atoms utilizing the charge-exchange reaction has already been considered.[1, 2] Pyle and co-workers have suggested that the collisional dissociation of H_2^+ ions, according to $H_2^+ \rightarrow H + H^+$, might also be a useful source of excited atoms;[3] such a mechanism would provide a source of excited hydrogen atoms of arbitrary energy, in contrast to the charge-exchange reaction, which is a useful source of excited hydrogen atoms in a relatively restricted energy range. This reaction is also under consideration by the Oak Ridge Thermonuclear Group.[4]

Sweetman has observed the formation of excited hydrogen atoms resulting from the dissociative collisions of 90-keV H_3^+ ions passing through water vapor and hydrogen gas. This process is analogous in most respects to the H_2^+ dissociation. However, at these lower energies the apparent distribution over the excited states of the resulting hydrogen atoms is not necessarily a reflection of the production of excited hydrogen atoms due to dissociative collisions of the molecular ions. At these energies the dissociative cross sections are typically 10^{-16} cm^2/molecule, while the charge-exchange cross section is approximately four times as large. Therefore, protons resulting from the primary molecular dissociative collision will have ample opportunity for charge exchange, and since the proton production in these collisions is comparable to the atom production, the final excited-state distribution may be more representative of the charge-exchange process than of the dissociative processes. To remove the ambiguities due to charge-exchange

---

[1] Donald R. Sweetman, Nucl. Fusion, Suppl. 1, 279 (1962).

[2] John R. Hiskes, Nucl. Fusion, 2, (1962).

[3] Robert V. Pyle (Lawrence Radiation Laboratory), private communication.

[4] Persa R. Bell, Jr., and Robert H. Mackin, (Oak Ridge National Laboratory), private communication.

and to measure the population distribution of the excited atoms due primarily to the dissociative process and the secondary excitation reactions will necessitate an experiment with molecular ion energies greater than a few hundred keV.

In conjunction with the proposed experiments in Berkeley an estimate has been made, based on symmetry considerations and the sum rules, of the relative population distribution for excited hydrogen atoms produced in the collision of H_2^+ ions and electrons. In the high-energy Born-approximation limit, the cross section leading to an atom in the nth level is given by the dipole matrix elements coupling the $1s\sigma_g$ ground electronic state with the $2n^2$ excited electronic states; only σ_g, σ_μ, π_g, π_μ, states need be considered; contributions to the σ_g, π_g, states vanish identically, and significant contributions to higher σ_μ states are eliminated by the $\sigma_g \rightarrow \sigma_\mu$ sum rule; primary contributions are due to $1s\sigma_g \rightarrow np\pi_\mu$ transitions. In the united-atom and separated-atom limits the distribution is proportional to $1/n^3$. From the $\sigma_g \rightarrow \pi_\mu$ sum rule[5] it follows that the distribution is equal to $2.3/n^3$, which is to be compared with the charge-exchange distribution, $3.2/n^3$. For intermediate internuclear separations the matrix elements change sign for those transitions leading to atoms in the n = 5, 6 and n = 10, 11, 12 levels, reducing the contributions to these levels relative to the $1/n^3$ distribution.

These considerations suggest that the population distribution of excited atoms produced by the dissociative collisions will be comparable to the distribution due to charge exchange.

---

[5] D. R. Bates, R. T. S. Darling, S. C. Hawe, and A. L. Stewart, Proc. Phys. Soc. (London) 67, 6-A (1954).

9. MAGNETIC SHOCKS

Stanley A. Zwick and Douglas E. Gonzales

Calculations based on two different models for the zero-temperature magnetic pulse have been attempted, in an effort to extend the range of available steady-state solutions. A summary of the latest results is presented below. The solutions will be discussed in greater detail in a paper now being prepared for publication.

The first type of calculation assumed that above the critical Alfvén-Mach number (Mach 2 for the solitary pulse) the positive ions follow looping trajectories, but the very light negative ions are constrained to move adiabatically with the magnetic flux. No such solutions could be found. On the basis of this result and certain qualitative arguments, we conclude that looping trajectories of both kinds of ion must be involved.

The second calculation assumed looping trajectories. It was based on an expansion of the particle equations of motion in powers of $\beta/\epsilon^{1/2}$, where $\beta = V/c$ is the ratio of pulse speed to the velocity of light, and $\epsilon = m/M$ is the ratio of light to heavy ion masses. For a hydrogen plasma

the leading terms in the expansion suffice for $\beta << 0.023$, which covers most cases of practical interest. These terms describe a plasma with negligible charge separation or electrostatic field, and lead to the steady-state pulse problem considered by other investigators.[1, 2, 3] The problem differs from the equal-mass problem only in a change of scale.

The extension involved in our present calculation, in comparison with those performed previously,[4] was the explicit treatment of excess applied stress. Steady-state particle trajectories in a plasma under pressure take on periodic properties, corresponding closely to a superposition of solitary pulse solutions with regular spacing along the direction of propagation. One may ascribe the excess stress to a repulsion between the elements of the periodic structure it produces.

Typical solutions are presented below in graphical form, in terms of the equal-mass displacement variables $\bar{x}$ and $\bar{y}$. Coordinates x, y_i, and y_e for the heavy positive particles (ions) and light negative particles (electrons) are related to $\bar{x}$, $\bar{y}$, and the mass ratio $\epsilon (\equiv m_e/m_i)$ by

$$x = \left(\frac{2\epsilon}{1+\epsilon}\right)^{1/2} \bar{x}; \quad y_i = \left(\frac{2\epsilon^2}{1+\epsilon}\right)^{1/2} \bar{y}, \quad y_e = \left(\frac{2}{1+\epsilon}\right)^{1/2} \bar{y}. \tag{1}$$

Characteristic parameters for a given solution are the scale (skin-depth constant) R, Alfvén-Mach number α, and stress constant σ, defined by

$$R = \left(\frac{Mc^2}{2\pi q^2 N}\right)^{1/2}, \quad \alpha = V\left(\frac{4\pi(m+M)N}{B_o^2}\right)^{1/2}, \tag{2}$$

$$\frac{B^2}{8\pi} + \Sigma m_k n_k \dot{x}_k^2 = \frac{B_o^2}{8\pi} + (m+M)\, NV^2\, (1+\sigma).$$

Here q is the ionic charge, N the number density of positive ions in the undisturbed plasma ($\sigma = 0$), and B_o the applied magnetic field. In the stress relation, the sum is taken over all ion and electron streams present at a point where the individual streams have velocity component $\dot{x}_k$ along the direction of pulse propagation. The actual field B may not reach the value B_o for $\sigma > 0$, and the actual particle densities n_k may similarly never take on their equilibrium value N.

---

[1] J. H. Adlam and J. E. Allen, Phil. Mag. 3, 448 (1958).

[2] L. Davis, R. Lüst, and A. Schlüter, Z. Naturforsch. 13a, 916 (1958).

[3] A. Baños, Jr., and R. Vernon, Nuovo Cimento 15, 269 (1960).

[4] A. A. Zwick, in Controlled Thermonuclear Research Quarterly Reports, UCRL-9243, June 1960, p. 103, and UCRL-9777, August 1961, p. 108.

Figure V-1 portrays a family of trajectories at Mach number $\alpha = 4$ and several values of σ, and Fig. V-2 an analogous family for $\alpha = 10$. Reduced magnetic and electrostatic field curves for the periodic loop trajectory with $\sigma = 0.50$ at $\alpha = 10$ are given in Fig. V-3, in terms of the variables

$$b = B/B_o, \quad e = (\epsilon^{1/2}/\beta)\ E/(1 - \epsilon) B_o . \tag{3}$$

Note that in a frame moving with the pulse at velocity V there will also exist a uniform electric induction field of magnitude $(V/c)\ B_o$. This field causes the particle trajectories to approach parabolic segments inside the loops at high Mach number and small σ, since the magnetic and electrostatic fields tend to be excluded from such loops.

General characteristics of the solutions may be described as follows:

a. For $\alpha > 2$, and σ between zero (solitary pulse) and $\sigma_{cusp} = (\alpha^2 - 4)/8$, there exists a family of looping trajectories. Nonlooping trajectories occur for σ above σ_{cusp}, but below a value σ_{mas} at which the amplitude of particle oscillation in the y direction reduces to zero (see Fig. V-1). For $\alpha > 3$, σ_{max} tends closely to σ_{cusp}.

b. Between $\alpha = 2$ and $\alpha - \alpha_1$ (≈ 9) the loop trajectories remain separate for all permissible σ. For α above α_1, the loops overlap for some range of σ (note Fig. V-2). At high Mach numbers, multiple overlapping occurs, and the affected range of σ tends to fill the interval from σ = zero to $\sigma = \sigma_{cusp}$. Solutions with overlap will not be obtained in the present calculation series, but can be generated by a simple extension of the equations. In a multiple-overlap solution with m-fold overlap, there are two regions of integration to consider, one containing $2m + 1$ independent streams and the other $2m + 3$.

c. Empirically, the pulse spacing λ(center-to-center) can be related to the extra stress by expressions of the forms

$$\sigma \approx \frac{1}{3\lambda^3} \quad \text{(for nonlooping trajectories)},$$

$$\sigma \approx \frac{A(\alpha)}{\lambda^5} \quad \text{(for single-loop trajectories)},$$

for $\lambda > 1.5$, where $A(\alpha) = 0.1$ for $\alpha = 4$, and $A = 3.2$ for $\alpha = 10$.

d. The loop width, height, etc., are of the order of

$$\left(1 - \frac{\sigma}{\sigma_{cusp}}\right) R\alpha = 2\left(1 - \frac{\quad}{\sigma_{cusp}}\right) \times \text{(Larmor radius)}. \tag{5}$$

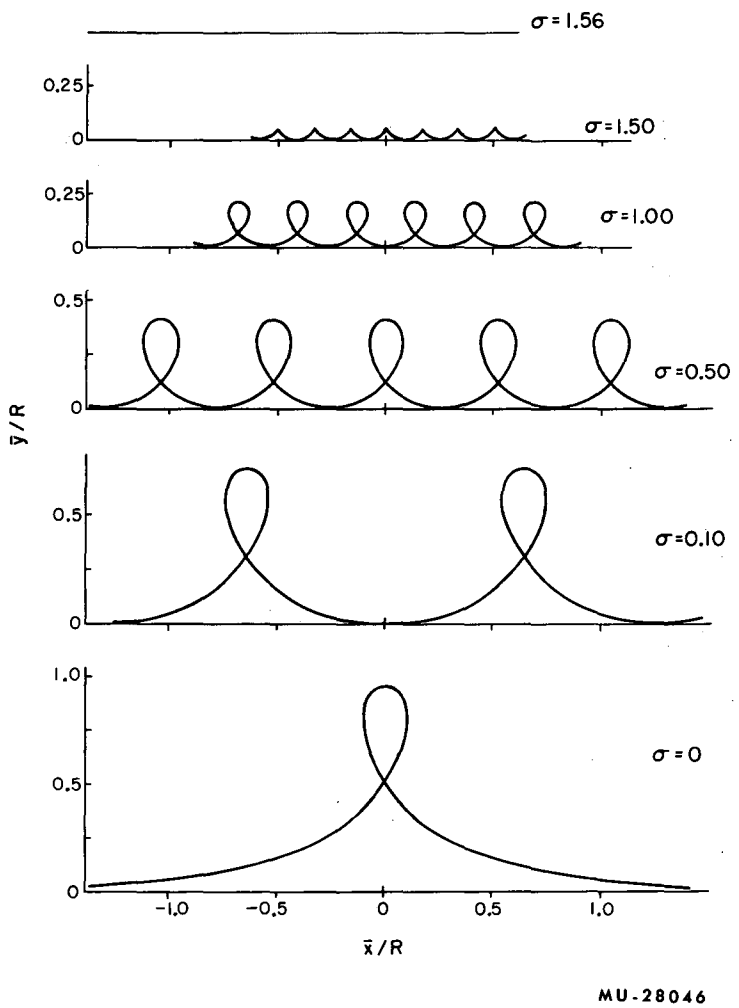

Fig. V-1. Family of particle trajectories at Mach 4 for $\sigma = 0$, 0.10, 0.50, 1.00, 1.50 (cusp trajectory), and 1.56 (limiting case).

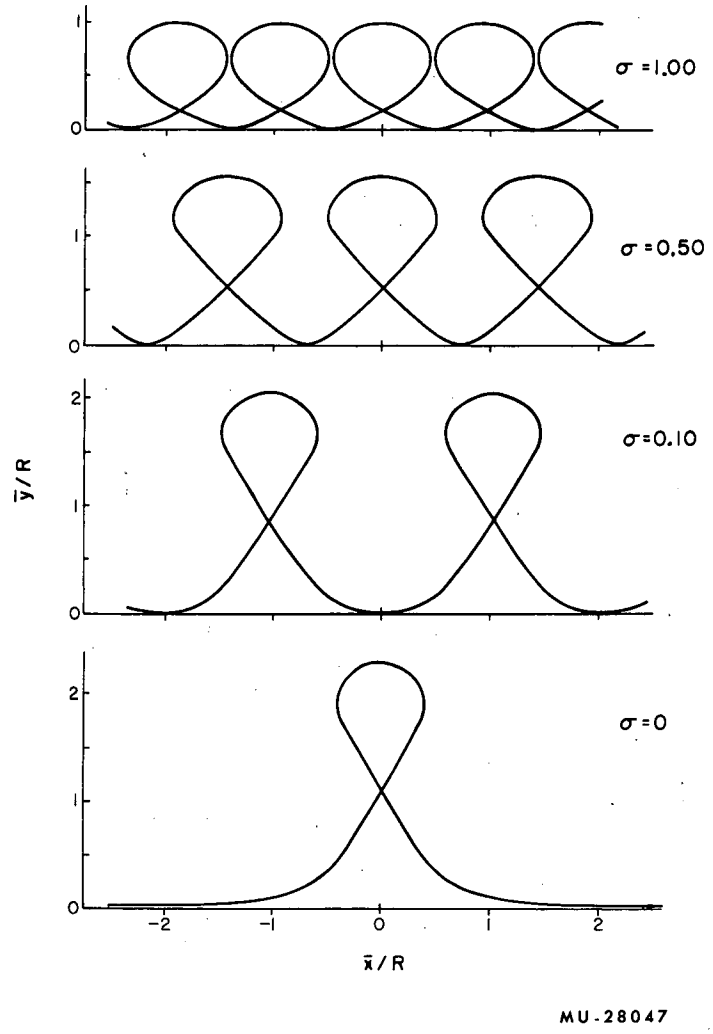

Fig. V-2. Mach 10 loop trajectories for $\sigma = 0$, 0.10, 0.50, and 1.00.

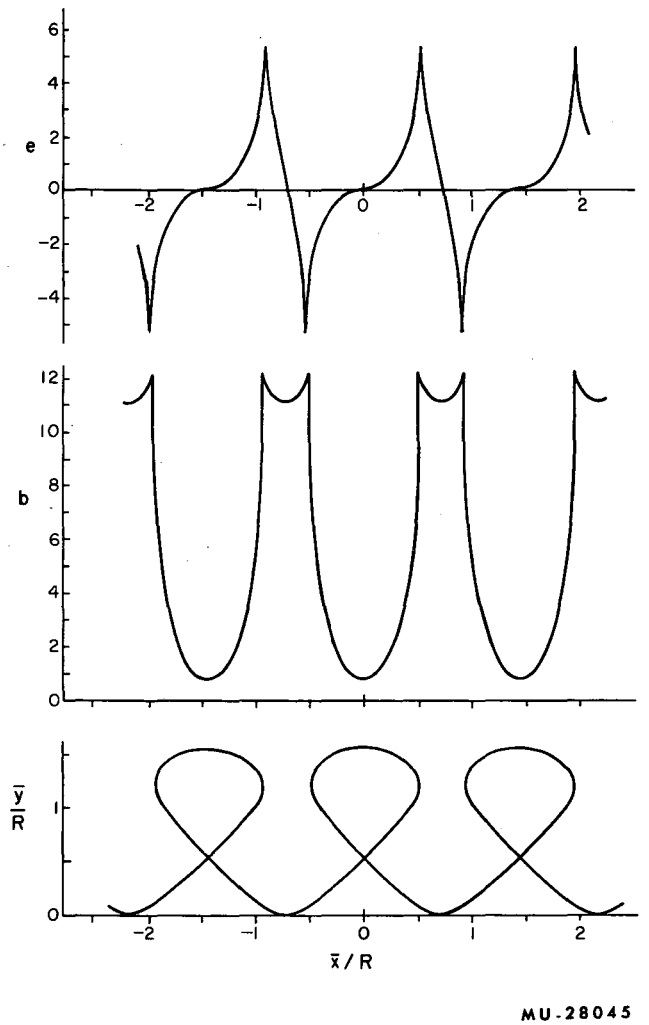

Fig. V-3. Particle trajectory with reduced magnetic and longitudinal electric fields $b = B/B_o$, $e = (\epsilon^{1/2}/\beta)\ E/(1 - \epsilon)\ B_o$, for $\sigma = 0.50$, Mach 10.

e. Quite accurately for $\alpha < 4$ or σ near σ_{cusp}, and to within a few percent for all single-loop trajectories calculated thus far, the sum of loop ordinates $\bar{y}_1 + \bar{y}_2 + \bar{y}_3$ is a constant through the loop region.

10. BUMPY TORUS AND POSITRON EXPERIMENT

Gordon Gibson,† Willard C. Jordan,‡ and Eugene J. Lauer

Positron Experiment

The experiment on the containment of positrons in mirror and cusp geometries has been terminated and final reports written Particle Behavior in Static, Axially Symmetric, Magnetic Mirror and Cusp Geometries, UCRL-6771, Gordon Gibson, Willard C. Jordan, and E. J. Lauer, March 9, 1962. Particle Behavior in a Static Asymmetric Mirror Geometry, UCRL-6856, Gordon Gibson, Willard C. Jordan, and Eugene J. Lauer, March 29, 1962.

Bumpy Torus

Injection Section

It is planned to set up the injection apparatus for the electron model[1] before the rest of the torus is available. This will consist of the gun, iron pole tips, injection coils and two main torus coils, associated power supplies, and diagnostic probes. It is expected that testing of this apparatus will commence in August. The most important purpose of this test will be to confirm the predicted motion of the electrons as they leave the gun, and the drift along the edge of the iron pole tips and around the horseshoe-shaped path between the injection coils. Tests of this apparatus can continue while the rest of the torus is being assembled, and then the injection apparatus can be moved from its temporary location and incorporated into the torus.

Stabilizing Field

In the Bumpy Torus geometry the field lines are closed and, under equilibrium conditions, surfaces of constant pressure are surfaces of constant $U = -\oint d\ell/B$, according to magnetohydrodynamic theory. The interactions of these surfaces with a midplane are nearly circles (not concentric) with their centers shifted inside the ring axis. According to this idealized theory, the plasma should experience the interchange instability.

---

†Westinghouse Electric Corporation, Atomic Power Dept., Pittsburgh, Pa.

‡The Bendix Corporation, Research Laboratories Division, Southfield, Mich.

[1] G. Gibson, W. C. Jordan, and E. J. Lauer, in Controlled Thermonuclear Research Semiannual Report, UCRL-9969, January 19, 1962, p. 166.

The low-β interchange instability is predicted to be stabilized if

(a) the magnetic field has shear (i. e. the flux lines spiral around a magnetic axis with the angle of rotation per trip around the torus being a function of distance from the axis), and

(b) plasma of infinite conductivity[2] exists everywhere along the flux lines.

Iron pole arrays are being designed which can be installed in some of the median planes between Bumpy Torus coils. A calculation is being carried out that will yield estimates of the shear as a function of the orientation and strength of the poles. None of the iron pieces will be placed in the vicinity of the injection section, so the field will not be significantly perturbed in this region. The effects of the shear on the single-particle motion has not yet been ascertained. In the initial experimentation with the complete torus, no shear will be introduced.

Loss-Rate Calculations

The calculations of the rate at which energetic plasma particles are lost owing to becoming trapped in the loss side of the horeshoe-shaped injection drift surfaces because of plasma scattering has been improved by incorporating accurate machine calculations of the field shape in the injection region. Studies are also continuing of the particle drift loss out of the injection section by using machine calculations of the particle trajectories.

Integration of Guiding-Center Equations

An expression for the gradient of the magnetic field of a Bumpy Torus composed of single-turn loops has been obtained. C. H. Woods and N. Hetherington have also derived this expression. The derivation is tedious and independent solutions seemed desirable to avoid errors. A code is in preparation[3] which will make use of these expressions in order to follow the guiding center of a particle's motion in a static field by solving the equations of motion obtained under the adiabatic assumptions.

It is the purpose of the calculations to check the precessional surfaces that are obtained by assuming the invariance of the momentum p, the transverse invariant $\mu = (p_\perp^2/B)$, and the longitudinal invariant $J (= \oint p_\parallel d\ell)$. In particular, the range of validity of the assumption that J is an invariant will be investigated, since μ and p are invariants for the equations that are to be solved.

If a particle is confined between adjacent mirrors, or if the particle is traversing the torus, J is approximately invariant in the adiabatic limit. By varying the adiabatic parameter it may be determined under which conditions the approximation tends to break down.

---

[2] The conductivity of a plasma consisting of 150-keV electrons and an equal density of positive ions having a nuclear charge of Z=7 is about 0.045 emu. Approximately 1/4 second would be required for a suddenly applied magnetic field to penetrate 1 cm into such a conductor.

[3] Programmer: Robert L. Herrick

A specific case of interest is that of a particle which is trapped between adjacent mirrors but, after precessing across lines of force, commences to traverse the torus. In a general Bumpy Torus geometry, at the time when the particle first passes through a mirror J changes in value. However, if for a given value of μ and of p the surfaces of constant J are found for particles that are (a) trapped between adjacent coils, and (b) traversing the torus, two sets of surfaces are found that join in a unique way, even though the value of J may change as the particle makes the transition. In the particular case of the Bumpy Torus with coils whose centers are coplanar and equally spaced, J values across a transition may be easily correlated because of the symmetry. (It was for this reason that a two-dimensional calculation[4] was meaningful.)

If at the time of transition the particle tends to "balance on a mirror" --i.e., the period associated with the longitudinal motion becomes long enough that the particle drifts an appreciable distance across lines of force per oscillation--the assumption of the invariance of J tends to break down even in the adiabatic limit. For given positions, the regions in velocity space for which J is not an invariant will be investigated.

[4] G. Gibson, W. C. Jordan, and E. J. Lauer, Phys. Rev. Letters 4, 217 (1960).

11. ATOMIC SCATTERING AND CROSS-SECTION MEASUREMENTS

Forrest S. Baker, Gilbert O. Brink, Edmund S. Chambers, Robert H. McFarland, and Edward A. Soltysik

Crossed-Beam Experiments

During the last six months several experiments have been begun on the crossed-beam machine and two have been completed. One of these has been described in a UCRL report and the other will be submitted for publication shortly.

Proton Production from H_2

During the last several years a controversy has arisen concerning the relative production of H^+ and H_2^+ from H_2 by electron bombardment. An experiment was performed that attempted to measure the ratio of the number of H^+ ions produced to the number of H_2^+ ions produced when a molecular beam of H_2 was bombarded with electrons.[1] Unfortunately no protons at all were observed, and only an upper limit to the ratio could be determined.

The main difficulty in this measurement is that the protons are produced with several electron volts of kinetic energy while the H_2^+ have thermal energies. It is difficult to design a detection system that will detect both types

[1] G. O. Brink and F. S. Baker, An Upper Limit to the Production of H^+ from H_2 by Electron Bombardment, June 1, 1962.

of ions with equal efficiency. The protons produced also have a non-isotropic angular distribution with respect to the electron beam. This distribution is peaked along the direction of the electron beam and has a minimum at 90° to the electron beam where most experiments are done.

Because of these considerations the Paul mass spectrometer was set up to look for ions coming directly along the electron beam. From the known solid angle it was possible to calculate the total number of protons produced from the number that were observed by the mass spectrometer. Suitable electric fields could then be applied to collect all of the slow H_2^+ ions and the ratio determined.

As was mentioned above no protons could be observed. This gives an upper limit to the ratio of H^+ to H_2^+ production of about 0.16.

Proton Production from H_2O

The relative cross section for the production of protons from water by electron bombardment was measured by the crossed-beam method. The shape of the curve is as expected with the exception of a slight shoulder in the region of 60 electron volts. This shoulder may indicate the presence of more than one mode of breakup of the H_2O molecule to form H^+ ions. The threshold for proton production was measured as 19.4 eV. This result agrees with the values obtained by other workers. This work will be submitted for publication in the near future.

Hydrogen Ion Source and Cross-Section Measurements

During this period the new mounting and vacuum system for the ion source was completed. A secondary electron detector was constructed and put into operation.

Preliminary measurements were carried out with this apparatus of the following atomic parameters:

1. Fast Neutral Production Cross Sections from H^+, H_2^+, or H_3^+ Ions in H_2 gas, 1.2 keV and 57.5 keV.

2. Dissociation (Breakup) Cross Sections of H_2^+ or H_3^+ Ions on H_2 Gas, 5 keV to 58 keV.

3. Secondary-Electron Emission Ratio from H^+, H_2^+, or H_3^+ Impinging on Copper-Beryllium, 1.2 keV to 57.5 keV.

The large vacuum system previously used with the ion source is being modified for use as a crossed-beam apparatus for the investigation of ion-neutral reactions.

Electron Production of Radiation

Additional experiments dealing with the inelastic scattering of electrons with gases have been completed. Molecular hydrogen has been bombarded with electrons ranging in energy from 15 to 400 eV. The molecular

and atomic spectrum has been surveyed for polarization at 25 eV from 3000 Å to 7000 Å. Although stronger Balmer lines were clearly resolved, there was no indication of polarization of the radiation.

The results observed were not unexpected, although positive polarization of the Lyman alpha line excited in atomic hydrogen has been reported,[2] as also has a preferred direction of dissociation by electron impact of molecular hydrogen.[3]

Basic information concerning a lack of understanding of inelastic scattering has been reported in UCRL reports numbered 6749, 6749 Rev., 6929 and 6949.

[2] W. L. Fite and R. T. Brackman, Phys. Rev. 112, 1157 (1958).

[3] Nobuji Saski and Tsuneyo Nakao, Proc. Imp. Acad. Japan 17, 75 (1941).

VI. ENGINEERING AND TECHNOLOGICAL DEVELOPMENT

1. ULTRAHIGH-VACUUM DEVELOPMENT

Norman Milleron and Leonard L. Levenson†

Oil Cracking in Diffusion Pumps

We tested oil cracking in two experimental oil diffusion pumps. Each pump had a ribbon heater and a jet stack made of 0.01-in.-thick 304 stainless steel. Using Veeco ionization gauges of the Bayard-Alpert type, we found the untrapped base pressure of each pump, at room temperature, to be about 5×10^{-7} torr when using Convoil-20, OS-124 or the new Dow-Corning oil. We attribute these high base pressures to catalytic action on metallic oxides, both on the ribbon heater and the jet stack surfaces. We are beginning tests with Teflon coatings on stainless steel as a possible solution to this cracking problem. Teflon coatings were subjected to impingement of hot oil vapor during four days of a preliminary test. No effect on the Teflon was seen.

Conductance Measurements

In addition to the rougher-than-rough surfaces reported last time we examined the conductance of some arrays in short tubes. One of these arrays was a set of spaced thin washers snugly housed in a tube. Let us discuss the scaling laws for the conductance of this washer array as a typical example. We compare the conductance of the array to the conductance of a plain rough-walled tube with the same i.d. as the washers and the same length as the housing tube. With two washers only, spaced far apart, at each end of the housing tube the array has a conductance greater than the equivalent plain tube. As the number of spaced washers is increased, with their i.d. and the length of the housing tube kept constant, the conductance of the array approaches that of the equivalent plain tube. Further increase in the number of thin washers, spaced apart, yields a minimum conductance 25% less than the equivalent plain tube. Increasing the number of washers to the limit of zero spacing raises the array conductance back up to the plain tube conductance. Details of this work are given in two papers: "The Effect of Rougher-Than-Rougher Surfaces on Molecular Flow Through Short Ducts," and "Free Molecular Gas Scattering from Arrays in Beam Tubes." These papers will be submitted for publication later this year.

Large Bakable Valve Design

Tests of a flat stainless steel-to-stainless steel valve closure employing about 100 lb per linear inch closing force have been completed. These tests were part of our optimum system design program and are for use in the straight-through and elbow-blocking plate designs. The valves can be baked

†Present address: Centre d'Etudes Nucléaires, Fontenay-aux-Roses (Seine), France.

in the closed position at 400°C against atmospheric pressure while the pump is running. By using differential pumping between two flat seats we obtained a leakage rate of 10^{-9} atm cc/sec on a 6-1/2-in.-diameter closure. It is worth pointing out, perhaps, that a closed conductance of only 8×10^{-4} atm cc/sec permits a 7-in.-diameter system to operate at 1×10^{-6} torr with atmospheric pressure on one side of the valve. This type of valve probably can be made to close in less than 0.2 sec.

2. MECHANICAL ENGINEERING DEVELOPMENT

Thomas H. Batzer

2 X Multistage Compression Facility

John R. Benapfl, Edward G. Scarlett, James F. Ryan, and James N. Doggett

Construction of the facilities for the 2 X machine is on schedule. The three-story capacitor bank structure, 20X100 ft, located on the north side of the main bay in Bldg. 180, is due to be completed on July 2, 1962. The machine foundations and footings are in. The 20X100-ft two-story capacitor bank is scheduled for completion on September 4, 1962. The control room, including electronic rack installation and 20-ton chiller system, is due for completion on August 15. The data-processing room is scheduled to be completed on August 1, including rack installation and 20-ton air conditioner.

All major mechanical parts of the machine have been designed and are on order. They include six aluminum tanks 5 ft in diameter by 5 ft long and a pumping manifold with adjustable structural support. Also included are 25 dc coils, 6 ft i.d. by 9 ft o.d. The facility is expected to be completed by November 1962.

Low-Energy Neutral-Beam Experiment

William S. Neef, Jr., Eugene T. Bradley, and James N. Doggett

Operation of the "Alice" machine began in April. The liquid-nitrogen-cooled field coils performed well at central fields up to 30,000 gauss. No attempt has been made to reach higher fields, but all indications point to satisfactory coil performance.

At very low magnet temperatures, small vacuum leaks developed at the joints between the pump boxes and the reaction chamber. Disassembly revealed foreign material across the sealing surfaces of the west pump box, and a severe scratch on the seal edge of the east pump box.

Heating tapes were added to these flanges to reduce differential expansion, and the damaged gasket surface was repaired. The system has been reassembled and pumped down and is now performing very satisfactorily from the vacuum standpoint.

Three new adjustable collimators were designed and are being constructed. Another stage of beam tube pumping has been designed and is being

added to combat the streaming problem from the water neutralizer. A solution to the streaming problem appears to be the "water vapor curtain," which was successfully tested recently. The collimated jet of water vapor directed across the beam tube collides with the water molecules streaming from the neutralizer. Both are then trapped on liquid-nitrogen-cooled surfaces.

The design of the axial limiter and radial profile detector was altered to use a large differentially pumped sliding vacuum seal to replace a long bellows and simplify the design. Fabrication will begin in July.

An ion-gauge calibration system similar to one recently built for NASA by the National Research Corporation has been designed. The first components are fabricated and are ready to test for vacuum performance.

A beam tube employing zeolite-filled cartridges cooled by liquid nitrogen has been designed and released for fabrication. Diffusion pumps with conventional cold traps are located at each end of the tube. A series of orifice plates separates the cartridges, which completely surround the beam passage with cold zeolite. Pumping tests using a simple hydrogen leak or an atomic beam (or both) will be conducted.

Astron

Charles A. Hurley and James F. Ryan

The debugging of the first mechanical assembly of the 720-kV electron gun is essentially complete. The modifications consisted of installing a new ceramic accelerating column, improved primary and ground connections, more and better insulation, and additional filters in the freon circulation system. This assembly, with all its connections except monitoring connections, is enclosed within the gun tank.

A decision to purchase a spare core stack presented an opportunity to improve the mechanical assembly considerably. The new design is complete and half the hardware is out for fabrication.

Auxiliary Astron Equipment

1. Installation jigs and handling gear for switch chassis and pulse shapers are complete.

2. Cable support trays inside the shielding wall were completed.

3. A large table-top device for making turning magnet field measurements has been designed and built.

4. Design is in progress on an optical diagnostic instrument for the beam experiment.

5. Work has begun on an ion source, which is to be tested in the 100-kV ion injector developed for the MTA high-current accelerator.

Induction Accelerator

Four accelerator units have been assembled and parts are on hand for the remaining four units. The blowers, air ducts, and plenum chambers for air-cooling the accelerator cores are on hand and are being installed. Three types of beam-focusing coils have been designed and four coils are completed. The rest are being made in the Coil Shop.

Beam Research Facility

The beam tube, 60 ft long by 18 in. in diameter, for the ARPA beam stability experiments is on hand. The parts for the focusing section and the differential pumping section are being procured; completion by Oct. 1 is expected.

Astron 90-Foot Trapping Chamber

The main Astron chamber is at high vacuum pumped by two of the four 20-in. diffusion pumps. No work has been done on the assembly of the cantilevers or any of the coils, as completion of the accelerator has first priority. The coaxial leads for the coils to be mounted on the ends of the cantilevers and the fine wire resistors for reducing the energy of the electrons during the injection process are being procured by the Electronics Engineering Department according to Mechanical Engineering design.

Bumpy Torus

J. Ralph Ullman, Eugene T. Bradley, and Manuel O. Calderon

All parts for the "weld test" assembly are due in July. Typical torus coil spools will be assembled with the adjacent pie-shaped sections to work out welding and other fabrication procedures.

The apparatus for the beam injection study has been designed and is on order. This assembly consists of 150-kV electron gun, flux leaders, split coils, beam probe, two torus main coils, vacuum vessel for the foregoing, and a vacuum pumping system. Apparatus to permit remote control of the electron gun bias voltage and filament current has been designed and detailed. Diagnostic probes to survey the trapping area are being designed.

Cryogenic Project

Clyde E. Taylor, Robert L. Nelson, and David C. Holten

The 8-in. i. d. $\times$ 16-in. o. d. $\times$ 12-in. -long sodium solenoid consisting of 78 turns of 5/8-in. square conductor has been cooled to 10° K by the pulsed refrigerator. The coil resistance is measured to be approximately $3\,\mu\Omega$ at this temperature, which indicates that the resistivity of the sodium in the coil is at least as low as that of the many small samples tested during the distillation process.

The lead-shot-filled refrigerator, an important component of the refrigeration system, has not been used because of seal failures in some ball valves. When current repairs on this refrigerator are completed, the coil can be energized to full power.

Component Development

Thomas H. Batzer and James F. Ryan

Further tests have been made on Monsanto OS-124 diffusion pump oil, with some modification to the original pumping system. The modifications consisted of substituting mild steel jets for the aluminum jets in the PMC 720 diffusion pump and designing an oil-free backing system using liquid-nitrogen-cooled zeolite and copper wool. The lowest pressure reached prior to the changes (with the same water-cooled baffle) was 4×10^{-8} torr. The base pressure after the changes was 4×10^{-9} torr.

Monsanto OS-138, a hexaphenyl ether, is currently being run in the same system. The results are not conclusive.

Bakable ultrahigh-vacuum flanges using 0.0015-in. soft aluminum foil have been developed. The engineering details of these flanges are described in Engineering Note 129. The flanges can be baked for long periods to temperatures above 400°C, and also can operate fully submerged in liquid nitrogen. The flanges tested were made of 304 stainless steel, but tests are currently being made using 6061-T6 aluminum flanges (5456 is a superior alloy for temperatures to 300°C) with soft aluminum foil, and indications are that they too will be very reliable. An aluminum vessel of roughly 50 liters, built of 6061-T6 aluminum with all the flanges made up of aluminum foil, has undergone preliminary bakeout and outgassing tests.

The second 10-in. bakable valve is fully assembled, and has been placed on a vacuum system for bakeout tests.

A bakable, ultra-high-vacuum pumping system is being assembled to determine the ability of a mercury pumped system to recover from an up-to-air accident.

3. ELECTRICAL ENGINEERING DEVELOPMENT

Vernon L. Smith

Pyrotron

David R. Branum

Table Top III

During the past six months the machine has been operated continuously. There were no major bank faults during this period.

An automatic "scope" camera positioner synchronized to the machine camera shutter controls was designed and built. This unit is now in operation on the Table Top machine.

A Livermore-constructed LASL-type plasma gun was installed on the second floor north of Bldg. 157, and is now being operated.

Various photomultiplier bases have been constructed for experiments on Table Top.

A new time-delay chassis is under design. It will have an overall delay range from 1 μsec to 1 sec. The jitter on the 1-μsec-to-1-msec ranges is less than 0.01%. The jitter on the 1-msec-to-1-sec ranges is less than 0.95%.

A specification has been written for purchase of a programmable getter supply.

Toy Top III S

In January of this year the pulsed field coils for the three-stage compression facility were redesigned. The months January to May were spent in building and testing the new pulse coils. These coils, designed by the Physics Group, were tested for 40-kV pulse breakdown voltage. In April, additional crowbar chains were added to banks 4AB and CD to improve the L/R field decay time and the bank crowbar efficiency.

There were a number of capacitor failures on Toy Top III's bank No. 1 earlier in the year. The capacitors failed in short and open conditions. Bank No. 1 was rebuilt, with new Cornell-Dubilier and Sangamo capacitors, and now will operate to the voltage limit (17 kV) of the WX4231 ignitrons. Since this conversion, there have been no troubles on bank No. 1.

A special 5-inch ignitron is under design for use as a high-current crowbar switch. The first trial tubes were used on the Table Top III bank No. 1 crowbar circuit. These became gassy after 1,000 pulses at 10,000 A peak current with a decay of 200 msec to the $1/\epsilon$ value. The tubes were cut open and showed no evidence of wall bombardment. Evidently the main problem was with the anode seal and the anode-to-cathode relative temperature differential. The anodes were cooler than the cathodes, thereby causing mercury to condense on the anode seal and short out the tube. This short caused the bank to discharge into the crowbar tubes at a current level limited only by the bank, line, and tube inductances and resistances. Several of these faults would greatly overheat the seals and cause a leak. A new 5-inch tube has been designed and is now being built by Westinghouse. This tube will be known as a WX4473 and will have better cooling of the cathode and a better anode seal configuration.

2X

This new multistage mirror machine is now under construction in Bldg. 180. Based on experience obtained from the Toy Top III machine and the capacitor samples bought earlier in the fall of 1961, a new complete capacitor specification was written. Five hundred of the 14.5-μf 20-kV capacitors and 200 of the 7.5-μf 20-kV capacitors were purchased from Westinghouse. All 700 capacitors were delivered in June of this year.

The ignitron switches chosen for this new experiment were the WX4231 size A and the new WX4681 size D ignitrons. The 4231 is a long-potted small ignitron with a graphite anode that has proved reliable at 30,000 A and 14 kV.

After conditioning, it will run up to 20 kV with only occasional prefire breakdowns. Three hundred and seventy of these small 4231 ignitrons were ordered and received from Westinghouse. The majority of these tubes will dc hipot in the 30-to 45-kV range.

The Type D ignitron, 4681, was specified because tests indicate they will be better than the standard 5555 ignitron. One hundred and sixty of these ignitrons were ordered from Westinghouse. Thirty tubes are still to be received. Those tubes that have been received have withstood a dc hipot from 30 kV to 50 kV.

Approximately 80% of the units on order have been received. All the ignitron parts have been received. Still outstanding are the bank buswork fabrications, pulse chassis, voltage detectors, and transmission-line fabrications.

The contractor is now assembling the north bay bank structure. The control room and the diagnostic room are also under construction.

The transmission-line runs from the 10^7-joule bank in Bldg. 156 to the 2X experiment in Bldg. 180 are now under design. The Plant Engineering group is designing the support structure and building modifications for the six large transmission lines.

The dc-cable runs from the Perkin power supplies in Bldg. 156 are now under design. These cable runs will not be constructed until the machine structure has been completed. This dc power supply system will be capable of a pulse peak dc output of 9.6 MW.

P-4

The two Eimac electron guns that failed earlier in the year were taken to Eimac for inspection. It was decided that the purchase of new guns would be less expensive than repair of the old electron guns.

Pyrotron

Hubert W. Van Ness

Alice

During this period all the following electrical systems for the Alice machine were completed and operated satisfactorily as initially designed: vacuum system power and control, bakeout power and temperature monitoring, ion source, mirror-field coil power supply control and monitoring, and operating-sequence control system.

The liquid-nitrogen-cooled mirror field-coil assembly is complete. During initial machine operation the coils have been energized to 3,000 A one-half the maximum design value of 6,000 A. In addition to monitoring the coil current and voltage, meters indicate the resistance of each modular section during the cool-down periods between operations. After the first two

weeks of operation, the operating-sequence control system was improved to make it more versatile and flexible.

Ion source operation has continued. The source magnet field was found to have a 0.5% 20-cps ripple, which is about five times as great as desirable. An LC filter section is being added to the output of the motor generator set supplying this field power.

A 60-kV 100 ma 0.1% voltage-regulated dc power supply has been ordered as per LRL Specification LES 11582. This power supply will replace the existing unregulated supply providing the accelerator voltage for the duoplasmatron ion source in the diagnostics development and test facility. The required modulation and detection equipment has been provided for the Lorentz-force reionization study in progress in this area.

A versatile high-vacuum ion-gauge test chassis, LE 8309-1, has been provided for the study of ion-gauge performance in the high-vacuum research area.

Cryogenics Coil Experiment

This facility was completed and initial operation started in February. The system provides up to 50,000 A into the cryogenically cooled test coil from a bank of twelve submarine batteries.

All power and control system are now in and operating. In no-load tests, the cryogenic coil has been cooled to liquid helium temperatures. Except for completion of the diagnostic system only minor engineering and installation effort are required.

Pinch Program

Hubert W. Van Ness

Levitron Experiment

During this period, the Levitron has been rebuilt to remedy internal insulation and vacuum problems. While the repair work was in progress, the gamma capacitor bank was modified. The modification involved paralleling capacitors in groups of five, firing through a single ignitron, plus the addition of load resistors and additional ignitor resistors. These changes provide more reliable bank operation at the slow current rise times (approximately 10^{-3} sec) involved in the Levitron operation.

The rebuilt Levitron is now ready for initial vacuum bakeout. This will be accomplished with the 10-kc 30-kW motor generator induction heater coupled to temporary Z windings on the Levitron.

A flash x-ray system with 0.1-μsec 100-kV pulse output has been purchased for use on the Levitron. This will be modified by the addition of a special tube to provide pulsed electron output into the Levitron through one of the ports on the device. The special tube will be designed and constructed in our Tube Shop.

Energy Storage System Investigation

Starting in February, a limited effort has been assigned to tests on a homopolar generator. Since then, initial calibration tests have been run up to 20,000 A output into the megampere switch and load circuit. All the equipment appears to be operating correctly at this level.

Field pulsing equipment has just been installed and initial tests of output with field pulsing are inder way. Tests will continue up to the 100,000-A level to obtain all possible data on both load switching and field-forcing modes of operation. Subsequently, tests will be run to determine the maximum capability of the equipment. It is hoped to obtain current pulse outputs approaching one million amperes from the generator.

Beta Pinch Capacitor Bank

The new capacitor bank for the Beta Pinch Experimental Area was decided upon in January. The bank will store 150 kilojoules at 20 kV. It will be divisible into four separate and independently controlled sections for versatility. The bank will provide a minimum output rise time of 5 μsec and a repetition rate of two operations per minute.

The bank construction is under way and about 10% completed. All capacitors have been received from the manufacturer and their assembly with ignitron mounting hardware is just starting.

Switch Development

David B. Cummings

Ignitron Development

The WX4564, the stabilized, low-inductance ignitron, was tested on the Table Top bank. Two tubes were used in series in the crowbar circuit for 1700 pulses. At this point one tube was gassy and the ignitors were down to about 5 ohms. The gassy tube was then cut open. There was no evidence of arc transfer to the wall. The pulses had a peak current of about 6,000 amperes with a decay constant of 0.05 sec. This is much longer than the arc transfer time for any other ignitron in use.

The WX4973 is an improvement of the WX4564, designed to be more easily produced with a glass seal instead of a ceramic one. These tubes should be delivered by October.

The remaining ZG7207 size D ignitrons were delivered by General Electric. Vacuum baking the graphite anodes to 2150°C was very hard on their ovens, and they will no longer accept orders to this specification. They have decided they don't feel it is necessary.

An order was placed with Westinghouse to make and test two types of molybdenum-anode ignitrons with special ignitors. These were the WX4838 and WX4839. The ignitors were designed to have hidden leads and radial electric fields. The intent was to avoid short-circulating the ignitor if the surface became wetted with mercury.

The WX4838 had a glass-coated tungsten rod dielectric starter. The WXk4839 had a boron carbide–boron nitride pellet sintered onto a tungsten rod and mounted on a ceramic seal. The average life was less than 100 pulses. The reasons for failure are not understood.

The WX4231, produced to our design, has been registered by Westinghouse for commercial production as the WL8306. This tube has a rounded throat and graphite anode and has been used extensively here.

Microwave Diagnostic Development

Charles B. Wharton

Alice Beam-Trapping Experiment, P-3

A cold plasma source intended for the study of breakup of the Alice beam uses a titanium hydride washer. The source is fired from a pulse line having a variable pulse length, from 15 μsec to 200 μsec, at voltages up to 20 kV.

Microwave diagnostics have been applied to measuring the plasma density, spatial extent, loss rate, and shot-to-shot fluctuations. The experiment is roughly as sketched in Fig. VI-1. Polarization diplexers allow two frequencies to be propagated over the same path simultaneously by orienting their polarizations perpendicular to each other. Three frequencies in all can be transmitted simultaneously; 25 and 35 Gc in the square-throated horns fed by the diplexers and 90 Gc between conventional horns. The antennas are small and spaced far enough apart that the far-field radiation theory applies.

Because of the small horn size the side lobe radiation was at first bothersome. Stray paths due to wall reflections gave spurious responses. A stainless steel liner, painted with a nonreflecting coating (see preceding semiannual report) reduced these spurious responses to a tolerable level.

Insulating sections in the waveguide runs were found necessary to eliminate pickup into the detectors from ground-current loops. Thin Mylar film between flanges (clamped with nylon screws) was found adequate, and introduced only small losses and standing waves.

The K-bank signal (25 Gc) gets cut off by plasma bursts at even low pulse voltages. The corresponding cutoff density is $n_{CO} = 10^{13}/cm^3$. Fig. VI-2 shows the 3-mm bank ($f = 90$ Gc, $n_{CO} = 10^{14}/cm^3$) and 8-mm band ($f = 35$ Gc, $n_{CO} = 2\times10^{13}/cm^3$) transmission signals for pulse voltages of 5 kV and 10 kV. At 5 kV neither signal reaches cutoff; at 10 kV both of them do, but at different times. The recurrent pulses are amplitude markers to show when the signal strength drops to zero. The data analysis of several hundred shots has permitted reaching of some fairly reasonable conclusions regarding source performance in the magnetic field.

The plasma column appears to be only a few centimeters in diameter and is suspected of being striated during the current pulse. The transmitted signal fluctuates considerably, as if the plasma were turbulent or unstable.

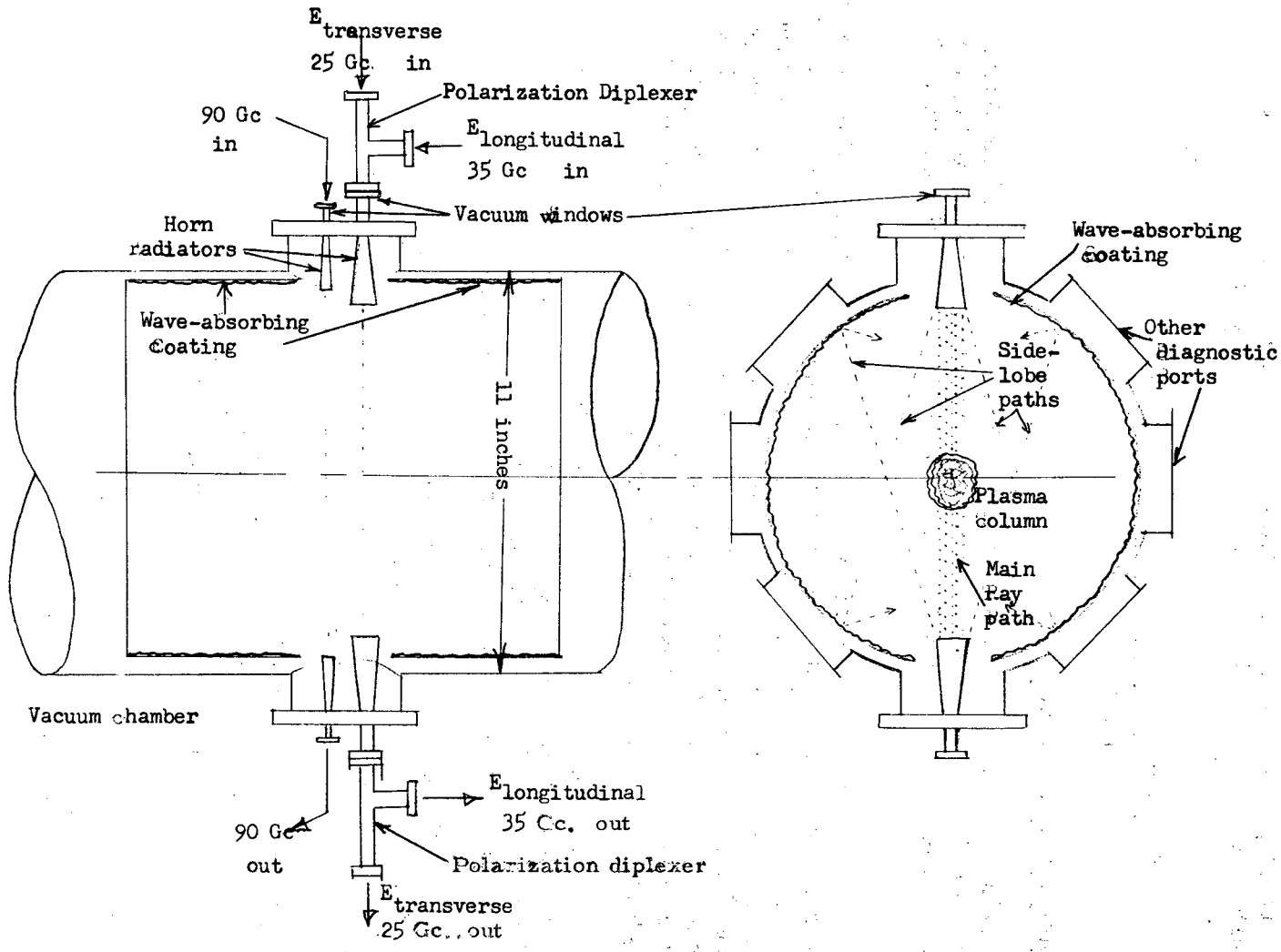

MUB-1325

Fig. VI-1. Microwave diagnostic attachments to the P-3 experiment.

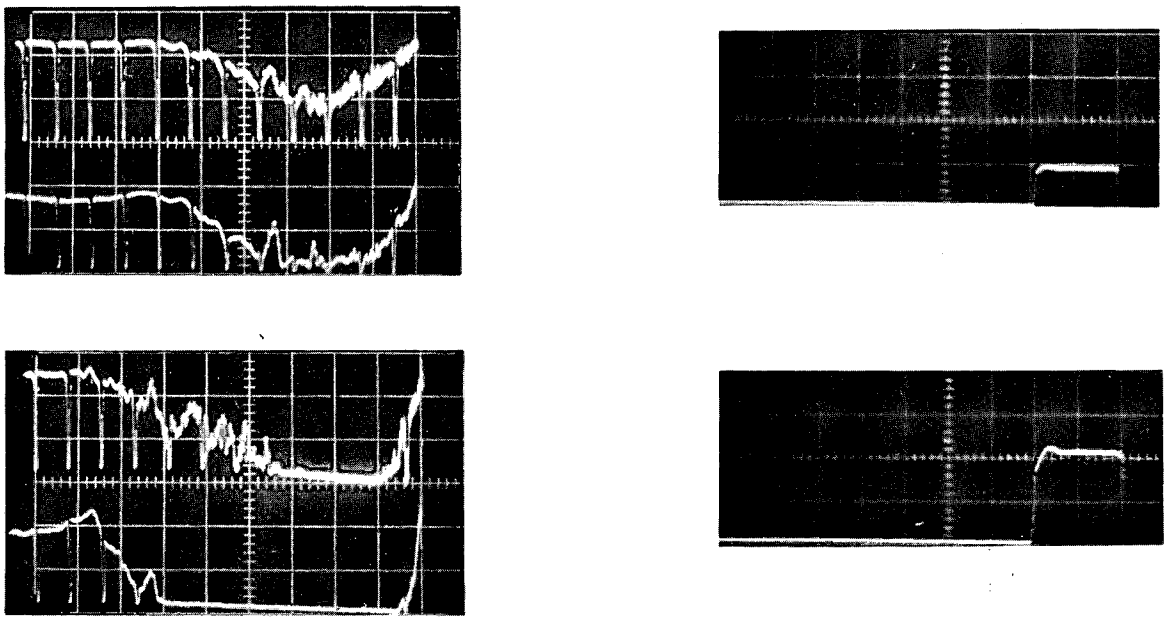

90 Gcs Transmission (top)

35 Gcs. Transmission (bottom)

Source Voltage

(5 KV / cm)

(550 amps/cm)

ZN-3254

Fig. VI-2. Microwave transmission attenuation, due to the plasma injected from the washer source. The current pulse lasts 200 μsec. Time scale is 100 μsec/cm for all traces.

These fluctuations smooth out during the afterglow, as one would expect. The plasma density seems to increase more or less linearly in time during the current pulse, clear out to 200 μsec. The constituents of the plasma are unknown and it may be either hydrogen or the contaminants that account for this buildup. The density decay is approximately logarithmic with time after the current ceases.

Collision rates seem fairly high, as deduced from wave attenuation on the low-density side of cutoff. Three-millimeter interferometer measurements especially showed up this effect, the first few fringes from cutoff being greatly attenuated in amplitude. An alternative explanation of this attenuation is that steep density gradients lead to severe scattering or that the small column size gives a refractive defocussing of the microwave beam. In most plasma experiments the latter effects are small compared with real absorption.

P-4 Instabilities Experiment

Not much that is new has been tried on the instabilities experiment during this period, owing to lack of time. We did insert a curved boron nitride dielectric rod radiator, to look first upstream (toward the injected electron beam) and then downstream (toward the plasma source). The received radiation bursts were of about the same magnitude from either direction when the tip of the rod was immersed in the plasma column. When the rod was a centimeter outside the plasma, the pulses were received only from the upstream direction.

Toy Top

Further bench work with microwave slot radiators is being done to be prepared for 70-Gc radiation and transmission measurements far up inside the machine. This method of wave launching permits access from the end of the machine, without side arms or coupling through glass walls. The AFC system, currently being developed for 3- and 4-mm systems, will be applied to the 70-Gc systems. Without stabilization, the klystron frequency drifts enough to make it difficult to hold a good null on the interferometer over long periods of time.

Astron System Engineering

Clelland D. Nail

The Electron Accelerator

Construction and Testing

Assembly of the Astron Electron Accelerator is progressing rapidly, with completion scheduled for the fall of this year. Much of the installation and practically all of the chassis construction is being done through outside contracts. Design decisions have been made on all system details. Some of these decisions are based on limited statistics and may require reconsideration after the accelerator enters the "debugging" stage.

Operational tests of parts of the system are continuing. A mock-up of eight cores and the associated equipment has been operating for several hundred hours. As final production models of various chassis become available from

vendors, they are installed in this test facility to obtain data for determination of the design adequacy. Results of these tests indicate a limited reliability when applied to the completed machine.

Details of Construction

In order to reduce the time required for construction, we have found it effective to purchase all electronic components, tubes, transistors, etc., while negotiating the assembly contracts. This shortens the time required by the vendor and assures that the Laboratory will receive hardware of the quality desired.

Another technique that has been followed wherever possible is to build two exact prototypes. One of these is supplied to the vendor; the other is placed on test. Usually by the time the contract is placed most of the design changes have been established and lost time is avoided. The contractor is required to furnish a production model for approval prior to starting the production run. If the production model does not perform exactly like the prototype, corrections can be made immediately.

A methodical technique for scheduling work, known as the CPM or Critical-Path Method, has been extensively applied to the accelerator construction program. By means of an "arrow diagram" the logical progression of each step in the procurement, testing, and installation of the components is established. Estimates of time and manpower are made and updated at frequent, regular intervals. Updating is done by the staff members most responsible for each detailed "arrow." These data are programmed into a computer and the longest or critical path to completion of the job is determined. By simple computer manipulation, the jobs may be listed in order of urgency, according to earliest possible start date, by craft required, or by any other logical progression. The result is a very complete analysis of work progression and shows areas where time and manpower economics may be effected.

This technique has made it possible to coordinate construction of all components so as to bring the predicted completion of the accelerator within the scheduled time.

The Astron Accelerator comprises, besides the cores, these major functional units: The pulse shaper, pulse-forming networks, switch chassis, core-reset pulser, trigger generator, system-timing generator, and charging power supplies (Fig. VI-3). Construction progress on each of these major units during this period has been as described below.

Pulse Shaper

The contract for assembly of the 500 pulse shapers illustrates the value of the paralleling technique for cutting production time. Data obtained from the critical-path method indicated a long delivery time for the pulse-shaper chassis. This estimate indicated the chassis, under normal procurement procedure, would not be ready for use by the time the machine was completed.

To avoid the delay, all the parts were placed on order; a personal

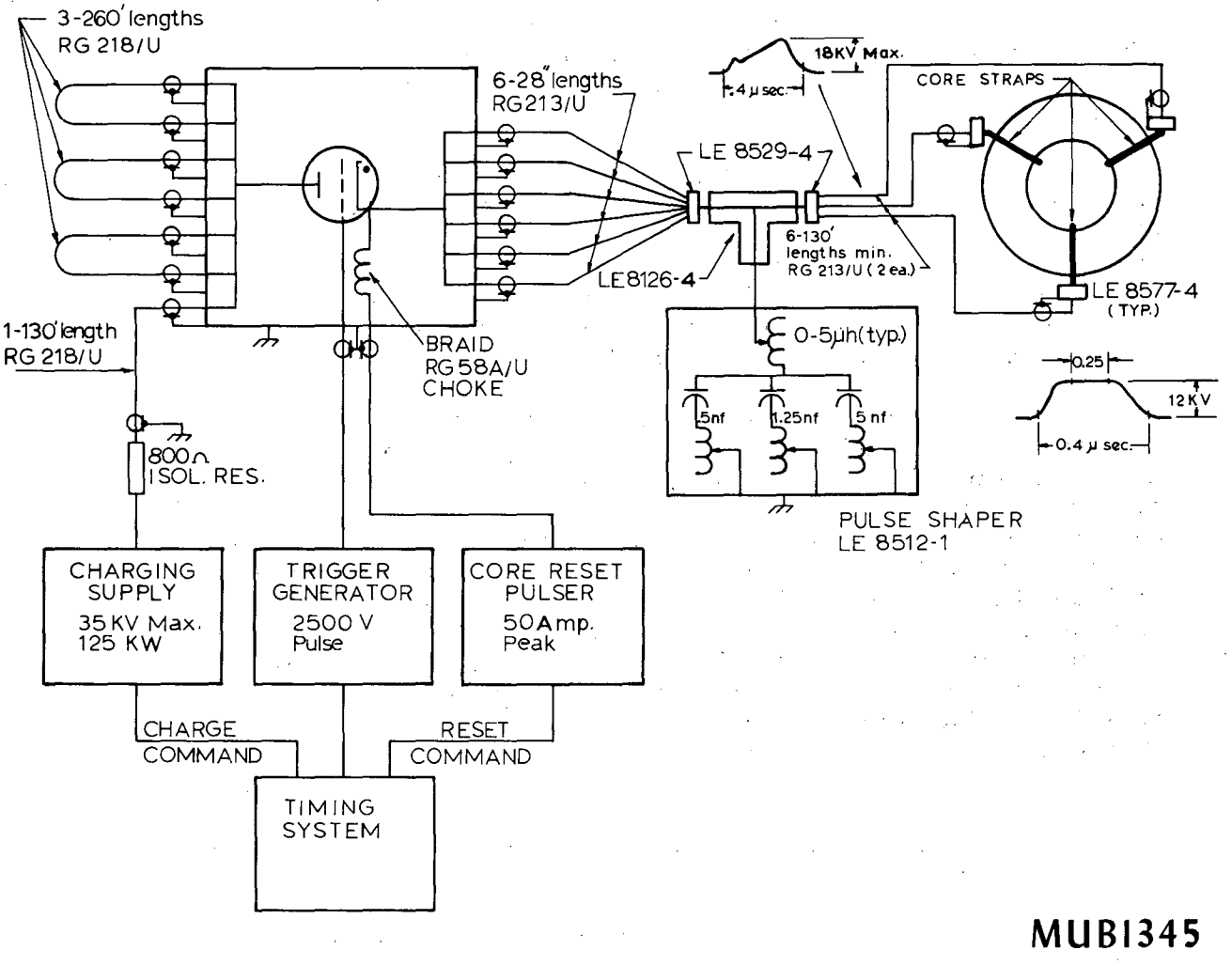

Fig. VI-3. Simplified block diagram of Modulator pulsing an accelerator core.

visit was made to the vendor responsible for inductors, and an assembly contract was negotiated. As the result of this paralleling of operations the production model has already been tested and a production schedule of 100 chassis per week is expected to start immediately.

The chassis will make use of the available ceramic capacitors even though these are known to be temperature-dependent. Samples of improved capacitors have been purchased, but no evaluation of these has yet been possible.

Pulse-Forming Network

The pulse-forming networks, consisting of RG-218/U coaxial cable, have been completed. The cables are coiled in 260-ft lengths on nearly 3,000 reels located on two platforms extending over the rack area. A contract is about half completed for connecting the cable ends to the connectors and high-voltage distribution cubicles.

Switch Chassis

The contractor has completed the required 500 thyratron switch chassis and a like number of input-output connector assemblies. Specially conditioned thyratrons are being installed in the chassis and tests run on a representative sample. Chassis and rack hardware are being carefully jigged so that all the units are interchangeable.

Core Reset Pulser

A contract has been awarded to construct the reset pulsers, and the production model has been approved. The circuit, designed by the Sherwood Research Group, uses solid-state techniques.

System-Timing Generator

The line-synchronized repetition-rate generator is ready for test. This drives a group of Digital Delay Generators to obtain the various times needed. Universal counter-timers have been purchased to monitor the timing of the system.

Output pulse amplifiers (or trigger generators, Fig. VI.3) are designed (but not constructed) to drive the reset pulsers, charging supplies, etc. on the output pulse amplifiers, the most difficult requirement is to drive the grids in the 500 thyratron switch chassis (50 ohms each at 2300 V). A magnetic modulator for this purpose was designed and tested. This circuit was found to possess many novel characteristics of interest; however, it was discarded in order to complete the machine in the scheduled time. In its place, four regular thyratron switch chassis are being substituted. The output of these chassis is stepped down through special pulse transformers from 12.5 to 2.3 kV.

The contractor for these transformers has submitted two designs for consideration. Neither has fully met the specifications but the second is close and will probably be acceptable after minor corrections.

Charging Power Supplies and Associated Equipment

All four of the charging power supplies which supply the 500 pulse-forming networks (Fig. VI-3) have now been delivered. However, to data, none of the units has been accepted and considerable difficulty has been experienced with tests.

In addition to the technical difficulties, the supplies were delivered six to eight months later than was specified in the contractual agreement. Special effort is being made to clear up these difficulties so that they will not delay scheduled completion of the accelerator.

Voltage distribution cubicles have been extensively redesigned to give automatic circuit protection when excessive current is drawn. Special fast-closing vacuum relays have been ordered. Contracts have been placed concurrently for the cubicle housings, the current-sensing coils, the electronic control circuits, and the wiring harness.

Control

The CPM analysis shows the completion of control chassis to be the most critical path. These items, while very detailed and complex, are "state-of-the-art devices" and will not require any additional development once the equipment is installed.

The Astron Facility

Magnet Power Supplies

Final specifications for the main field power supplies are being revised. The ripple and regulation response time requirements have been relaxed and a higher noise level (70 db) has been permitted.

Deceleration Resistors

The specifications and drawings of the deceleration resistors are complete and are out for bid.

Basic Experimental Physics

Atomic and Molecular Physics

David R. Branum

The ion-detection system was designed to operate a 2 cycles per second. A mercury relay detector was used to indicate phase matching. Nonlinearity in the output circuit was corrected with an impedance changer. The phase control was modified to use a square wave delay unit designed for minimum jitter and temperature characteristics.

The rf oscillator associated with the ion-detector mass spectrometer was designed to produce frequencies between 0.5 and 3 Mc. The oscillator includes link coupling to provide rack-mounted controls away from the main experiment.

The glass vacuum system was altered to contain the ion source. A high-power rf oscillator (16 Mc) and a 35-kV power supply were built and installed.

An angular position indicator was installed to control the position of the rotating vacuum chamber. Panel controls and monitoring were provided.

The work done with the radioactive potassium required a counting system. A system including a Hamner Model No. 276-N was installed and tested. Noise effects associated with the photomultiplier and the cathode follower were studied and evaluated.

A counting system was developed for the detection of ion signals. The system includes a summation counter and an automatic printout unit. Stability tests are still in progress.

The racks and associated control equipment to be used in the new facilities for the Cross-Section Group are on order.

Bumpy Torus Experiment

Hubert W. Van Ness

Design of major electrical system components is now complete and fabrication and installation of these components is now under way. Design of the control system and control rack layout is not 30% complete.

Megajoule Electrolytic Capacitor Bank

Donald B. Hopkins

The megajoule electrolytic capacitor bank[1] in Berkeley is nearing completion. It is intended to supply power to generate pulsed magnetic fields for up to five different experiments on a sequenced time-sharing basis. It is basically 80,000 μF of capacitance, rated at 5 kV, and capable of being discharged in a minimum quarter-cycle time of 200 μsec. It consists of 80 modular drawers of 144 capacitors, each rated at 1000 μF, 450 V, in a 12-by-12 series parallel array. Each module has its own set of output switching ignitrons and a reactance-limited charging supply, and it is essentially an independent 12.5-kJ bank in itself, requiring only primary ac power and ignitron-firing pulse inputs. Figure VI-4 is a photograph of half the bank at an uncompleted stage of development, and Fig. VI-5 is a photograph of a single modular drawer.

Figure VI-6 is a photograph of the bank control console located at each of the five experimental stations. Each user has, in his turn, independent control over bank capacity (in increments of one-quarter bank), bank voltage, and

[1] Donald B. Hopkins and Pierre F. Pellissier, A High-Voltage Electrolytic Capacitor Bank, UCRL-9968, December 11, 1961.

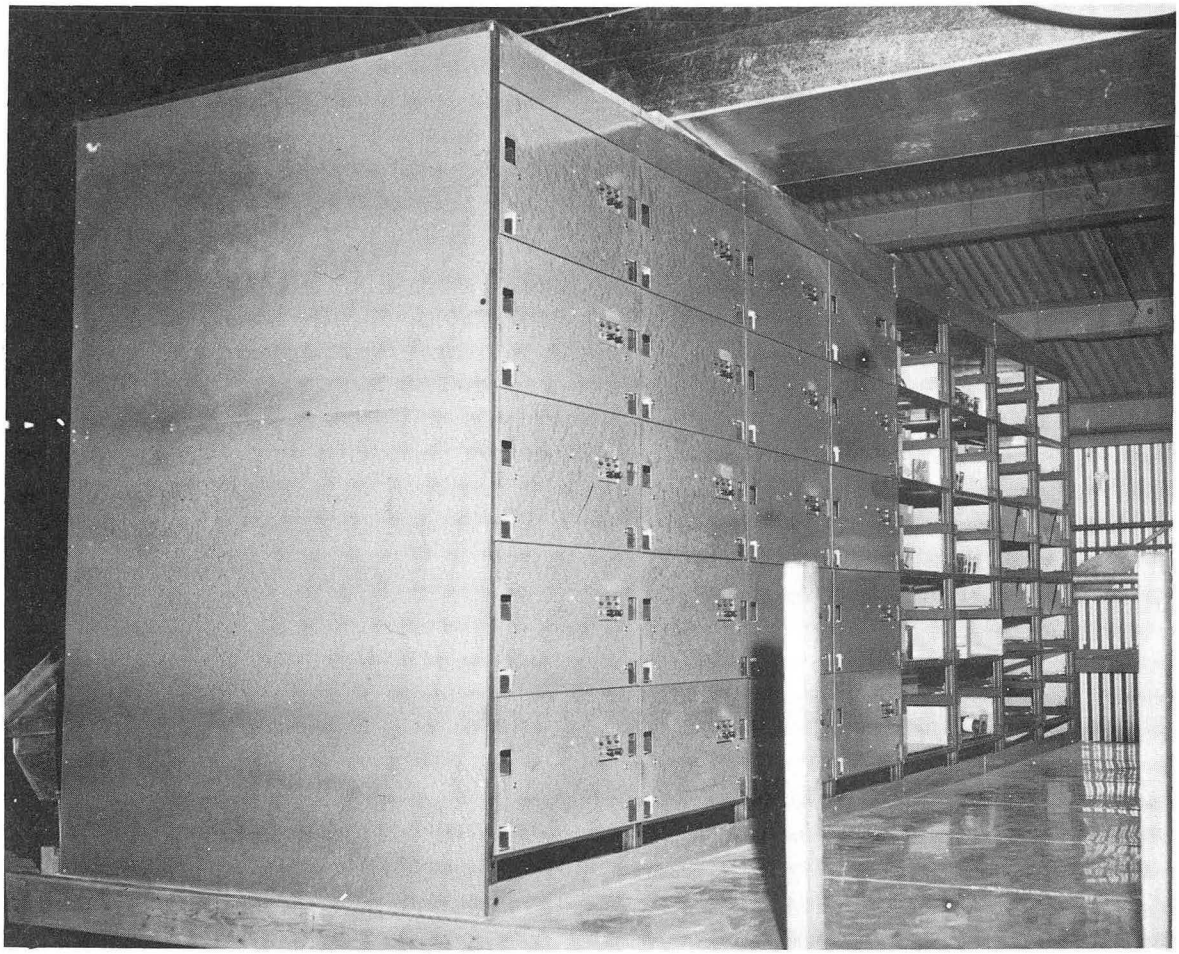

ZN-2984

Fig. VI-4. One half of megajoule bank.

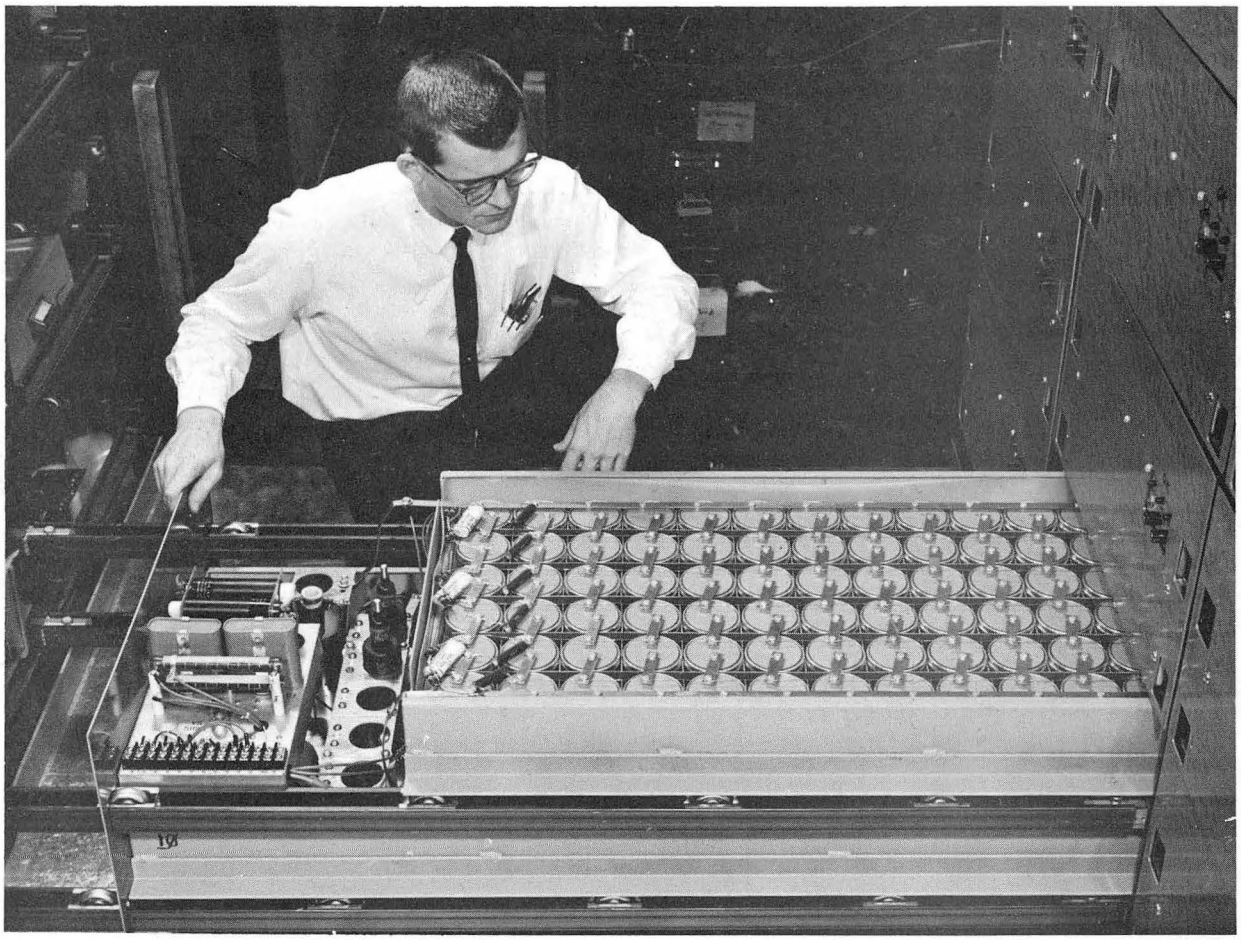

ZN-2985

Fig. VI-5. Megajoule bank modular drawer.

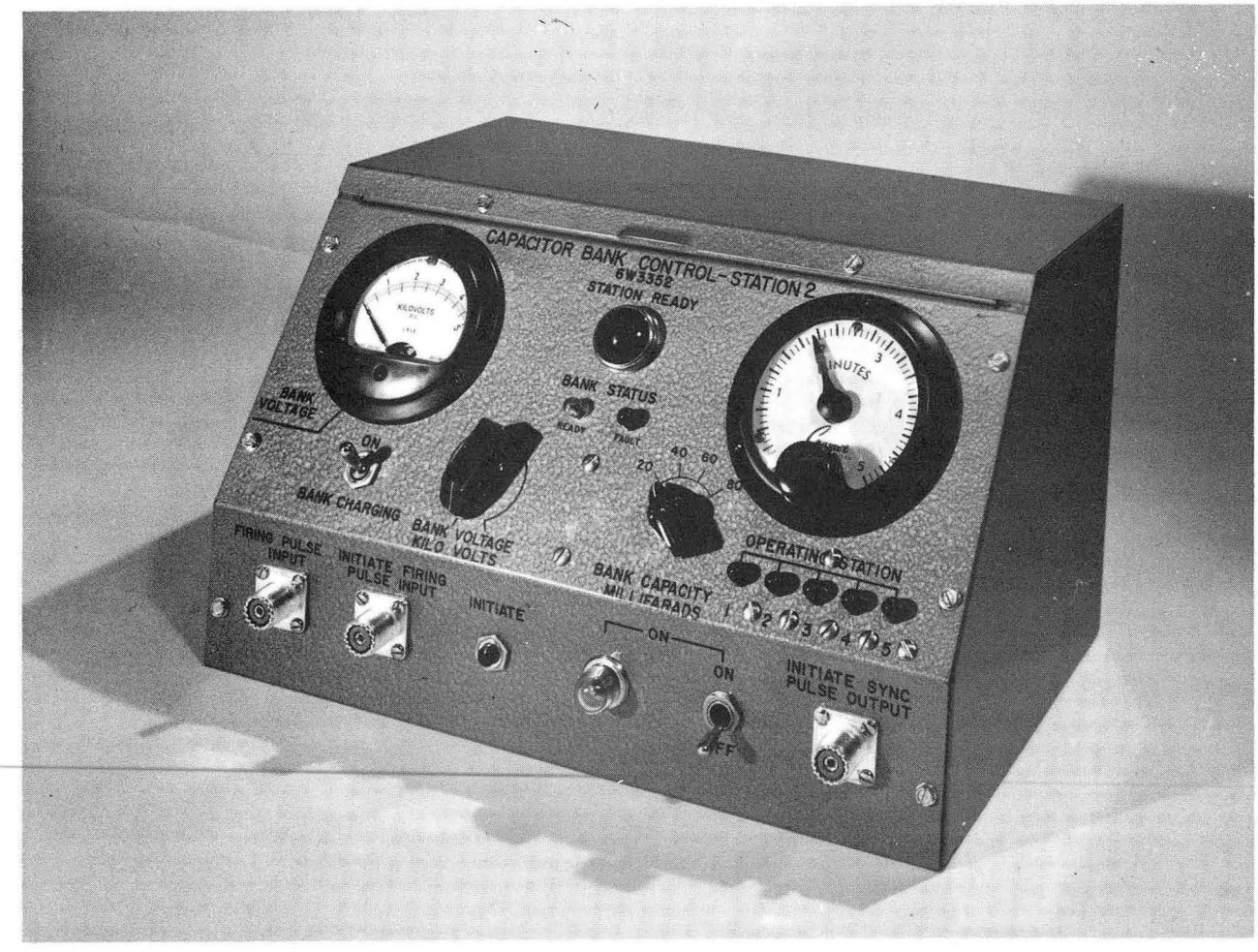

ZN-2986

Fig. VI-6. Megajoule bank control console.

firing time. Provisions are made for charging only the portion of the bank selected. An adjustable timer limits the operating cycle time allotted to any station to a maximum of 5 minutes. Charging time, depending on the desired bank voltage, ranges from 30 to 90 sec.

Typical operating quarter-cycle times are from 5 to 20 msec. For consistent firing, it was necessary to install voltage equalization circuitry on some modules to maintain the voltage of all modules within about a 200-V tolerance range. It was also necessary to provide the module-firing ignitrons with a long ignitor pulse, approximately 1.2 msec, of 2 kV amplitude. Four pulse lines, one for each quarter-bank, each using three series strings of twelve of the same type of electrolytic capacitors used in the bank, generate these pulses. The capacitors in the bank apparently deform fairly rapidly. It is necessary to "form them in" at full voltage for 15 min each morning to ensure reliable firing during the day.

The bank has obvious advantages of size, cost, and flexibility. Required floor space, including access and service area, is less than 250 ft^2. The total cost, including charging supplies, controls, and labor, is about 14 cents per joule. Including external voltage dividers and internal leakage current, about 24 w/kJ is required to maintain the bank at full voltage.

VII. TALKS AND PUBLICATIONS

APS 1962 Annual Meeting, New York, N. Y., January 24-27, 1962

Gilbert O. Brink, The Ionization of Potassium by Electron Impact, Bull. Am. Phys. Soc. Ser. II 7, 70 (1962)(UCRL-6688-T Abst., Nov. 6, 1961).

Marvin H. Mittleman, Rearrangement Collisions, Bull. Am. Phys. Soc. Ser II 7, 40 (1962)(UCRL-6682-T Abst. Nov. 3, 1961).

AIEE General Meeting, New York, N. Y., January 29-February 2, 1962

D. B. Cummings, Ignitron Discharge Growth During High Current Pulses, UCRL-6635 Abst., Sept. 26, 1961.

Science Lecture Program, North American Aviation, Inc., Los Angeles, Calif., February 2, 1962

Richard F. Post, Some Aspects of the Problem of Controlled Fusion, UCRL-6738-T Abst., Jan. 8, 1962; invited paper.

Beam-Plasma Conference, Massachusetts Institute of Technology, Research Laboratory of Electronics, February 17-18, 1962

Andrew L. Gardner, Beam Plasma Experiments at LRL, Livermore; informal talk.

APS 1962 Spring Meeting, Washington, D. C., April 23-26, 1962

Wulf B. Kunkel, The Polarization of the Two Magnetoacoustic Wave Modes, Bull. Am. Phys. Soc. Ser. II 7, 260 (1962)(UCRL-10039 Abst., Feb. 1962).

L. L. Levenson, N. Milleron, and D. H. Davis, Effect of Rougher Than Rough Surfaces on Molecular Flow Through Short Ducts, Bull. Am. Phys. Soc. Ser. II 7, 260 (1962)(UCRL-6787-T Abst., Feb. 6, 1962).

Charles W. Hartman and Stirling A. Colgate, Electrostatic Shock in Collisionless Plasma, Bull. Am. Phys. Soc. Ser. II 7, 273(1962) (UCRL-6783-T Abst., Feb. 6, 1962).

John M. Wilcox, Forrest I. Boley, Alan W. DeSilva, C. N. Watson-Munro, Gordon W. Hamilton, and Peter R. Forman, Ion Cyclotron Resonance in a Highly Ionized Plasma, Bull. Am. Phys. Soc. Ser. II 7, 274 (1962) (UCRL-10037 Abst., Feb. 1962).

Stirling A. Colgate and Richard H. White, The Dynamics of a Supernova Explosion, Bull. Am. Phys. Soc. Ser. II 7, 320 (1962)(UCRL-6777-T Abst., Feb. 5, 1962).

Robert V. Pyle and George A. Paulikas, Search for Enhanced Interactions in a Positive Column, Bull. Am. Phys. Soc. Ser. II 7, 328 (1962) (UCRL-10038 Abst., Feb. 1962).

Kenneth W. Ehlers, Color Production from Energetic Ions Impinging on Metals, UCRL-9920 Abst., Apr. 1962 (postdeadline paper).

AEC Sherwood Theoretical Meeting, New York University, New York, N. Y. April 30-May 1, 1962

W. Heckrotte and V. Kelvin Neil, Theoretical Description of the Astron E Layer, UCRL-6881-T Abst., April 10, 1962.

Seventh Symposium on Hydrogen Thyratrons and Modulators, Fort Monmouth, New Jersey, May 22-24, 1962

Bernard M. Loth, Development of a 50-Megawatt Magnetic Modulator to Simultaneously Trigger 500 Thyratrons, UCRL-6811-T Abst., Mar. 8, 1962.

Vernon L. Smith, Performance Tests and Life Data of the 36-Megawatt Modulators Developed for the Astron 1000-Megawatt Electron Accelerator, UCRL-6810-T Abst., Mar. 8, 1962.

Sixth Brookhaven Conference on Molecular Beams, Upton, Long Island, N. Y. June 10-13, 1962

F. S. Baker and G. O. Brink, Deposition of Molecular and Atomic Beams on Surfaces, UCRL-6866 Abst., Mar. 23, 1962.

G. O. Brink, An rf Mass Spectrometer as a Universal Detector, UCRL-6905 Abst., Apr. 25, 1962.

American Nuclear Society Meeting, Boston, Mass., June 18-21, 1962.

John R. Hiskes, Injection into Fusion Machines Using the Lorentz Force, UCRL-6799-T Abst., Feb. 21, 1962; invited paper.

APS 1962 Summer Meeting in the East, Northwestern University, Evanston, Ill., June 19-21, 1962

L. S. Hall, On a Statistical Theory for the Derivation of Transport Equations, Bull. Am. Phys. Soc. Ser. II 7, 400 (1962)(UCRL-6869-T Abst., Mar. 27, 1962).

H. P. Furth, Instability of Reverse-Field Theta Pinches, Bull. Am. Phys. Soc.Ser. II 7, 405 (1962)(UCRL-6884-T Abst., Apr. 11, 1962).

Publications

International Science and Technology

Stirling A. Colgate and Harold P. Furth, Thermonuclear Plasmas 1, No. 2, 34-41 (1962) (original title, Progress in Controlled Fusion Research, UCRL-6670, Oct. 24, 1961).

IRE Transactions on Nuclear Science

W. A. S. Lamb, Design Features of a High-Current Pulsed Electron Accelerator, NS-9, 53(1962) (UCRL-6699, Nov. 15, 1961).

Vernon L. Smith, Development of 36-Megawatt Modulators for the Astron 1000-Megawatt Electron Accelerator, NS-9, 57 (1962) (UCRL-6469, Dec. 29, 1961).

Journal of Applied Physics

Harold P. Furth and Morton A. Levine, Force-Free Coils and Superconductors, 33, 747 (L) (1962) (UCRL-6498, June 26, 1961).

Lewi Tonks, Magnetic-Field Reversal by Relativistic Electrons Which Slow Down While Circulating in a Uniform Impressed Magnetic Field, 33, 1987 (1962) (UCRL-5733, Sept. 7, 1961).

Nuclear Fusion

Lewi Tonks, The Structure of the Astron E-Layer, 1, 273 (1961) (UCRL-6379, June 10, 1961).

C. C. Damm, A. H. Futch, F. Gordon, A. L. Hunt, E. C. Popp, R. F. Post, and J. F. Steinhaus, Plasma Production by the Trapping of Energetic Atoms 1, 280 (1961) (UCRL-6393, June 12, 1961).

The Physical Review

M. H. Mittleman and Robert Pu, Optical Potential for Closely Coupled States, 126, 370 (1962) (UCRL-6663-T, Oct. 1961).

M. H. Mittleman, Formal Theory of Rearrangement Collisions. II, 126, 373 (1962) (UCRL-6674-T, Oct. 1961).

The Physics of Fluids

V. Kelvin Neil, Stability of Thin Electron Layers, 5, 14 (1962) (UCRL-6463, May 12, 1961).

George A. Paulikas and Robert V. Pyle, Macroscopic Instability of the Positive Column in a Magnetic Field, 5, 348 (1962) (UCRL-9682 Rev., Oct. 2, 1961).

This report was prepared as an account of Government sponsored work. Neither the United States, nor the Commission, nor any person acting on behalf of the Commission:

A. Makes any warranty or representation, expressed or implied, with respect to the accuracy, completeness, or usefulness of the information contained in this report, or that the use of any information, apparatus, method, or process disclosed in this report may not infringe privately owned rights; or

B. Assumes any liabilities with respect to the use of, or for damages resulting from the use of any information, apparatus, method, or process disclosed in this report.

As used in the above, "person acting on behalf of the Commission" includes any employee or contractor of the Commission, or employee of such contractor, to the extent that such employee or contractor of the Commission, or employee of such contractor prepares, disseminates, or provides access to, any information pursuant to his employment or contract with the Commission, or his employment with such contractor.